

**Analysis of morphology development during the mixing process of  
rubber-clay nanocomposites and correlation to their mechanical-  
physical properties**

Dissertation

zur Erlangung des akademischen Grades

Doktor-Ingenieur (Dr. -Ing.)

vorgelegt dem

Zentrum für Ingenieurwissenschaften  
der Martin-Luther-Universität Halle-Wittenberg

von MSc Zulfiqar Ali

geb. am 20.04.1974 in Hafizabad (Pakistan)

Halle, den 5.08.2009

**Dedicated to My Loving Parents**

## Acknowledgement

It is great opportunity for me to express my thanks to all the people who accompanied and shared me directly or indirectly for completion of this work.

I would like to sincerely acknowledge my supervisor Prof. Dr. Ing. habil. Hans -Jochain Radusch for his continuous guidance, inspiration and enthusiasm throughout my work and providing me an opportunity to work in his group. I am also thankful to him for his help in solving my day to day problems that any student might face in a foreign land. During my stay as MSc and PhD student in his group, I have always found my Prof. as sympathetic, and person of principles.

I would like to express my deep sense of gratitude, sincere thanks to my advisor Dr. Hai Hong Le for his valuable suggestions, discussions, continued encouragement and inspirations throughout my stay here. I have always found him a humble and kind colleague, who is always willing in helping, providing opportunities and exposing his students to the scientific environment on a large scale. The expertise and extensive experience of Dr. Le in the field of elastomer technology proved a substantial helpful to accomplish this task.

I am also obliged to Dr. Sybill Ilisch for her continuous support during course of the whole research work. Her scientific cognition and experience proved me enormous helpful.

I also would like to thank Dr. R. Androsch, Dr. A. Wutzler and Dr. L. Fiedler, for their help and cooperation over the course of my work in their laboratories. I am grateful to all colleagues, H.-J. Wilke, A. Hähndel, D. Heidenreich, D. Mileva, Q. Zia, M. Hübner, C. Uhlemann, Y. Schwarz, C. Busch and J.-M. Grothe for their cooperation and nice company during my stay.

I would like to thank Prof. Dr. Thomas Thurn-Albrecht, Dr. K. Busse, Dr. E. Hempel, for valuable discussions and SAXS analysis. I am also thankful to Dr. S. Funke for surface tension analysis, Prof. Dr. Goerg H. Michler and Dipl.-Ing. Sylvia Goerlitz for TEM analysis.

I would like to acknowledge HEC Pakistan for financial support of this work.

Last but not least, I feel a deep sense of gratitude for my parents who formed part of my vision and taught me the good things that really matter in life. I wish to give a very special thank to my wife for moral support, and unlimited patience for her understanding and help during my stay in Germany. Finally I am grateful to my brother and sisters, for rendering me the sense and the value of brotherhood. I am glad to be one of them.

MSc Zulfiqar Ali

<b>1</b>	<b>Introduction</b>	<b>1</b>
<b>2</b>	<b>Nanoclay filled rubber and rubber blends</b>	<b>3</b>
2.1	Clay as filler for polymers	3
2.1.1	Clays	3
2.1.1.1	Smectite	4
2.1.1.2	Montmorillonite	5
2.1.2	Modification of clay with organic substances	6
2.1.3	Organoclay in polymer matrices	9
2.1.3.1	Generation of polymer nanocomposites	9
2.1.3.2	Clay dispersion in rubber	11
2.1.3.3	Thermodynamics of organoclay dispersion	12
2.1.3.4	Effect of technological parameters on the clay dispersion	13
2.1.3.5	Effect of material parameters on the clay dispersion	15
2.1.3.6	Correlation between clay dispersion and mechanical properties	17
2.2	Organoclay in blends	19
2.2.1	Immiscible polymer blends	19
2.2.1.1	Compatibilization efficiency of organoclay	20
2.2.1.2	Phase specific localization of organoclay in the blends	22
2.2.2	Methods for characterization of organoclay dispersion and distribution in rubber compounds and rubber blends	24
2.3	Monitoring of clay dispersion during mixing process	26
2.3.1	Electrical conductivity of polymer-clay nanocomposites	26
2.3.2	Correlation between the conductance and clay dispersion	27
2.3.3	Online measured electrical conductance method for carbon black and application of the method to clay dispersion	28
<b>3</b>	<b>Aim of work</b>	<b>31</b>
<b>4</b>	<b>Experimental</b>	<b>32</b>
4.1	Materials	32
4.2	Internal mixer	33
4.3	Sample preparation	34
4.4	Methods of morphology evaluation and property characterization	36
4.4.1	Morphological characterization	36



4.4.1.1	Optical microscopy	36
4.4.1.2	Atomic force microscopy	37
4.4.1.3	Transmission electron microscopy	38
4.4.1.4	Small angle X-ray scattering analysis	38
4.4.2	Surface investigation	39
4.4.2.1	Measurement of bounded rubber layer on the organoclay surface	39
4.4.2.2	Extraction experiment	39
4.4.2.3	Surface tension	39
4.4.3	Electrical conductance	40
4.4.3.1	Online conductance	40
4.4.3.2	Offline conductivity	40
4.4.4	Mechanical and thermal performance	41
4.4.4.1	Stress-strain relationship	41
4.4.4.2	Dynamic mechanical thermal analysis	41
4.4.4.3	Thermogravimetric analysis	41
<b>5</b>	<b>Results and Discussion</b>	<b>42</b>
5.1	Online conductance of rubber clay nanocomposites	42
5.2	Hydrogenated carboxylated acrylonitrile butadiene rubber XHNBR-clay nanocomposites	42
5.2.1	Online conductance of XHNBR-clay nanocomposites	42
5.2.2	Correlation between online conductance and structure of HNBR-clay nanocomposites	46
5.2.2.1	Rubber layer investigation	46
5.2.2.2	Macrodispersion	47
5.2.2.3	Microdispersion	49
5.2.2.3.1	Atomic force microscopy	49
5.2.2.3.2	Transmission electron microscopy	52
5.2.2.3.3	Small angle X-ray scattering analysis	53
5.2.3	Mechanical properties	55
5.3	Hydrogenated nitrile butadiene rubber (HNBR)-clay nanocomposites	57
5.3.1	Online conductance chart of HNBR-clay nanocomposites	57
5.3.2	Characterization of clay dispersion in HNBR	58

5.3.2.1	SAXS analysis	58
5.3.2.2	Atomic force microscopy	59
5.4	Natural rubber NR-clay nanocomposites	62
5.4.1	Conductance of NR-clay nanocomposites	62
5.4.2	Characterization of clay dispersion in NR	63
5.4.2.1	SAXS analysis	63
5.4.2.2	Atomic force microscopy	64
5.4.2.3	Transmission electron microscopy	65
5.5	Epoxidized natural rubber ENR-clay nanocomposites	67
5.5.1	Online conductance of ENR-clay nanocomposites	67
5.5.2	Characterization of clay dispersion in ENR	68
5.5.2.1	SAXS analysis	68
5.5.2.2	Transmission electron microscopy	70
5.5.3	Variation of clay types and concentrations of organoclay	72
5.6	Blends of HNBR and NR (polar/non-polar blend system)	74
5.6.1	Correlation of online conductance and development of the structure of the blend	74
5.6.1.1	Clay localization	75
5.6.1.2	Morphology development in organoclay filled HNBR/NR blend	78
5.6.2	Mechanical properties	83
5.6.2.1	Stress strain relationship	83
5.6.2.2	Dynamic mechanical thermal analysis	85
5.7	Blends of HNBR and ENR (polar/polar blend system)	87
5.7.1	Online conductance of unfilled and filled HNBR/ENR-clay blends	87
5.7.2	Relationship between online conductance and morphology of blends	88
5.7.2.1	Investigation of clay transfer and distribution	88
5.7.2.2	Morphology development in organoclay filled HNBR/ENR blends	92
5.7.3	Investigation of mechanical behavior of the blend nanocomposites	97
<b>6</b>	<b>Summary</b>	<b>99</b>
<b>7</b>	<b>Zusammenfassung</b>	<b>103</b>
<b>8</b>	<b>Literature</b>	<b>107</b>

## List of Abbreviations and Symbols

### Abbreviation

AFM	Atomic force microscopy
BIT	Black incorporation time
BR	Polybutadiene rubber
CB	Carbon black
CEC	Cation exchange capacity
CNT	Carbon nanotubes
CP	Characteristic point
DMTA	Dynamic mechanical thermal analysis
ENR	Epoxidized natural rubber
EPDM	Ethylene propylene ter polymer
FTIR	Fourier transformed infrared spectroscopy
HNBR	Hydrogenated acrylonitrile-butadiene rubber
IR	Infrared
MA	Maleic anhydride
MMT	Montmorillonite
NBR	Nitrile butadiene rubber
NIR	Near infrared
nm	Nanometer
NMR	Nuclear magnetic resonance
NR	Natural rubber
<i>o</i>	Octahedral
OMEC	Online measured electrical conductance
PE	Polyethylene
phr	Parts per hundred part of rubber
PP	Polypropylene
SAXS	Small angle X-ray scattering
SEM	Scanning electron microscopy
SMR	Standard Malaysian rubber

SBR	Styrene butadiene rubber
$T$	Tetrahedral
TEM	Transmission electron microscopy
TGA	Thermogravimetric analysis
TMTM	Tetramethylthiuram monosulfide
XHNBR	Carboxylated hydrogenated acrylonitrilebutadiene rubber
XRD	X-ray diffraction
ZDMDC	Zinc dimethyldithiocarbamate

## List of symbols

$\text{\AA}$	Angstrom
$A/A_0$	Area of the non-dispersed tactoids/total area of the micrographs
$c_R$	Mass concentration of organoclay in the mixture
$C_{\text{off}}$	Offline conductance
$\sigma_{\text{comp}}$	Conductance of the nanocomposites
$\sigma_{\text{rubber}}$	Conductance of the rubber
$\sigma_{\text{clay}}$	Conductance of the clay
C4	Butyl (hydrocarbon with four carbon atoms)
C8	Octyl (hydrocarbon with eight carbon atoms)
C18	Octadecyl (hydrocarbon with eighteen carbon atoms)
CH <sub>2</sub>	Methylene
°C	Degree centigrade
$d$	Interlayer spacing
$E_A$	Van der Waals interaction energy
$E$	Tensile modulus
Hz	Hertz
$h.\Delta s$	Entropy change per unit area
$h.\Delta g$	Enthalpy change per unit area
$L$	Rubber layer
$m_1$	Mass of the rubber compound

$m_2$	Mass of the rubber-filler gel
l	Litre
m	Meter
S	Siemens
Pa	Pascal
N	Newton
q	Scattering vector
rpm	Rotations per minute
s	Second
$\dot{\gamma}$	Shear rate
$t_{90}$	Time to vulcanizing 90 % of elastomer
$T_g$	Glass transition temperature
$\lambda$	Wavelength
$W_I$	Mass of inorganic part of the organoclay
$W_S$	Mass of surfactant in organoclay

# 1 Introduction

Rubber finds a large number of practical applications in automotives, mainly as tires and gaskets, in medicine, agriculture, building/construction, conveyer belts, sealing articles, water and fuel pipes, elastic binders/damping parts and many other fields. Market trends demand economic materials that cover a broad spectrum of applications with superior properties, ranging from those of unfilled vulcanizates up to highly filled vulcanizates. This can be achieved by appropriate selection of elastomer types, elastomer blends, vulcanization recipe and fillers. Thus, for the successful preparation and application of the rubber parts or products, a combined knowledge of chemistry, physics and engineering plays a key role. The selection of material or processing conditions is a great scientific challenge for tailoring the properties of the rubber.

During the last 10 years, nanoclay has gained a rising interest as filler for rubber, because of its specific properties. Rubber-clay nanocomposites offer a number of advantages over conventional composites at low filler loading. The effectivity of nanoclay for polymers strongly depends on its degree of intercalation and exfoliation. In the last decade most of research in conjunction with clay nanocomposites has been performed to improve the microstructure and the impact on the material properties. Different attempts, in terms of variation of polymer matrix or chemistry of clay, especially the creation of organophilic modified species, called organoclay, as well as processing conditions, have been made to exfoliate clay platelets in rubber compounds. Despite the current progress, in polymer nanocomposite technology there are fundamental unanswered questions related to the kinetics of intercalation and exfoliation processes. The intercalation/exfoliation of polymer clay nanocomposites is frequently characterized by microscopic techniques like transmission electron microscopy (TEM), atomic force microscopy (AFM) [1,2] and also by small angle X-rays scattering (SAXS) [3]. Some other techniques like nuclear magnetic resonance (NMR) [4], Fourier transformed infrared spectroscopy (FTIR) [5], neutron scattering [6], rheology [7] and dielectric spectroscopy [8] have also been used to investigate the nanocomposites structures. The post processing or offline experimental characterization techniques are not only time consuming, labor intensive, expensive, requiring a high expertise but also crucial in determining the influence of processing parameters on the resulting microstructure. Due to the increasing requirements with respect to productivity and quality, the field of real-time monitoring of polymer processing has been tremendously grown

within the last years. Since process control for complex systems, such as nanocomposites or blends will provide the highest benefit, therefore a fast and accurate determination of morphology is urgently needed. Replacing the offline measurements and minimizing them with in-process or online measurement methods, which would quite economic and easy to handle, is strongly desirable.

In the last decade some methods like dielectric relaxation spectroscopy [8], near infrared (NIR), Raman, ultrasonic, ultra-violet/visible light spectroscopies [9-11], have been used during the extrusion for *in situ* monitoring, either to analyze the degradation of polymers or morphology development in the composites or blend systems. In these investigations the sensor has been installed in the slit die, which lies behind the screw tip of the used extruder. These techniques provide information about the chemical structure or morphology of the system only at one point of complete spectrum of development. So it is highly required to have a technique that not only provides the online information but also delivers the complete chart of development of morphological and mechanical characteristics at different stages, also showing the advantages of being rapid, reliable and non-invasive analytical technique. In order to understand the processing of nanocomposites, it is essential to analyze the complete morphology development during melt mixing process.

Polymer clay nanocomposites show higher conductance, which is ionic in nature, than that of pristine polymer matrix [12,13]. Online measured electrical conductance (OMEC) is based on the electrical conductivity and has already been successfully used for the analysis of the dispersion and distribution of carbon black as well as carbon nanotubes in rubber compounds and rubber blends [14,15]. The received electrical signal in the nanocomposites may be used to analyze the clay dispersion in the host polymer during the mixing process.

This PhD work is conducted to apply the OMEC for the characterization of kinetics of intercalation/exfoliation of organoclay in the rubber matrix. Elastomer types of different polarity, viscosity and chemical structure (XHNBR, HNBR, ENR and NR) as well as different types of organoclays are used in order to investigate their effect on the intercalation/exfoliation behavior and its correlation to the OMEC chart. The morphology of the nanocomposites along the mixing time and the most important relevant properties were determined and correlated with the online conductance. Furthermore the method was also extended to binary rubber blends in order to find a correlation between the dispersion state, morphology development and the OMEC spectrum.

## 2 Nanoclay filled rubber and rubber blends

### 2.1 Clay as filler for polymers

#### 2.1.1 Clays

The clay minerals are substances, which consist of crystals formed by stacks of platelets with approximately 1 nm thickness, high aspect ratio and large specific surface area. Majority of clay minerals are phyllosilicates or layered silicates with Al, Mg, Fe and other elements. The principle building structure of clays consist of tetrahedral arrays of silicon-oxygen and octahedral of aluminum or magnesium-oxygen/hydroxyl, which are superimposed in different fashions. The clay minerals are classified by their arrangements of tetrahedral and octahedral sheets. The 1:1 clay minerals contain one tetrahedral and one octahedral sheet per clay layer (TO); 2:1 clay minerals contain two tetrahedral sheets with an octahedral sheet between them (TOT); and 2:1:1 (TOTO) clay minerals contain an octahedral sheet that is adjacent to a 2:1 layer. Clay is named on the basis of chemical composition. For example, three types of swelling clay minerals are the 2:1 ditetrahedral smectite termed as montmorillonite (MMT), hectorite and saponite as shown in the table 2.1.

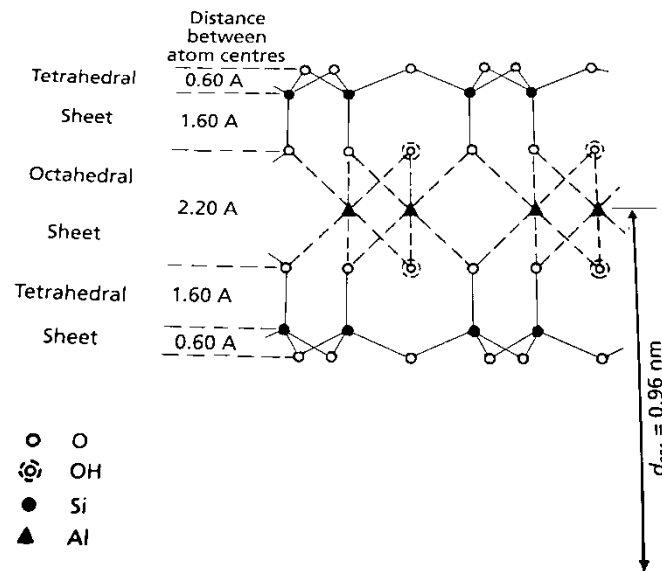
**Table 2.1:** Classification and example of clay minerals [16,17]

Structure		Mineral Example	
Type	Group		Ideal composition
2:1 (TOT)	Smectite	Montmorillonite	$[(Al_{3.5-2.8}Mg_{0.5-0.2})(Si_8)O_{20}(OH)_4] Ex_{0.5-1.2}$
		Hectorite	$[(Mg_{5.5-4.8}Li_{0.5-1.2})(Si_8)O_{20}(OH)_4] Ex_{0.5-1.2}$
		Saponite	$[(Mg_6)(Si_{7.5-6.8}Al_{0.5-1.2})O_{20}(OH)_4] Ex_{0.5-1.2}$
2:1 (TOT)	Illite (micas)	Illite	$[(Al_4)(Si_{7.5-6.5}Al_{0.5-1.5})O_{20}(OH)_4]K_{0.5-1.5}$
2:1 (TOT)	Vermiculite	Vermiculite	$[(Al_4)(Si_{6.8-6.2}Al_{1.2-1.8})O_{20}(OH)_4]Ex_{1.2-1.8}$
1:1 (TO)	Kaolin	Kaolinite	$Al_4Si_4O_{10}(OH)_8$
1:1 (TO)	Serpentine	Antigorite	$(Mg,Fe)_3Si_2O_5(OH)_4$
2:1:1 (TOTO)	Chlorite	Tricoctahedral chlorite	$Mg_6Si_4O_{10}(OH)_8$



### 2.1.1.1 Smectite

These 2:1 clays are most frequently used for a variety of non-ceramic applications. The structure of smectite consists of an octahedral sheet sandwiched by two tetrahedral sheets. The tetrahedral sheet is composed of corner lined tetrahedral, whose central ions are predominantly  $\text{Si}^{+4}$ . The basal oxygen of the tetrahedron is shared by the neighboring octahedral forming hexagonal patterns. Thus the crystal lattice of 2:1 phyllosilicate consists of about 1 nm thin layers with an octahedral alumina sheet sandwiched between two tetrahedral silica sheets. It is usually the variation of swellability, which arises from the isomorphous substitution in the tetrahedral and octahedral sheets, which give rise to the negative charge on 2:1 layers, e.g. in octahedral sheet  $\text{Al}^{+3}$  is replaced by  $\text{Mg}^{+2}$  or  $\text{Fe}^{+2}$  ions [17]. Owing to this, the charge deficit arose by this isomorphous substitution of charged ions is compensated by interlayer cations ( $\text{Na}^+$ ,  $\text{Ca}^+$ , and  $\text{Li}^+$ ). The triple sheet layers form stacks with the interlamellar gallery between them. The gallery height is determined by the type of cations positioned in the gallery and degree of hydration. The nominal value for interlayer spacing ( $d_{001}$ ) is taken as 0.96 nm due to the presence of counter balancing ions. The van der Waals interaction energy ( $E_A$ ) that holds the stacks together depends very much on the distance between the platelets of the interlamellar spacing.

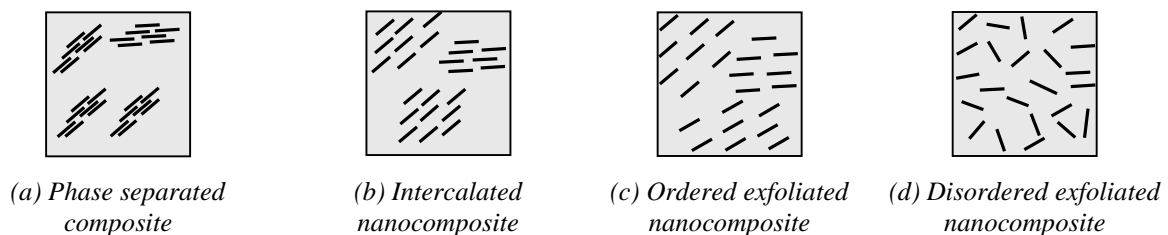


**Figure 2.1:** Unit cell structure of 2:1 phyllosilicate  $[\text{Al}_2(\text{OH})_2(\text{Si}_2\text{O}_5)_2]_2 + 5 \text{ wt } \% \text{ H}_2\text{O}$  [18]

### 2.1.1.2 Montmorillonite

Montmorillonite is the most common member of the smectite clay family. It is a phyllosilicate mineral and also the most common material used in production of nanocomposites. It was named after Montmorillon in France, where MMT was identified by Knight in 1896. The idealized structure of Na-MMT is shown in the figure 2.1. MMT has unique properties that enable it a preferred material for preparation of nanocomposites. An idealized MMT has 0.67 units of negative charge so it behaves like a weak acid. The cation exchange capacity (CEC) = 0.915 meq/g, in other words one ion per 1.36 nm<sup>2</sup>, i.e. anionic groups are spaced about 1.2 nm apart. The specific surface area of MMT is about 750-800 m<sup>2</sup>/g (theoretically value is 834 m<sup>2</sup>/g). MMT undergoes two types of processes before making the nanocomposites, acid treatment and preparation of organoclay. The aim of the former is purification, replacement of Ca<sup>2+</sup> for H<sup>+</sup> dissolution of some Fe, Al, and Mg ions from the octahedral layers. The latter process renders the hydrophilic clay as hydrophobic organoclay.

The properties of nanocomposites are greatly influenced by the dispersion degree of MMT. Depending on the nature of the used components and the method of preparation, significant differences in composites structure may be obtained [19]. Figure 2.2 shows four types of dispersion of clay layers in a polymer matrix. Phase separated composites are obtained, when the polymer is unable to intercalate between the silicate sheet (figure 2.2a), and the properties stay in the same range as that of traditional microcomposites.



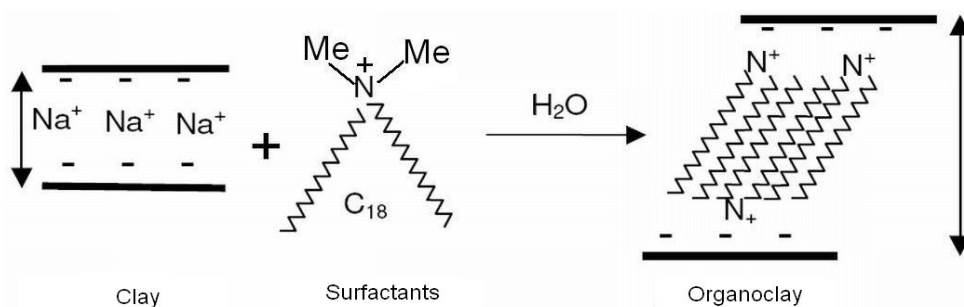
**Figure 2.2:** Schematic representation of clay dispersion in polymer matrix [1,20]

An intercalated structure is obtained, when a single extended polymer chain can penetrate between the clay layers (figure 2.2b), a well-ordered multilayer morphology results with alternating polymeric and inorganic layers. The exfoliated structures are obtained when  $d_{001} > 8.8$  nm with the individual platelets either ordered (because of stress field or concentration effects) or not, respectively (figure 2.2c and d). However, fully exfoliated structure is rarely seen

in practice. An exfoliated structure as shown in the figure 2.2d is an idealized reference morphology that arise from only looking at local scale. In reality, the morphology is a mixed intercalated/exfoliated structure.

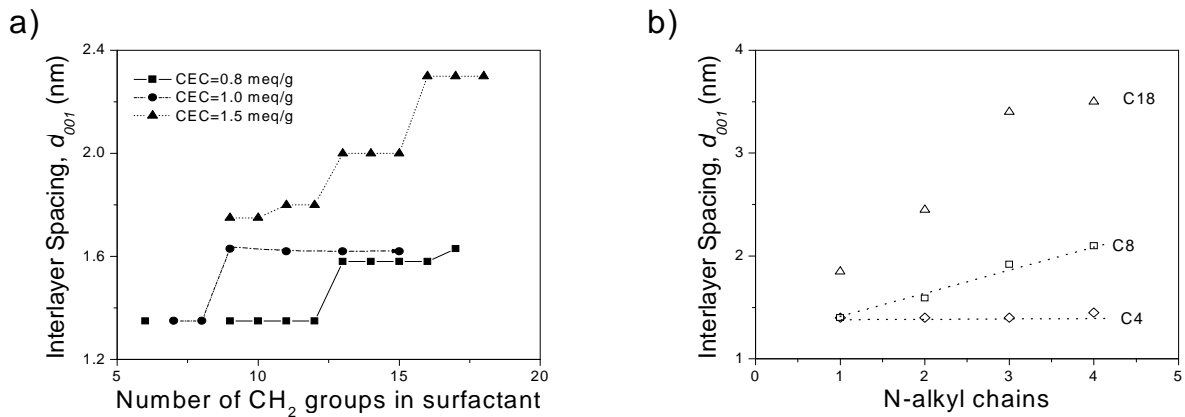
### 2.1.2 Modification of clay with organic substances

The clays are naturally polar and hydrophilic in nature. This makes them incompatible for mixing and interaction with mostly organic polymers. Moreover, the clay layers are held together by electrostatic forces, which hinder the dispersion of hydrophilic clay. In order to render the clay miscible with polymer matrices, it is required to convert the normally hydrophilic clay to an organophilic one. A popular and relatively easy way of modifying the clay surface, making it more compatible with an organic matrix, is ion exchanging. Generally, the ion exchange is carried out by mechanically mixing the aqueous slurry of sodium montmorillonite with organic cation either in the shear field or subjected to ultrasonic as reported by Pérez et al. [21]. A reaction scheme of ionic exchange in clay is shown in figure 2.3.



**Figure 2.3:** Schematic diagram of the ion exchange reaction in clay

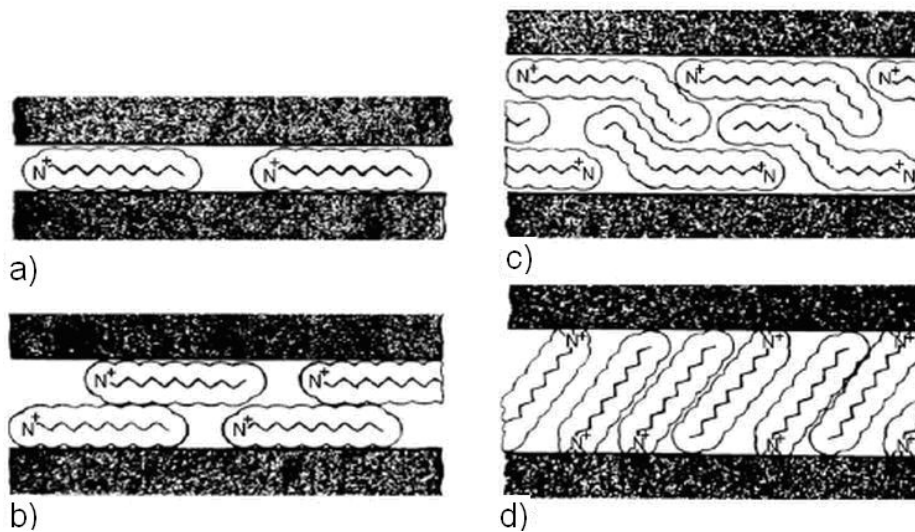
The  $\text{Na}^+$  ion in clay can be exchanged with alkyl ammonium ions including primary, secondary, tertiary and quaternary alkyl ammonium cations under proper conditions [22]. The conversion of hydrophilic inorganic clay to a hydrophobic organoclay also improves the interfacial adhesion properties between the organic and inorganic phases when a hydrophobic polymer matrix is involved. At the same time, this process helps to separate the clay platelets so that they can be more easily intercalated and exfoliated. The  $d_{001}$  spacing between the clay layers of the organoclay depends on length of alkyl chain, number of alkyl chains, the ratio of cross-sectional area to available area per cations and cation exchange capacity of the clays [22-24] as shown in figure 2.4.



**Figure 2.4:** (a) Interlayer spacing of clay as a function of alkyl chain length and CEC [24] and (b) dependence of the basal-plane spacing on the number of alkyl chains of different length in the organic cation at room temperature [22]

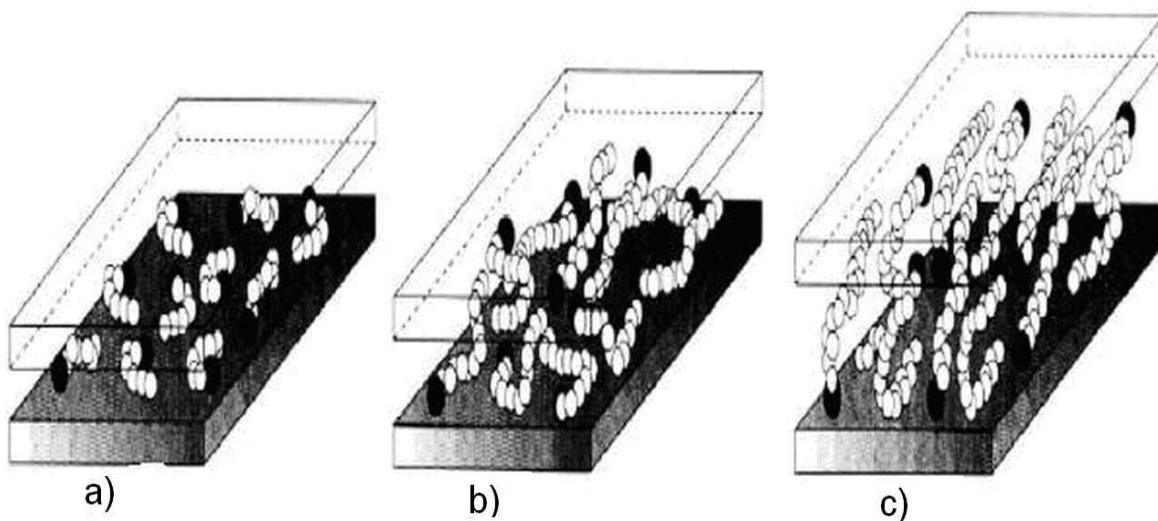
### Structural models of surfactants

The structure and interaction of surfactant-clay is of crucial importance to design, fabrication and characterization of exfoliated nanocomposites. Lagaly [25] has proposed a simple and idealistic model for surfactants in the 2:1 clay minerals. According to his model the surfactants lay either parallel to the clay surface, forming mono- and bilayers or radiating away from the surface, forming paraffin-type arrangement (figure 2.5).



**Figure 2.5:** Alkyl chain aggregations in 2:1 phyllosilicates: (a) monolayer, (b) bilayers and (c) pseudotrimolecular layers of chains lying flat on the surface, and (d) paraffin-type monolayer [25]

In the pseudo tri molecular arrangement, some chain ends are shifted above one another, so the spacing is determined by the thickness of three alkyl chains [25]. Vaia et al. [26] have employed Fourier transformed infrared spectroscopy to determine the conformation of surfactants by monitoring frequency shifts of CH<sub>2</sub> (methylene) stretching and scissoring vibrations as a function of interlayer packing density, chain length and temperature. They have proposed a wide range of molecular arrangements, varying from solid like to liquid like or even to intermediate liquid crystalline case, depending on the packing density and chain length. Increasing the packing density or chain length, improves the ordering of the chains. However, high temperature favors the disordered, liquid like conformation. When the available surface area per molecule is within a certain range, the chains are not completely disordered but retain some orientational order similar to that in the liquid crystalline state depending on the packing density and chain length (figure 2.6).



**Figure 2.6:** Alkyl chain aggregations in 2:1 phyllosilicates: (a) the molecules are effectively isolated from each other at the shortest lengths, (b) quasi-discrete layers form with various degree of in plane disorder and interdigitation between the layers at medium lengths, and (c) interlayer order increases leading to a liquid crystalline polymer environment at long lengths. Open circles represent CH<sub>2</sub> segments while cationic head groups are represented by filled circles [26]

Nuclear magnetic resonance spectroscopy has been used by Wang et al. [27] to investigate the conformation of surfactant in MMT. They have demonstrated a co-existence of ordered (all trans) and disordered conformations (mixture of trans and gauche). Different experimental techniques like IR, NMR, XRD and DSC have been used by Osman et al. [22] to study the

structure and chain dynamics of self-assembled monolayers of mono, di, tri and tetra alkyl ammonium cations of varying length (C<sub>4</sub>, C<sub>8</sub>, C<sub>18</sub>) on MMT platelets. At ambient temperature the surfactant monolayer assembled on the MMT adopt a two dimensional ordered or disordered state depending on the cross sectional area of the molecules, cations available on the substrate and the alkyl chain length. At low temperatures, the alkyl chains preferentially assume an all trans conformation. Conformation transformation of the chain takes place with increasing temperature leading to a disordered phase (liquid like) in which the chains assume a random conformation.

### **2.1.3 Organoclay in polymer matrices**

#### **2.1.3.1 Generation of polymer nanocomposites**

Although nanocomposites can be prepared by a number of methods, much of the research and development activity leading to commercial interest is based on melt compounding, for both manufacturing flexibility and economic considerations. Vaia et al. [28] were among the pioneers who observed the direct intercalation behavior of a molten polymer into an organically modified clay by employing polystyrene and an alkylammonium modified montmorillonite. The processing parameters are of critical importance while dispersing of nanofillers in the polymer matrix. The degree of intercalation/exfoliation of organoclay in polymer matrix is generally governed by compatibility, polymer diffusivity and processing conditions. Under these circumstances rubber as polymer matrix could find a preferred place, due to its viscosity, and the swelling ability of the pristine or organoclay in solutions, for production of rubber clay nanocomposites by solution, latex or melt mixing route. Despite such advantages overwhelming research has been devoted to thermoplastics and thermosetting resin, but less attention has been paid to rubber. In general, the preparation methods for the rubber clay nanocomposites can be divided into four major categories depending on the processing techniques [29,30].

#### *In situ polymerization*

In this method organoclay is swollen within monomer solution or liquid monomers so that the polymer formation can occur in between the intercalated sheets. Polymerization can be initiated either by heat or radiation, by the diffusion of a suitable initiator, or by an organic initiator or

catalyst fixed through cation exchange inside the interlayer before the swelling step by the monomer or by increasing the temperature if it is sufficiently active [29,30].

#### *Latex compounding*

Latex compounding is a promising route in preparing rubber-clay nanocomposites. Rubber is usually available in the form of latex, which is an aqueous dispersion of rubber particles in the submicron to micron range. In this technique, the clay is dispersed in water which acts as swelling agent due to hydration of inter-gallery cations. The water swelling capability of the natural clays are not the same but depend upon the type of clay, its cation exchange capacity and hence the mixing of the latex with the layered clays (having high cation exchange capacity) followed by co-precipitation (coagulation) [29]. Several options are available to add and disperse the clay in the latex like dispersing the clay directly in the latex, by using a silicate slurry, restabilization of the clays containing latex prior to appropriate comminuting operations like ball milling, etc. [30-32].

#### *Solution blending*

In this method organoclay is first swollen in the solvent, which is capable of dissolving both of organoclay and rubber matrix. Rubber is then dissolved in the solvent and added to the solution. The curatives may be added before solvent removal, but they are usually compounded with the intercalated material after partial or complete solvent removal, the clay re-assemble around the polymer, resulting in rubber-clay nanocomposites and then vulcanized at a specific temperature [30,33,34].

#### *Direct melt mixing*

This is the most promising method with great advantages over the previously mentioned methods, being industrially viable process and environmentally benign, due to absence of solvents. Direct melt intercalation of polymers in organoclay is primarily driven by enthalpic polymer-host interactions whereas the driving force for polymer intercalation from solution is the entropy gained by desorption of small molecules from the host galleries [28]. In this method both organoclay and rubber mixture are blended in the molten state under shear. The rubber chains diffuse from the molten mass into the clay galleries to yield intercalated or exfoliated nanocomposites [29,30].

### 2.1.3.2 Clay dispersion in rubber

Since the pioneer work in early 90s by researchers in Toyota Central Research Laboratories (Japan) on nylon 6-clay nanocomposites [76], there has been a variety of publications on polymer-clay nanocomposites particularly for thermoplastics and epoxy thermosets. Less attention was paid to elastomers during this era of polymer-clay nanocomposites research, only some sporadic works appeared in the field of rubber-clay nanocomposites [35,36]. In recent years rubber-clay nanocomposites have attracted the attention of both industrial and academic researchers as they often exhibit outstanding properties at low loading of clay. For either of the processing methods, several rubbers served as matrices in organoclay filled systems, e.g. nitrile butadiene rubber (NBR) [2,37-46 ], natural rubber (NR) [47-50], epoxidized natural rubber (ENR) [51-53], ethylene propylene ter monomer (EPDM) [54-57] and styrene butadiene rubber (SBR) [34,58-60 ]. From practice point of view manufacturing of rubber-clay nanocomposites by melt mixing and latex blending have got the interest of industry. In rubber, similar to the thermoplastics, high molecular weight [61], polarity of the macromolecules [76], modification of the polymer matrix by introduction of compatibilizer [62] and proper processing conditions [63] favor the preparation of nanocomposites [34,42,54,55 ].

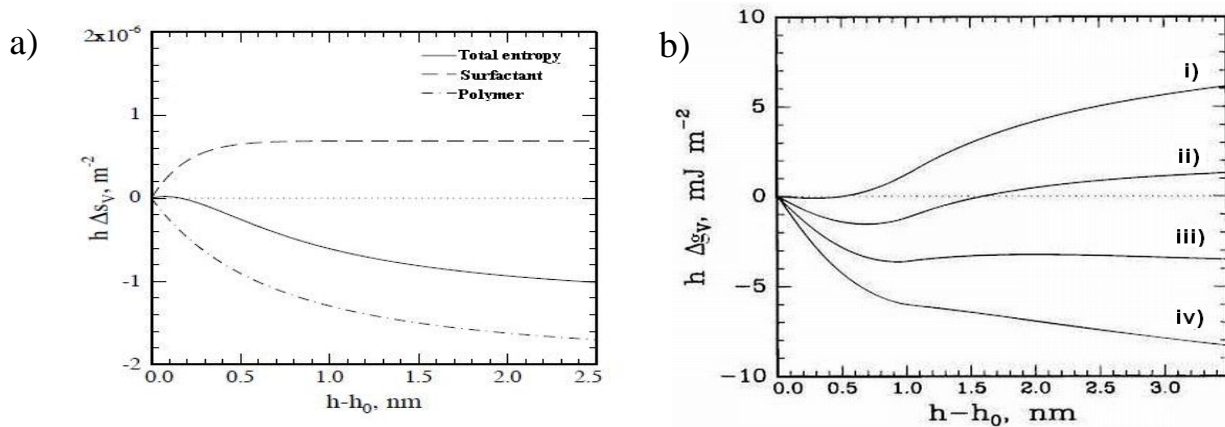
Most of the rubber-clay nanocomposites research in last decade has been focused on the mechanism and parameters affecting the nanocomposites formation [38-43,48,49,51]. The knowledge obtained in the last two decades on the mechanisms affecting thermoplastics and thermosets-clay nanocomposites has been utilized for the manufacturing the rubber-clay nanocomposites. Vulcanization process itself may be a suitable tool to control the morphology of the rubber-clay nanocomposites [57,58]. Jacob [49] prepared natural rubber (NR)-clay nanocomposites using different concentrations of clay and showed the formation of an intercalated structure. Wu et al. [32] reported that carboxylated acrylonitrile-butadiene rubber (XNBR)-clay nanocomposites prepared by emulsion process exhibit a total exfoliated state. However, Sahdu et al. [2] used TEM and AFM technique to show that hydrogenated acrylonitrile-butadiene rubber (HNBR)-clay nanocomposites form intercalated and exfoliated structures both with the unmodified and the modified clay. Kim [38] investigated the effect of the chain length (number of carbon atoms) of the surfactant on the clay dispersion in NBR and found that clay modified with shorter chains of surfactants yield intercalated structure, whereas surfactants with longer chains produce exfoliated nanocomposites. Recent studies have demonstrated that besides a proper choice of materials the conditions of processing play a key



role in achieving exfoliation [37,64,65 ]. Despite the current progress in polymer nanocomposite technology, there are many fundamental unanswered questions related to the kinetics of intercalation and exfoliation processes. Only few researchers describe the effect of pristine clay and organoclay on the vulcanization kinetics of rubber nanocomposites [48]. Similarly, also much of rubber-clay nanocomposites research was focused on the structure development and property correlation, but less attention has been paid to online characterization of the nanocomposites. In order to fully explore the potential, scientific and industrial applications of the nanocomposites, the kinetics of clay dispersion and thermodynamics of the process must be realized. Thus, there is a need for fundamental understanding, capable of describing and predicting the properties of nanoscale structures.

### 2.1.3.3 Thermodynamics of organoclay dispersion

Vaia et al. [66] used the lattice based thermodynamic model, which provides some basic predictions regarding the equilibrium states (i.e. phase separated, intercalated, or exfoliated) in relation to the enthalpic and entropic factors of the interaction constituents, namely surfactant, polymer and clay platelets.



**Figure 2.7:** (a) Entropy change per unit area as a function of the change in the gallery height, (b) Change of free energy per area versus the change in gallery height based on the thermodynamic model presented in [66], for various surface-polymer affinities.

According to this model, polymer confinement in clay galleries results in entropy loss but the latter may be compensated in part by the entropy gain induced through the increase in conformational freedom of the tethered surfactant chains upon layer separation (figure 2.7a).

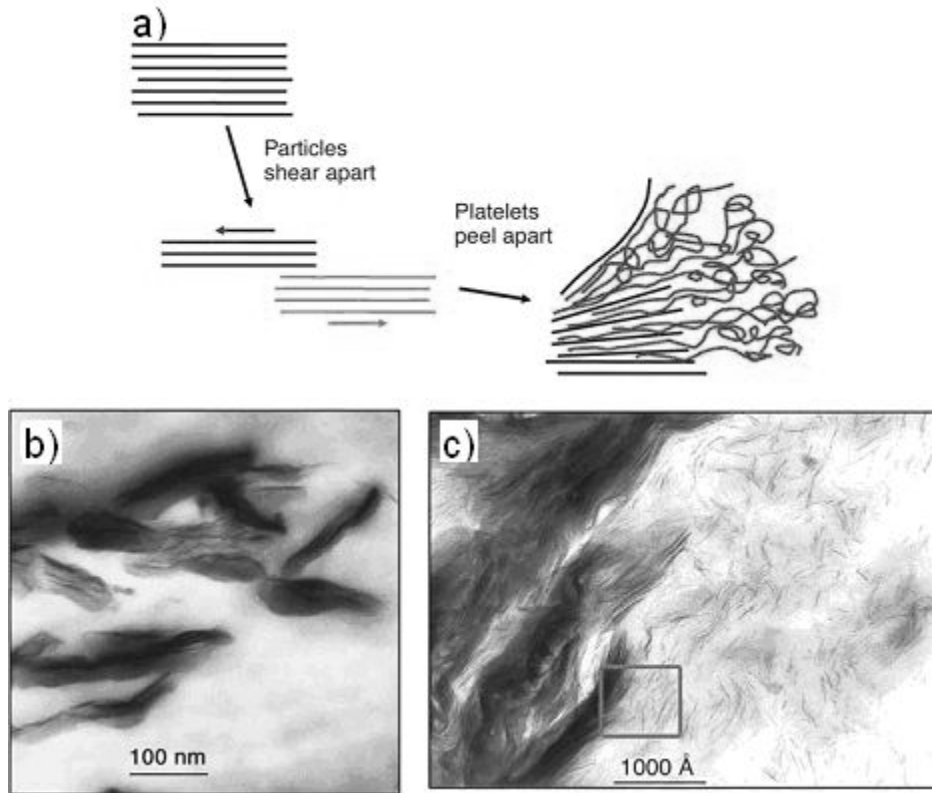
As a consequence, melt intercalation is predicted to depend primarily on energetic (enthalpic) factors [66]. Complete layer separation depends on the establishment of very favorable polymer-surface interactions to overcome the penalty of polymer confinement (figure 2.7b). The free energy curve (i) in figure 2.7b is always positive at all gallery heights, indicating that polymer intercalation is unfavorable because the polymer and organoclay is immiscible. Type (ii) curve displays only one minimum and polymer intercalation is favorable up to a finite layer separation. Type (iii) curve displays more than one free energy minimum. Thus type (iii) system exhibits ill-defined intercalated structures for intermediate intercalated structures before complete layered exfoliation. Type (iv) curve shows a continuous decrease in the free energy as the gallery height increases. This type corresponds to complete polymer-clay miscibility, leading to the formation of exfoliated structure. Vaia et al. [66] developed an expression, for the enthalpy that contains the contributions from both van der Waals interaction and polar (Lewis acid/base) interactions. The later could lead to a favorable enthalpy of mixing, which is rendered by maximizing the magnitude and number of favorable polymer-surface interactions while minimizing the magnitude and number of unfavorable, i.e. apolar, interactions between the polymer and the surfactants.

The lattice based model has ability to determine analytically the effect of various aspects of polymer and organoclay on the nanocomposites formation. This also provides a first understanding of the complex role of the thermodynamics in determining the dispersion of nanoparticles in polymers. A recent model by Mackay et al. [67] has suggested that the dispersion of nanoparticles in a polymer results in increased molecular contacts between polymer and the nanoparticles. This increased accessible area of contact due to dispersion of nanoparticles results of favorable enthalpy of mixing. Their results indicate that nanoparticles are capable of dispersing in polymers if the size of the nanoparticle is smaller than the radius of gyration of the polymer molecules.

#### **2.1.3.4 Effect of technological parameters on the clay dispersion**

A proper selection of technological parameters, like shear intensity, rotor/screw speed, residence time/mixing time, temperature, pressure and mixer or extruder types is essential to control the degree of intercalation/exfoliation of organoclay and thus enhancement in properties and performance of the nanocomposites [63-65,68,69 ]. The results of these investigations indicate

that the dispersion and distribution of organoclay is facilitated by optimum balance between shear intensity and mixing time as well as proper selection of temperature.



**Figure 2.8:** (a) Shearing-peeling mechanism for exfoliation of clay platelets in a polymer, (b) transmission electron micrographs showing evidence for the combination of shearing tactoids to consistent thickness and (c) peeling platelets off a tactoid [65]

Dennis et al. [65] have studied extensively the effect of extruder types, screw design and residence time on the degree of dispersion of clay in polyamide. They demonstrated that the morphology of nanocomposites is drastically influenced by processing conditions. The dispersion of organoclay agglomerates can be achieved, when the cohesive force of agglomerates is exceeded by the hydrodynamic separating force or shear stress applied by the matrix polymer during melts processing. Kim et al. [68] have demonstrated that the applied shear seems to contribute to breaking up of clay tactoids and improve the sample uniformity. The breaking up of the organoclay agglomerates into primary particles facilitates the polymer chains to diffuse easily into the gallery of layered clay and enhance the degree of exfoliation under suitable mixing conditions. The shear stress applied during mixing seems to play a secondary role [68]. This is

similar to the shearing process exfoliation mechanism proposed by Dennis et al. [65], whereby a combination of mechanical and chemical forces reduces hundreds or thousands of tactoids composing the 8-10  $\mu\text{m}$  particles to smaller ribbon like structures. The peeling of individual platelets from the ribbons accomplishes the exfoliation process. Figure 2.8a schematically illustrates this process, and figures 2.8b and c show evidence for this mechanism from transmission electron microscopy (TEM) images taken in the early stages of exfoliation of the organoclay in a nylon 6 matrix. Park et al. [70] have also proposed a similar mechanism for exfoliation of clay platelets in epoxy nanocomposites.

Mixing time is another technological parameter which also affects the dispersion of organoclay in the polymer matrix. Generally, increasing the mixing time in internal mixer or residence time in the extruder improves the delamination and dispersion of clay. It is connected with rotor/screw speed. For higher rotor/screw speed less residence time is needed, whereas for low speed more residence time is required for exfoliation of organoclay in the polymer matrix [65,71].

Temperature is also an essential parameter that affects the exfoliation of organoclay in the polymer matrix. Kim et al. [68] investigated the exfoliation of clay in nylon 6 matrix even at lower shear rate, when the processing temperature is high, due to the fact that the diffusion of polymer into the interlayer is enhanced. This also indicates that the exfoliation of clay layers is also closely related to diffusion of polymer matrix into the gallery of clay layers, which is closely connected with the interaction of the filler with the material parameters.

#### **2.1.3.5 Effect of material parameters on the clay dispersion**

The intercalation/exfoliation is greatly enhanced by maximizing the number of clay-polymer host interactions through appropriate selection of various material parameters [28]. Despite this, optimum processing conditions play a crucial role for the dispersion of organoclay [64,65]. In addition to this, the proper choice of the material parameters, e.g. molecular weight, polarity, chemistry of the main chain and branches, viscosity of the polymer matrix as well as addition of compatibilizer and last but not least chemistry of the organoclay and its concentration play an important role and determine the exfoliation of the clay platelets. The interaction mechanism between polymer matrix and organoclay primarily controls the exfoliation of clay layers [68]. This depends on the polarity, molecular weight, hydrophobicity, reactive groups of the polymer, clay types and modification of clay [72]. Jiankun et al. [73] have found that catalytic effect

during cross linking, penetrating ability of curing agents to clay and long chains of the surfactants promote the exfoliation of clay platelets in the polymer matrix.

Fornes et al. [61] investigated the effects of the viscosity, which is determined by the molecular weight of the polymer matrix, on the exfoliation of clay platelets by preparing the nanocomposites with three different molecular weight grades of nylon 6 (low, medium, and high). The morphological investigation based on TEM and SAXS revealed that for the low molecular weight nylon 6-clay nanocomposites, a mixed structure, having regions of intercalated and exfoliated structures, was obtained. For medium and high molecular weight nylon 6 well exfoliated structures were obtained. The number of clay platelets per unit increases with increasing molecular weight, thereby revealing the dependence of exfoliation of clay on the molecular weight of the matrix in order higher > medium > lower [61]. In contrast, Strobl [74] found that an increase in the molecular weight decreases the diffusibility of polymer chains. Ishida et al. [75] have observed a decrease in degree of intercalation-/exfoliation with increase of molecular weight. The intercalation/exfoliation of organoclay in nanocomposites depends on different mechanisms, either shear, diffusion or combination of both.

It is imperative that the surface polarity of polymer is high in order to fully wet and intercalate clay tactoids. Highly polar polymers, such as nylon [76] and polyimide [77] systems have achieved exfoliated state and yielded nanocomposites with remarkable properties. If the matrix is non-polar or moderately polar, an intercalated structure, or a combined intercalated and exfoliated morphology is obtained. Examples of such behavior have been observed for various polymer matrixes [2,34,47,57]. Young et al. [57] reported an intercalated structures for non-polar EPDM-organoclay nanocomposites and low molecular weight EPDM (liquid EPDM), in which the presence of large stacks of clay layers indicate poor dispersion. Non-polar polymers are very difficult to intercalate into clays, because of the lack of thermodynamic driving forces for intercalation/exfoliation and higher polarity of clays.

This challenge, for the moderate or non-polar polymers, has been met by premixing an oligomer (having both of polar and non-polar end) having compatibility with both of the clay and polymer matrix [62,78-81]. Melt-mixing the organoclays with maleic anhydride-grafted polypropylene (MA-PP) oligomers results in MA-PP intercalation. This premixed MA-PP and organoclay is then melt-mixed with polypropylene matrix. There should be an optimum quantity of maleic anhydride that creates enough polarity to intercalate well, but also non-polar enough to mix with PP. Unfortunately, the oligomer limits the extent of properties. Similarly, maleic anhydride

grafted PE (MA-PE) also interacts with organoclay during melt-compounding to form exfoliated PE nanocomposites. The use of MA-PP or MA-PE results in a two-step (masterbatch) process, where care should be taken on the extent of maleic anhydride (MA) functionalization of PE or PP. As pointed out by Manias et al. [82] a too low MA content does not promote nanocomposite formation, while too high MA content leads to immiscibility between the neat (unfunctionalized) polymer and the masterbatch. Coupling agents like silane enhances the dispersion of the organoclay in NBR and NR matrix [78,79].

The interlayer spacing between the clay platelets as well as interaction of the filler and polymer can be increased by tailoring of the chemistry of surfactants, length of the alkyl chains, number of alky chains and concentration [21-24].

#### **2.1.3.6 Correlation between clay dispersion and mechanical properties**

The performance of polymer–clay nanocomposites is highly dependent on their microstructure, which in turn depends directly on the degree of intercalation/exfoliation of clay platelets in the polymer matrix and clay contents. Good dispersion of the clay platelets in the polymer matrix generally yields enhanced Young's modulus, storage modulus and tensile strength.

It has been found that the tensile modulus of polyamide 6 increases by 37 % for poorly dispersed clay and about by 66 % for exfoliated and well dispersed organoclay with only 5 % loading [65]. For exfoliated morphology of nanocomposites the increase in the tensile strength is higher even at low clay contents. The reinforcing effect is lower for nanocomposites, with clay platelets being partially exfoliated and stacked. With increasing exfoliation degree, a monotonous increase in the yield stress and decrease in the yield strain are observed [81].

Sadhu et al. [34] have studied the influence of the structural and processing parameters on nanocomposites prepared with organoclay and SBR with different styrene contents (15, 23, and 40 %). They have noted that even with a very low organoclay loading, the SBR-organoclay nanocomposites displayed improved mechanical properties. Upon the incorporation of unmodified clay and organoclay, the degree of property improvement was much higher for the rubber having higher styrene content and reinforced with organoclay. The authors explained the above results by assuming decoiling of the SBR chains in toluene as a result of similar polarity and solubility parameter values leading to complete exfoliation of the organoclay.

In another study, Sadhu and Bhowmick [42] have prepared a series of nanocomposites by mixing NBR, SBR and polybutadiene rubber (BR) with organoclay. The mechanical properties of the

rubber/clay nanocomposites were correlated with TEM and XRD results. In all cases, the nanocomposites showed improved mechanical properties and the extent of the increase in strength varied from 38 to 166 % depending on the nature of the base rubber and its polarity. A comparison of the mechanical properties of SBR, BR, and NBR (with 34 % acrylonitrile content) showed that the extent of the improvement in the mechanical properties was different and these were explained with the help of XRD and TEM. Among the NBRs, the improvement in the strength was found to be higher for NBR with higher acrylonitrile content due to better exfoliation of clay platelets. This was explained by the authors due to some hydrogen bonding phenomena involved by the hydroxyl groups on the clay surface and nitrile groups of NBR.

Usuki et al. [56] have prepared EPDM-clay nanocomposites by mixing at 200 °C and using different accelerators during vulcanization process. The EPDM-clay exfoliated nanocomposites were prepared successfully only when tetramethylthiuram monosulfide (TMTM) or zinc dimethyldithiocarbamate (ZDMDC) were used as the vulcanization accelerators. The tensile strength of the EPDM-clay nanocomposites using TMTM and ZDMDC as the vulcanization accelerator was two times higher than that of neat EPDM. The tensile stress at 100 % of the EPDM-clay nanocomposites also increased by 40 % compared with that of virgin EPDM. The elongation of the EPDM-clay nanocomposite using ZDMDC was highest among all the samples and was 85 % higher than that of neat EPDM. The storage moduli of the EPDM-clay nanocomposites were higher than that of neat EPDM. The authors have proposed that the vulcanization accelerators dissociate into radicals and combine with EPDM chain to polarize the EPDM molecules. These EPDM molecules intercalate into the clay galleries and finally exfoliate the clay platelets through H-bonding between clay surface and polar EPDM.

The stiffness of polymer-clay nanocomposites increase with increasing molecular weight of polymer matrix, which facilitate better dispersion of clay platelets in the polymer [61]. Similarly, the difference of organoclay treatments, which affects the clay dispersion in the polymer matrix, also influences the mechanical performance of the nanocomposites [65]. The impact strength and elongation at break values remain at the levels of neat nylon 6 up to about 5 wt % of the organoclay and then decrease, as the clay cannot be exfoliated for the higher contents but remains as tactoids. Mixtures containing 20 wt % organoclay are very brittle [64,83] due to agglomeration the clay tactoids. The beneficial effects of clay additions on the tensile strength accompanied by an increase in elongation at break could be attributed to the synergistic action of platelets orientation and chain slippage [58].

## **2.2 Organoclay in blends**

### **2.2.1 Immiscible polymer blends**

Polymer blends have emerged as an attractive field not only for scientists but also for researchers in industry to commercialize the polymers. Blending of elastomer phases has been recognized as the most versatile, economic method to produce materials able to satisfy complex demands for performance, as it allow the users to access properties of the final blended and vulcanized elastomer that are not accessible from a single, commercially available elastomer alone. The properties of blends depend on phase morphology, polymer component ratio, interfacial adhesion, cross-linking, distribution of filler between the phases, distribution of plasticizer between the polymer phases, distribution of cross-links of elastomers. Tokita et al. [84] have studied the mixing of EPDM with the diene rubbers as a function of relative viscosity. The detailed morphology of elastomer blends depends on the mixing procedure, the rheology of the blend components, and the interfacial energy. If the volume ratio of both of the phases is equal , the elastomer of lower viscosity tends to be the continuous phase.

Most of the polymer phases are immiscible. The application of any processes or technique, which are used to tailor the phase morphology and interfaces of blend interphase, is called compatibilization. The basic strategies for compatibilization of two phase polymer blends can be divided into at least three major categories: co-crystallization of two phases, dynamic vulcanization, and addition of third material as compatibilizing agent [85]. Generally, the compatibilization of polymer phases is carried out by addition of copolymers, miscible with both of phases, reactive blending or mechano-chemical blending. Compatibility is a relative term, so often domain size is used to describe extent of mixing, smaller the domain sizes, more compatibility and vice versa [86].

Recently, organoclays have shown quite interesting effect on the compatibilizing behavior of the immiscible polymer blends [87-89]. The use of copolymer and grafted copolymer as compatibilizer could adversely affect the mechanical properties of the blend, or the compatibilization is brought about at the cost of some properties. The use of organoclay not only compatibilizes the immiscible blend, but could also improve the various properties.



### 2.2.1.1 Compatibilization efficiency of organoclay

Compatibilization of highly incompatible elastomers has only been used to a limited extent [90,91]. For binary blends of elastomers with large differences in solubility parameters, as in diene elastomers with polar elastomers, the properties depend on the morphology, which is dominated by the large domain size and the lack of interfacial adhesion. Therefore, controlling the phase behaviour and morphology becomes a key factor in determining the performance of polymer blends, which mainly rely on the interface, and polarity of the polymer components. Since most of polymer pairs are immiscible they are usually compatibilized to get the blend with desired morphology and properties.

Traditionally, block and graft copolymers are used to strengthen the interface and stabilize the morphology. However, they are system specific, relatively expensive to engineer, and very difficult to produce for systems with more than two components.

Organoclays have emerged as an attractive alternative to traditional compatibilizers because of their low cost and ease in processing with polymers. They have potential to improve the compatibilization efficiency of many different polymer blends. Organoclays frequently exhibit synergistic effects in a blend, i.e. improve the compatibility between the phases and enhances the properties of the blends [83,92,93]. In the last decade, elastomer blend-clay nanocomposites have received significant attention for both the fundamental as well as the applied research as they often exhibit remarkable improvements of the mechanical and thermo-mechanical properties, enhanced barrier properties or reduced flammability, either due intrinsic differences in the constituents or differences in the reinforcement and vulcanization of the elastomer phases [90]. However, the efficiency of organoclay with regard to improving the solid-state properties of rubber blends is extremely dependent on the degree of clay dispersion (intercalation/exfoliation), clay contents as well as the blend morphology. Moreover, the kinetics and morphological development of phase separation of the blends are significantly influenced by the addition of organoclay.

Several studies of polymer blend-clay systems [94-98] have usually indicated the compatibilizing effect of clay in immiscible blends. The domain size of dispersed phase in NBR/SBR [97], HDPE/PA6 [94,95] PS/poly (vinyl-methyl-ether) (PVME) [99], PA6/EPR [98], PA6/PPO [100] and PBT/PE blend [101] reduces drastically by addition of clay due to its efficiency to improve the compatibilization of the immiscible polymer blends. Fisher et al. [102] have proposed another mechanism by which clay can form *in-situ* grafts by adsorbing large amounts of polymer,

which in turn are very effective at reducing the interfacial tension and inducing compatibilization in highly immiscible blends. In relation to this, Wang et al. [103] tried to determine how organoclay compatibilizes the PS/PP system. They attributed this phenomenon to the fact that the two immiscible polymer chains can co-exist between the intercalated clay platelets. These two chains play the role of a block copolymer, which acts as a compatibilizer for the PS/PP system. The clay platelets located at the interface are stiffer than the polymers, resulting in a high bending energy of the interfaces. This favors the formation of small domains and further promotes the compatibilization process. Gelfer et al. [94] have concluded that the reduction of domain size of the dispersed phase in the polymer blend is due to the excessive amount of surfactant in the organoclay and the clay could act as compatibilizer. They have suggested that clay alone is not responsible for the improved miscibility between PS and PMMA, but it may be due to a combined effect of clay and the surfactants which could play the role of compatibilizer. None of surfactant or clay alone could improve the compatibilization efficiency and modify the blend to such extent as reported [94].

The average diameter size of the dispersed EPR domains in 80/20 (wt %) nylon 6/EPR blends decreases significantly even when a small amount (0.5 phr) of the clay is added [98]. Based on SEM investigations it has reported that the curve, obtained plotting average diameter size of dispersed phase and clay concentration (phr), is similar to the emulsification curve, which has been reported for an immiscible blend with a block (or graft) copolymer as compatibilizer. Based on the TEM and SEM analysis Sharif et al. [104] have also shown that morphology of the dispersed phase is fine and distributed homogeneously in the matrix. He concluded that it is a compatibility phenomenon of the organoclay which results in the formation of nanocomposites. Ray et al. [105,106] have investigated that organoclay reduces the interfacial tension gap of the phases in immiscible blends, which also clearly indicates the compatibilization of the blend. It has been shown, while utilizing different organoclays with different surfactants and interlayer spacing, that the key factor for improving the compatibilization efficiency of organoclay is the initial interlayer spacing. The increase in the order of interlayer spacing correlated with the order of domain size reduction of the dispersed phase [105]. Vo et al. [107] have observed, while varying the material and technological parameters, that clay act as compatibilizer and improve various thermo-mechanical properties. In short, organoclay improves the compatibility by altering the interfacial tension of the phases, that ultimately leads to refined morphology and improved mechanical performance.

### **2.2.1.2 Phase specific localization of organoclay in the blends**

Elastomers are viscoelastic fluids at processing temperatures, with persistent transport phenomenon. In immiscible blends, this leads to change in the size and shape of the elastomer phases and migration of the fillers and plasticizers from one phase to another. Interphase transfer of fillers (silica, carbon black) in elastomer blends has been observed [108]. Changing the properties of elastomers by uneven distribution of fillers and vulcanization is, however, the more common case of blends of immiscible elastomers [109]. This migration of filler in a specific phase is due to greater solvation between filler and one of the polymer phases in the melt mixed blends. The engineering properties of cross-linked elastomer blends depend not only on the elastomer phase itself, but also on the amount and localization of the fillers and plasticizers as well as on the extent of the cure. The localization of the fillers is sensitive to polarity of the polymer phase [94], chemical nature of filler [107], processing conditions [87], amount of the filler [101] and viscosity.

If the organoclay has a different chemical affinity to the components of binary immiscible blends, it selectively localizes in a specific phase and results in a significant change in viscosity ratio of the blend component by its reinforcing effect, which is rarely observed in the case of polymer blend mixed with a traditional copolymer. So the reinforcing effects of organoclay on a polymer blend can be determined depending on its degree of dispersion and its localization. Regarding the inhomogeneous distribution of clay in polymer blends, different work showed that clay preferentially resides in the blend phase having better affinity to organoclay [94,98,100]. If clay shows the same affinity to both blend phases, it concentrates dominantly at the interphase [87,110]. These two positions indicate two roles for the organoclay as nanofiller: it stabilizes the polymer phases and improves the mechanical properties by influencing the morphology of the blends [107].

However, if the organoclay has a specific affinity for one component of a multi-component system, then there is little opportunity for the organoclay to diffuse into the interface. Gefler et al. [94] found that in PMMA/PS blends most of the clay resides and is finely dispersed in the PMMA phase and interfacial region between PS and PMMA. They have attributed this tendency to more affinity of organoclay to the polar PMMA phase. Khatua et al. [98] have observed that for nylon 6/EPR blends, approximately all the organoclay preferred to exist in the nylon phase, which could be due to differences in the miscibility of organoclay with each of the polymer phases and higher polarity of nylon than EPR. Li et al. [100] have found that in case of

nylon/PPO blend clay stays preferably in the nylon matrix. Sharif et al. [104] have found that organoclay has tendency to shift to the more polar phase, i.e. EVA, when it was loaded in NR/EVA blends. In short, the tendency of clay to transfer to a specific phase depends on the affinity to the specific phase.

Vo et al. [107] have investigated the effect of different organoclays having different surfactants and polarities in Nylon 6/PVDF blends. Two types of organoclays have been used for the investigations: one was more polar (Cloisite 30 B) where as the second organoclay is less polar (Cloisite 20 A). It has been found that more polar organoclay (Cloisite 30 B) in the blends interacts favorable with both polymer phases but it prefers more the nylon 6 phase, so was more likely to disperse in the nylon phase. On the other hand less polar organoclay (Cloisite 20 A) prefers to reside at the interface. The differences in the functional groups of the surfactants in organoclay offer varying affinities to the polymers such that the location of clay can be tuned to modify the blend properties.

The concentration of organoclay also plays a vital role for the localization of the filler in the specific phase [101]. The morphological investigations show that location of organoclay depends on amount of organoclay and its affinity to the specific phase. It was noted that when small quantity (1 %) was added in PE/PBT blends, it localizes at the interface. For higher concentration it shifted to PBT phase [101].

Hong et al. [101] have studied thoroughly the shear induced migration of organoclay in the PBT/PS binary blends. When master batch either of PS or PBT and clay was annealed with the second plain phase at processing temperature for a longer time, no obvious migration of organoclay across the interphase has been observed, although organoclay is thermodynamically more stable in PBT phase, due to its higher polarity, than in PS phase. When PS-clay master batch was mixed with the plain PBT at different shear rates (1, 10 and 50  $s^{-1}$ ) for different mixing times, it has been found that for higher applied shear force more and more clay tactoids from the interface migrate into PBT phase in shorter time. The clay particles can only move through the interphase, if the magnitude of shear force exceeds a certain critical value [101]. The size of the filler is also of critical importance for phase specific localization of the filler [101]. The particle migration through the interphase is accelerated by increasing the shear rate ( $\dot{\gamma}$ ), which supplies large amount of force for the hydrodynamic shear flow.

Viscosity is an important parameter which also influences the localization of filler, but a more critical factor to induce the clay migration in the blend system is the chemical affinity between the polymer phases and the organoclay. Organoclay prefers to reside in the phase where it is thermodynamically more stable, even if the specific phase has higher viscosity [101].

### **2.2.2 Methods for characterization of organoclay dispersion and distribution in rubber compounds and rubber blends**

The most prominent methods used to determine the structure of the nanocomposites are transmission electron microscopy [1] and X-ray diffraction (usually SAXS) [3]. SAXS is based on the well-known Bragg's equation, and can quantify the periodicity of well-stacked clay in parallel registry. By monitoring the position, shape and intensity of the basal reflection from the distributed clay layers, the nanocomposites structure may be identified either intercalated or exfoliated. Although, SAXS offers a convenient method to determine the interlayer spacing of clay layers, nevertheless it is seldom used as the definitive proof of exfoliation, because issues such as surface sensitivity and orientation of the platelets can result in ambiguous results. On the other hand, transmission electron microscopy can provide useful information in a localized area on the morphology, structure and spatial distribution of the dispersed phase of the nanocomposites. Both, the low and high magnification micrographs are essential elements of the analysis. The low magnification micrograph emphasizes the overall clay dispersion, while the high magnification micrograph allows the observation of the individual clay layers, so that the morphology, intercalated or exfoliated, can be assigned. Thus SAXS and TEM techniques can be regarded as complementary to each other for characterization of the morphology of polymer-clay nanocomposites [1]. There are some other methods that have been used in addition to SAXS and TEM for investigations to characterize the dispersion of clay in the polymer nanocomposites including AFM [2], NMR [4], FTIR [5], neutron scattering [6], rheology [7] and dielectric spectroscopy [8].

The dispersion and distribution of organoclay in polymer blends as well as the development of blend morphology is characterized by usual microscopic techniques for nanocomposites like TEM, SEM etc. [89,98,104]. Additionally the location of organoclay in specific phase has also been characterized by DMA [110,111].

All of these methods are post processing techniques employed for the characterization of nanocomposites. These are not only labor intensive but also fail for monitoring the extent of

exfoliation of clay platelets during compounding process. During processing the clay dispersion is sensitive to material and technological parameters, additionally the upper limit of processing temperature of most thermoplastic materials could also damage organoclay, so a vast area of materials properties as a function of intercalation/exfoliation remains unexplored. The relationship between processing parameters and a complete chart of dispersion ranges from immiscible to intercalated/exfoliated structures in the real-time measurements remains unknown. This situation has greatly impeded advances in understanding of clay nanocomposite performance and compromised the industrial and commercial applications of nanocomposite. With increasing demands with respect to productivity, quality and commercialization of the products, it is highly required to establish the means for controlling the amount of exfoliation during processing of nanocomposites. For more complex systems like clay in binary blends, the process control in the real time will provide the highest benefit; therefore a fast and accurate determination of morphology is severely needed. These problems could be rendered either by replacing or at least minimizing the existing offline characterization techniques by online methods, which would be quite viable to examine the intercalation/exfoliation of organoclay during processing.

Online controls are being developed either to monitor the uniform distribution of the nanofiller to produce homogeneous bulk properties or spatially variation of the nanofillers concentration to meet the specific design criteria. The second critical aspect for the real time monitoring of processing nanocomposites is the integration of high throughput, is to probe the state of dispersion with changes in processing and material parameters, and correlate with multitude of properties. So it could be helpful to develop detailed structure-processing-property correlations in a rapid and system specific manner. The benefits associated with the application of these techniques can be directly related to improved quality and reduced production costs. In recent years, many inline and online methods for monitoring the dispersion of fillers such as carbon black (CB), silica, carbon nanotubes (CNT) and polymer structure directly in the mixing device has been developed, e.g. near and mid infrared spectroscopy [9,112], Raman and UV / VIS spectroscopy [113], Remote Laser Micro Analysis [114], ultrasound [115,116], inline rheology [117], inline monitoring of density and viscosity [118] and dielectric spectroscopy [8,119]. Regarding the polymer nanocomposites, Bur et al. [8,119] have detected electrical signals of polyamide (PA)-clay composites during the extrusion process. He supposed that the appearance of conduction may be related to the change of the microstructure of the nanocomposites.

In most of these investigations the sensor has been installed in a slit die, which lies behind the screw of the extruder. The information obtained by these techniques only corresponds to one point i.e. where the sensor or transducer is installed, but fails to elaborate the complete spectrum of development. Therefore it is highly required to have an online technique that not only provide real time information but also provide a complete spectrum of the development of morphological changes at different stages. Furthermore the method has potential to be extended to blend-organoclay system, which could be used for characterization of phase specific localization of organoclay as well as development of the blend morphology. Moreover, it also shows the advantage of being rapid, reliable and industrially viable.

## **2.3 Monitoring of clay dispersion during mixing process**

### **2.3.1 Electrical conductivity of polymer-clay nanocomposites**

There are some exclusive electrical properties exhibited by organoclay minerals which are mainly attribute to the ionic conductivity. Vaia et al. [120] have observed that the preparation of PEO/clay nanocomposites could increase the ionic conductivity as compared to that of PEO. Intercalated nanocomposites prepared by melt intercalation of PEO into Li-MMT have shown to enhance the stability of the ionic conductivity at lower temperature when compared to a more conventional PEO/LiBF<sub>4</sub> mixture. The higher conductivity at room temperature compared to conventional PEO/LiBF<sub>4</sub> electrolytes with a single ionic conductor character makes those nanocomposites new promising electrolyte materials. Some other authors [8,12,13,121,122 ] also reported about the appearance of a conductance signal while manufacturing of polymer-organoclay nanocomposites. Kortaberria [12], Hussain [13] and Jang [121] have used dielectrical measurements for the characterization of the curing kinetics of epoxy matrices modified with organoclay. They showed that the addition of organoclay alters the electrical properties of the epoxy matrix. Higher conductivity values have been obtained for higher clay contents. They suggested that the conductivity exists because of the high ion transfer through inter- and intra-region of clay galleries. Aranda [122] characterized the ionic conduction mechanism of intracrystalline polymer-salt complexes obtained by insertion of poly(ethylene oxide) (PEO) and Crown ether compounds in an unmodified clay, containing Na<sup>+</sup> exchangeable cations in their interlayer space. PEO compounds (Crown ethers and PEO) are able to associate interlayer Na<sup>+</sup> cations modifying dramatically the ionic conductivity of the natural clay. The conductivity of

these compounds with intercalated clay structures depends on the interaction strengths between the interlayer  $\text{Na}^+$  cation and the oxyethylene compound. Macrocyclic polyethers which form very stable complexes restrain the  $\text{Na}^+$  ion mobility, and consequently the observed conductivity is low. PEO involves weaker cation-interactions, which can be invoked to explain the significant enhancement of the conductivity. It is noteworthy that in these materials the contribution of the anions to the ionic conductivity can be considered as zero, because the negatively charged clay layers constitute the anionic entities (infinite anionic radius), and consequently the transport cationic number for these systems must be assumed to be unity, in view of the immobility of the anions [122]. This situation is quite different from conventional PEO salt complexes, where an organic macromolecule acts as a solvent of the salt and dissociates partially, making it possible for the system to operate as a mixed cationic/anionic ion-conductor. The intercalated materials exhibit exclusively cationic conductivity [122]. Okamoto et al. [123] have reported the correlation between internal structure and ionic conductivity behavior of PMMA/clay and PS/clay nanocomposites having various dispersed morphologies of the clay layers by using an impedance analyzer in the temperature range of 90–150 °C. The nanocomposites having finer dispersion of the clay layers exhibit higher ionic conductivity rather than the other systems such as PMMA-clay nanocomposite with stacking layer structure [123]. The activation energy of the conductivity in finer dispersed morphology systems becomes larger than the other systems and the corresponding organoclay solids.

Even though the pure clays are insulator, the interlayer cations and their mobility ensure a significant ionic conductivity of the polymer-clay nanocomposites. Thus, solids exhibiting ionic or mixed ionic and electronic conductivities can be selectively prepared, which render a large variety of nanocomposite materials presenting suitable electrical properties for different applications. The intercalation of the polymer chains not only influence the thermo-mechanical properties but could also affect significantly the ionic mobility of cations, electrical conductivity and other electrical parameters associated with the ions from the clay interlayer [124].

### **2.3.2 Correlation between the conductance and clay dispersion**

As mentioned above, the addition of organoclay changes the electrical properties, which is mainly attributed due to the ionic conductivity of the free released surfactants [8,12,13]. The release of surfactants influence the conductivity, which increases by either higher loading of organoclay or exfoliation of the clay platelets. Intercalation process causes a moderate increase



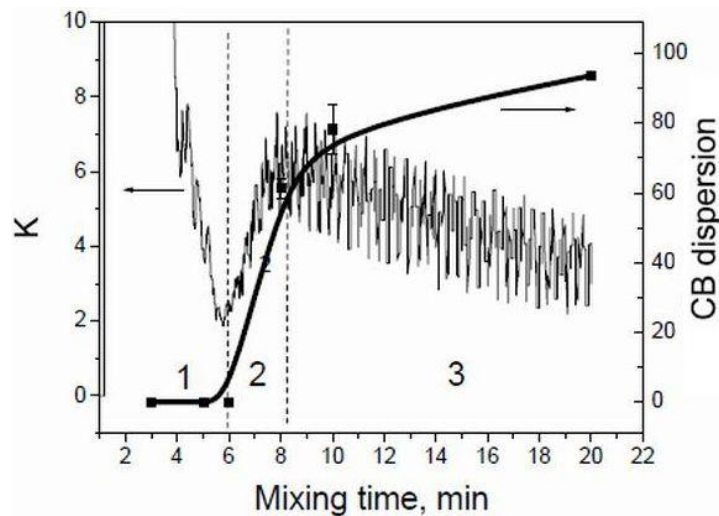
of conductance whereas exfoliation imparts higher conductance [123]. It is supposed that there exists a correlation between conductance and clay dispersion as well as clay contents. Regarding this, it has also been presumed that along the mixing time organoclay undergoes different dispersion stages that releases surfactants trapped inside the clay galleries and influences the electrical conductance.

### **2.3.3 Online measured electrical conductance method for carbon black and application of the method to clay dispersion**

The OMEC method was used by Le et al. [14] for systematic characterization of dispersion and distribution of carbon black in the rubber matrix. The electrical conductance of the composites is measured directly in the mixing equipment. This method based on principle that the change of electrical conductivity of polymer-CB composites is in dependence on concentration as well as the dispersion and distribution of electrical conductive filler in the polymer matrix [14,125-128]. OMEC chart and CB dispersion of the gum NR is presented in figure 2.9 [14]. Conductance and dispersion show three distinct stages. In the stage 1, the sensor is surrounded by free carbon black, which causes a short circuit showing a very high electrical conductance. With progressive encapsulation of carbon black through the rubber matrix, the fraction of the free carbon black continuously decreases until a clear decrease in the conductance is observed. In this stage, the CB dispersion shows a value near to zero. After passing a minimal value, the conductance of the mixture increases again and reaches a local maximum as observed in the stage 2. At the same time the values of the CB dispersion sharply increases.

The change of the OMEC and CB dispersion are determined by a very complex behavior of the mass transfer in the mixing chamber. Three main processes can take place simultaneously in this stage: the infiltration of the rubber chains into the voids within the CB agglomerates, the detachment of fine particles on the periphery of the agglomerates (erosion), the breakup of agglomerates and the distribution of the fine CB particles throughout the rubber matrix. The increase of OMEC value and its correlation to the CB dispersion during the second stage has been explained on the basis of the “onion model” proposed by Shiga and Furuta [129]. Infiltrated rubber and the clouds surrounding different agglomerates can touch each other and build a network, which leads to an increasing contribution of the conductance. Furthermore, due to the shear forces and the mass transfer the fine particles are distributed throughout the rubber matrix. The CB network is destroyed that causes a decreasing contribution of the online conductance.

The mixing time corresponding to the local maximum in conductance-time curve is called black incorporation time (BIT). At this time the infiltration process seems to be completed. Beyond the BIT, in the stage 3, the CB dispersion rate progressively reduces, while the small aggregates are intensively distributed. The pronounced decay of the conductance is mainly caused by the better distribution process of the small aggregates throughout the rubber matrix and therefore the increasing distances between the aggregates.



**Figure 2.9:** Relation between OMEC (K) of NR-CB mixture and dispersion of the filler [14]

An intensive investigation has been carried out by various authors to characterize the dispersion of organoclay and its effect on properties in the polymer matrix using dielectric spectroscopy [8,13,122,130]. Davis et al. [130] used dielectric spectroscopy during twin screw extrusion processing of polymer nanocomposites to characterize the clay contents and the dispersion process. Dielectric results were correlated with TEM and XRD results. It has been found that all nylon 6-clay nanocomposites show two types of dielectric relaxations,  $\alpha$  and Maxwell–Wagner, associated with rotational mobility of PA6 for amide linkages and ion accumulation at the layered clay-polymer interface, respectively. The plain polymer had only  $\alpha$ -relaxation. It was proposed [130] that difference between baseline alpha-relaxations for Nylon-6 and Maxwell-Wagner relaxation seen for nanocomposite, can be used to describe quantitatively clay concentration in a polymer matrix. Noda et al. [119] have also used online dielectric slit die sensor to examine the morphology development during melting mixing of nylon 6 clay nanocomposites. The data obtained from the online instrument was correlated with the offline

TEM and dielectric measurements to establish the relationship between the filler dispersion and the dielectric relaxation behaviour. The extent of exfoliation of various types of clays in nylon [6,11,12] has been analyzed by passing through a slit die at the end of the extruder [8]. The slit die had a specialized dielectric and an optical transmission sensor. It has been found that the optical transmittance increases as exfoliation of clay increases [8]. Data from the dielectric relaxation and the optical transmission correlated to clay dispersion as observed by TEM.

Although extensive work has been reported for the online characterization of clay dispersion in the polymer matrix by using dielectric spectroscopy, there are still many open questions relating to kinetics of morphology development which need to be explored. In addition, these methods have only been applied to single phase polymer clay nanocomposites but not to the blend-clay system. The results obtained in all the processes correspond to the single point of the whole spectrum of the development, i.e. the point where transducer has been installed. So there is missing link between online conductance chart and complete kinetics of clay dispersion.

The online method, based on the electrical conductivity of the composites as a function of filler dispersion, has been modified and applied in this work to characterize the intercalation and exfoliation of organoclay in the rubber compounds. Furthermore, the method has also been extended to characterize the phase specific localization of organoclay and development of morphology in the rubber blends.

### **3 Aim of the work**

The demand for real time characterization of polymer nanocomposites is showing increased popularity in recent years among researchers. This has triggered the scientists to improve many of the existing techniques as well as explore new methods. Polymer-clay nanocomposites show improved dielectric properties due to intercalation/exfoliation of clay platelets in the polymer matrix. This has prompted us to apply online measured electrical conductance (OMEC) method, to characterize the dispersion and distribution of organoclay in rubber compounds and rubber blends. The benefits associated with the application of this method can be directly related to improved quality and reduced production costs.

The objective of the present work is to use the online conductance method to characterize the kinetics of clay dispersion as well as development of morphology in rubber-clay nanocomposites, also to investigate the effect of technological parameter, like shear force, on nanocomposite preparation. Furthermore the development of structure as well as physical and mechanical properties has been correlated to the online method. The final properties of the rubber nanocomposites could be tailored by controlling the organoclay dispersion.

The method is applied to a number of rubber systems with different polarities (XHNBR, HNBR, ENR 50, and NR) and organoclay. The data obtained from the online instrument have to be correlated with offline techniques TEM, AFM, SAXS etc. to establish the relationship between filler microstructure and OMEC behavior to lay down a relationship between filler microstructure and online conductance spectrum. The correlation between the conductance measured directly in the mixing chamber of the internal mixer and the development of morphology for either rubber-clay nanocomposites or the rubber blend-clay nanocomposites needs to be realized and thoroughly investigated using different characterization techniques.

Moreover, the OMEC method will also be used to investigate the effect of organoclay in rubber blends with different polarities and compatibilities like polar/non-polar (HNBR/NR) blends and polar/polar (HNBR/ENR) rubber blends. The filler phase specific localization and development of the blend morphology would be characterized by offline techniques. A further objective of the work is to determine the performance of the rubber nanocomposites, derive the structure-property relationship and finally correlate with the online measured data both for the plain rubber matrix and the rubber blends as well as their nanocomposites.

The success of work in lab scale will initiate the application of the method of the online conductance for monitoring of the production of organoclay filled polymers on industrial scale.

## 4 Experimental

### 4.1 Materials

For dispersion of organoclay in the single phase polymer and blends following materials according to their different polarities and modifications have been selected.

**Table 4.1:** Materials, abbreviation, trade name, manufacturers and general properties of used materials

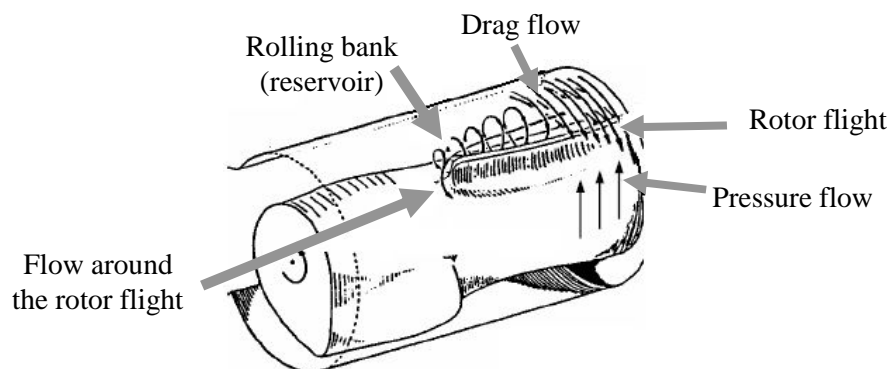
Material	Abbreviation	Trade name	Suppliers	Properties
Carboxylated hydrogenated nitrile butadiene rubber	XHNBR	Therban XT VP KA 8889	Lanxess Deutschland GmbH, Germany	Acrylonitrile content of 33 % , mooney viscosity ML (1+4, 100°C) 77 MU, residual double bonds about 3.5 % and volatile matter $\leq$ 0.49 wt % , specific gravity 0.97 and soluble in acetone and it is methyl ethyl ketone (MEK) [131].
Hydrogenated acrylonitrile butadiene rubber	HNBR	Zetpol 2030L	Zeon Deutschland GmbH, Germany	Acrylonitrile content of 35 wt% , mooney viscosity ML (1+4, 100°C) 55 MU, ash contents on ignition 0.5 wt % , heat loss 0.5 wt % , iodine value 55 mg/100 mg, and it is soluble in acetone [132].
Natural rubber	NR	Standard Malaysian Rubber SMR10	Astlett Rubber Inc. Canada	Ash contents on ignition 0.75 % and volatile matter 0.80 % , density 0.92 g/cm <sup>3</sup> , glass transition temperature -54 °C, dirt 0.08 % , It is soluble in toluene and cyclohexane [133]
Epoxidized natural rubber 50	ENR	ENR 50	Weber & Schaer GmbH & Co. KG Germany	Mooney viscosity ML (1+4, 100 °C) 80 MU, ash residue after ignition 1-2 % , density 1.02 mg/m <sup>3</sup> , glass transition temperature -24 °C, epoxidation grade 50 % . The epoxy groups are statistically distributed along the main chain of the polymer [134]
Peroxide	Peroxide	Luperox 101	ATOFINA Deutschland GmbH, Germany	Molecular weight 290.4 g, melting point 5 °C, and suggested temperature curing range 160-210 °C.

Modified clay	Organoclay	Nanofil 9	Süd Chemie Gemrany	Layer spacing 2 nm, average particle size of about 35 $\mu\text{m}$ , weight loss on ignition of 35 %, specific gravity 1.8 $\text{g}/\text{cm}^3$ , powder density 180 $\text{g}/\text{cm}^3$ and humidity ~3 %.
Unmodified clay	Clay	Cloisite $\text{Na}^+$	Rockwood Additives Inc. USA	It is basically montmorillonite; hydrated aluminum silicate, with totally silica contents $\leq$ 0.3%, specific density 2.85 $\text{g}/\text{cm}^3$ , insoluble in water and in organic solvents, with weight loss on ignition 7%, particle size ~ 13 $\mu\text{m}$ and layer spacing 1.17 nm [135]

## 4.2 Internal mixer

In internal mixer, different parts exert different forces which could influence the mixing process. The rotor flight plays a key role for mixing of rubber compounds and dispersion of filler in the matrix [136]. The material is swept in either half of the mixing chamber and into the area in front of the flight by the rotor flight. The fill factor and the relative position determine the collected material [136]. During one rotor turn the materials is distributed with the mixing chamber by a flow between rotor tip and chamber wall and between rotor shaft and chamber wall as well as by the flow around the end of the rotor flight, as illustrated in the figure 4.1, the remaining material returns to the reservoir. In internal mixer, the region between the rotor flight and the chamber wall is the most important for good mixing efficiency. In this region the shear forces and elongation deformations are high: it is the only region within internal mixer with unidirectional flow [137].

The flow of the material in the front of flight is the summation of drag flow and pressure flow, former is caused by rotation of rotor whereas the later is due to pressure difference behind the rotors and in front of rotors as shown in the figure 4.1. However, behind the rotor tip, voids are present at even at every fill factor, resulting in a low pressure and providing the basis for disordering, necessary for intensive and extensive mixing.



**Figure 4.1:** Flow path within half of internal mixer [137]

Various parameters like time profiles of temperature, torque, energy input, ram pressure or other parameters monitored during mixing can act as fingerprints to control and analyze the mixing process. Especially, during the mixing of rubber compounds, the torque parameter gives valuable information about the different steps of mixing process. Furthermore, the parameters which mostly influence the mixing efficiency are given by:

- a) Fill factor,
- b) Rotor speed,
- c) Geometrical design of the mixing chamber and the rotor,
- d) Temperature control,
- e) Ram pressure.

### 4.3 Sample preparation

The samples were prepared in an internal mixer PolyLab system Rheocord (Thermo Electron/Haake) provided with rotors of roller types. The experiments were based on the fact that firstly the online method for characterization of intercalation/exfoliation of organoclay has been applied to single phase rubber compounds. The effects of technological parameters, like rotor speed and material parameters like varying the polymer matrix and clay types have been investigated. Then the method was applied to investigate the effect of organoclay on the phase specific localization as well as development of morphology in two types of elastomer blends, polar/non-polar and polar/polar blends respectively.

XHNBR was mixed with peroxide in an internal mixer PolyLab System Rheocord (Thermo Electron/Haake) equipped with rotors of roller types at an initial chamber temperature of 50 °C and a rotor speed of 70 rpm. Clay was added after 7 minutes. A clay concentration of 5 phr was

kept constant for all nanocomposites. For the characterization of the dispersion kinetics of organoclay samples were taken out after different mixing times of 1, 3, 4, 10, 25 and 30 minutes. The mixing time denotes the time after addition of organoclay. A reference series was also prepared by a rotor speed of 25 rpm, and an initial chamber temperature of 70 °C was chosen in order to keep the mass temperature similar for both series. For a second series the mixtures were prepared for different time intervals of 10 seconds, 1, 2, 7, 10, 20 and 45 minutes. The mixtures were compression-molded (Laboratory press P200 Fa. Collin, Germany) at 170 °C to  $t_{90}$  and vulcanized for 1 mm thick plates. Similar mixing procedure along with the processing conditions has been followed for other elastomer as shown in table 4.2. ENR was mixed with organoclay for different mixing time as shown in the table 4.2. Furthermore, in order to discard the effect of decomposition of ENR at mixing temperature, ENR was milled at two roll mill for various times before mixing with organoclay.

**Table 4.2:** Names of samples and mixing conditions

Elastomer	Rubber trade name	Clay, phr	Speed, rpm	Mixing time, min
XHNBR	Therban XT VP KA 8889	5	70	1, 3, 4, 10, 25, 30
HNBR	Zetpol 2030L	5	70	1, 2, 4, 10, 30
NR	SMR 10	5	70	1, 4, 10, 30
ENR	ENR	5	50	1, 2, 4, 6, 10

Two sets of blends, first polar/non-polar and second polar/polar blends were prepared.

The polar/non-polar blend was prepared in two steps. In the first mixing step, NR was mixed with 10 phr organoclay at the same mixing condition as mentioned above (organoclay in SMR 10) to produce a NR-clay masterbatch. Mixing time of 10 minutes was kept for all masterbatches. In the second step, plain HNBR was mixed with the NR-organoclay masterbatch to get 50/50 HNBR/NR blends having a total clay concentration of 5 phr, i.e. NBR/NR/clay in ratio 50/50/5. In the following they are called HNBR/(NR-clay masterbatch) blends. For comparison purpose, an unfilled 50/50 HNBR/NR blend was prepared at same processing conditions as for filled blends. The kinetics of development of blend morphology and phase specific location of organoclay have been characterized by taking out samples of the mixing chamber at various



mixing times, i.e. 2, 5, 10, 15, 25, 40 minutes. The mixtures were compression-molded and vulcanized at 170 °C to  $t_{90}$ .

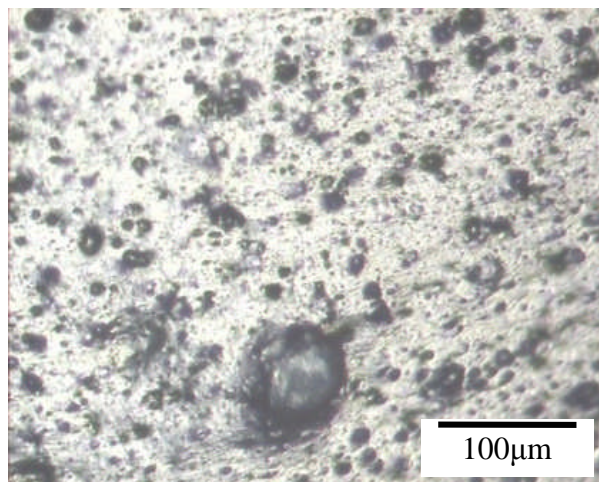
In order to investigate the effect of organoclay in polar/polar matrices, HNBR and ENR were blended together. The sample preparation procedure has been similar to the [HNBR/(NR-clay masterbatch)] i.e. in two steps. ENR was mixed with 10 phr organoclay at 50 °C, 50 rpm rotor speed for mixing time of 10 minutes. In the second step, ENR-clay masterbatch was mixed with plain HNBR to get 50/50 HNBR/ENR blends with total clay contents of 5 phr. The kinetics of development of blend morphology and tendency of the filler to transfer in the specific phase was characterized by taking out samples at various times 1.5, 2, 4, 6, 10, 20, 40 minutes relative to online conductance spectrum. The mixing time denotes the time after mixing plain HNBR and ENR-master batch. For a comparison purpose unfilled HNBR/ENR blends were also prepared at same processing conditions as that of HNBR/(ENR-clay masterbatch) blends. The mixtures were compression-molded and vulcanized at 170 °C to  $t_{90}$ .

## **4.4 Methods of morphology evaluation and property characterization**

### **4.4.1 Morphological characterization**

#### **4.4.1.1 Optical microscopy**

The macrodispersion has been investigated by optical microscopy, which is one of the most reliable methods for direct assessment of the filler dispersion in the polymer matrix. Reflecting optical microscopy (Leica DM-RX, Leica) has been used for the morphological investigations of the cut surface of the samples at room temperature. The filler aggregates of diameter smaller than 3  $\mu\text{m}$  were not visible.



**Figure 4.2:** Optical micrograph of XHNBR-clay nanocomposite mixed at 70 rpm after 1 min of mixing time

The quantitative morphological analysis has been computed from the images of optical micrographs using the image analyzing software QWin (Leica). Optical micrographs have been analyzed by the method described by Leigh-Dugmore [138] for carbon black and modified by us for organoclay. The area of the non-dispersed tactoids (dark grey part in figure 4.2)  $A$  is calculated and related to the total area of the micrographs  $A_0$  (figure 4.2). The dispersion degree  $A/A_0$ , is the ratio of clay tactoids with an average diameter greater than  $3 \mu\text{m}$  and the total area of the image.

#### 4.4.1.2 Atomic force microscopy

The surface-structure of the flat microtomed surface of the sample was analyzed using a Quesant Q-Scope (Quesant, USA), equipped with a  $40 \mu\text{m} \times 40 \mu\text{m}$  scanner operating in intermittent mode. Standard silicon cantilevers NSC 16 with a resonance frequency and force constant of about 170 kHz and  $40 \text{ N m}^{-1}$ , respectively, were used for scanning the microtomed samples. Damping, amplitude and other parameters are adjusted to optimal values to get the better images. Height and phase images were simultaneously measured, although only the phase images are presented here.

Samples for AFM measurement were fine trimmed using cryo-chamber CN 30 of a rotary microtome HM 360 (Microm, Germany) by means of a diamond knife (Diatome, Germany) at  $-120 \text{ }^\circ\text{C}$ . The flat surface thus obtained was scanned for the characterization of morphology. The surface was not etched additionally by chemicals.

The quantitative morphological analysis has been computed from the AFM micrographs using the image analyzing software. The computed data from the image analysis has been statistically secured by calculating approximately all, number particles and blend phases to quantify the filler particle size and phase sizes, respectively.

#### 4.4.1.3 Transmission electron microscopy

Microstructure was examined using a transmission electron microscope JEM 2010 (Jeol, Japan), operated at 200 kV. Ultrathin sections of each sample (ca. 100 nm) were prepared at  $-100\text{ }^{\circ}\text{C}$  from a bulk specimen using an ultra microtome Ultracut E (Leica, Germany) with cryo-system FC6 (Leica, Germany). The samples were not exposed to any chemical to enhance the contrast.

#### 4.4.1.4 Small angle X-ray scattering analysis

Small-angle X-ray scattering (SAXS) measurements were performed at room temperature using a rotating anode X-ray source RU-3HR (Rigaku) equipped with a nickel-filtered Cu  $K\alpha$  tube ( $\lambda = 0.154\text{ nm}$ ) for detection of the state of exfoliation. The generator voltage was 40 kV and generator current was 60 mA. Typically diffracted intensity is plotted as a function of  $2\theta$  using the Bragg's law,

$$n\lambda = 2d \sin \theta \quad (4.1)$$

where  $\lambda$  is the wavelength of X-ray radiation used in the diffraction experiment and  $d$  is the spacing between the diffraction lattice planes. Since the  $d$ -spacing is of interest one might wonder why diffraction data is not plotted as a function of  $\sin \theta$ . This is in fact done with the use of the scattering vector  $q$ .

$$q = \frac{4\pi}{\lambda} \sin \theta \quad (4.2)$$

Substituting equation (4.2) in equation (4.1), Bragg's law of diffraction yields:

$$d = \frac{2\pi}{q} \quad (4.3)$$

The first order Bragg peak in the Lorentz corrected intensity curves were fitted by using a Gaussian function with linear background subtraction; this gives a good description of diffraction in  $q$  or  $s$  reciprocal space, giving the interlayer distance and the relative peak strength. All samples had a uniform thickness of 1.0 mm, i.e. the obtained peak area corresponds to the amount of ordered structures.

## 4.4.2 Surface investigation

### 4.4.2.1 Measurement of bounded rubber layer on the organoclay surface

The wetting behaviour of rubber on organoclay surface has been characterized on the basis of method developed by Le et al. [139]. When organoclay is mixed with a rubber, a part of the rubber chains will be bonded to the existing reactive groups which are available on the surface of the clay. Unvulcanized raw rubber compound was extracted with suitable solvent (acetone was used for XHNBR-clay nanocomposites). The bound part of the rubber forming a layer around the filler particles remains in the rubber-filler gel. The determination of the amount of rubber  $L$  bound to the surface of the organoclay was carried out according to equation. 4.4 [139].

$$L = \frac{m_2 - m_1 \cdot c_R}{m_2} \quad (4.4)$$

The mass  $m_1$  corresponds to the rubber compound before extracting; it is the sum of the mass of the insoluble rubber, the mass of the soluble rubber and of organoclay, whereas  $m_2$  is the mass of the rubber-filler gel, which is the sum of the insoluble rubber and the mass of organoclay.  $c_R$  is the mass concentration of organoclay in the mixture. This value is dimensionless and lies between 0 and 1. For the experimental work 0.25 g of the uncured mixture were stored at room temperature in 100 ml acetone. After three days the rubber-filler gel was taken out, dried up to a constant mass and analyzed.

### 4.4.2.2 Extraction experiment

Extraction experiment has been carried out for quantitative investigation of phase specific localization of filler in heterogeneous blend. 0.25 g of the uncured HNBR/(NR-clay master batch) blends were stored at room temperature in 100 ml cyclohexane. The NR phase and the clay distributed in it were extracted. After three days the rubber-filler gel was taken out and dried to a constant mass. The thermogravimetric analysis of the rubber-filler gel was carried out. By evaluation of the curve of the mass the clay loading distributed in the HNBR phase was determined.

### 4.4.2.3 Surface tension

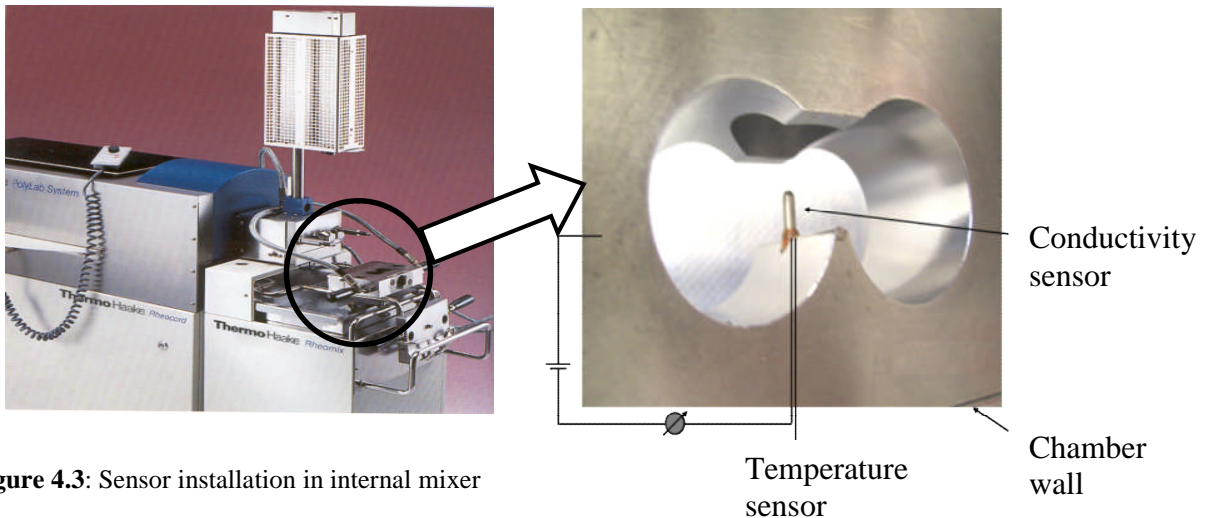
The contact angle of the sample surface against water was measured. A drop of freshly bi-distilled water was placed on each sample, which was then sealed with a glass cover. The sessile

drop analyses were performed with an OCA 20 (Data Physics Instruments GmbH, Germany) contact-angle instrument, employing both digital imaging and drop-shape analysis at 20 °C. Pictures taken at various stages of the procedure were evaluated for determination of the surface tension.

### 4.4.3 Electrical conductance

#### 4.4.3.1 Online conductance

A conductivity sensor has been installed in the chamber of the internal mixer, as show in the figure 4.3, to measure the conductance signal of the mix volume between the sensor and the chamber wall as used by Le et al. [14]. The construction and position of the conductivity sensor was modified to detect the conductance signal of the investigated system with good reproducibility. Furthermore, a thermocouple has also been installed in the chamber in order to measure and control the temperature.



**Figure 4.3:** Sensor installation in internal mixer

#### 4.4.3.2 Offline conductivity

Offline conductivity measurements were performed at room temperature using the sandwich principle by means of an electrometer 6517 A (Keithley, USA). By this method the volume resistivity of the material samples was measured as  $C_{off}$  in  $\Omega\text{cm}$ , normalized to a definite measured volume.

#### **4.4.4 Mechanical and thermal performance**

##### **4.4.4.1 Stress-strain relationship**

The uniaxial tensile properties of the materials were measured by stress-strain measurements according to DIN ISO 37 using tensile testing machine Z005 (Zwick/Roell AG, Germany), specimen holders 8397. The dog bone type specimens were examined at room temperature, at the crosshead speed of 200 mm/min and preload 0.1 MPa. All the test specimens had a thickness of 1 mm and an initial length of 50 mm. Data obtained has been computed by software and also calculated manually from the stress-strain curves. The tensile modulus, stress at 100 % or 200 % elongation, stress at break and strain at break were determined. All the data presented are an average of five measured specimens for each of the sample.

##### **4.4.4.2 Dynamic mechanical thermal analysis**

The peak position of loss factor has been successfully used to characterize the phase specific localization of the fillers in rubber matrix [140]. The dynamic mechanical properties were characterized using a dynamic mechanical tester Qualimeter 500 N (Fa. Gabo, Germany) equipped with liquid nitrogen accessory for controlled cooling. Compression molded bars were tested at temperatures ranging from -100 °C to 100 °C, frequency of 1 Hz and heating rate of 2 K/min. The storage modulus  $G'$ , loss modulus  $G''$  as well as the loss factor  $\tan \delta$  were determined in the prescribed temperature range.

##### **4.4.4.3 Thermogravimetric analysis**

The thermogravimetric analysis of the samples was carried out by a thermo balance TGA /SDTA 851 (Mettler Toledo). Samples were heated up to 800 °C with a heating rate of 20 K/min in an air atmosphere. The loss of sample weight was recorded. The mass curves of the rubber filler gel have been analyzed, which revealed the mass of surfactants and clay loading before and after extraction. Furthermore, the evaluation of the curve of mass of clay loading in blend has been used for the quantitative distribution of clay in one of the specific phases.

## 5 Results and Discussion

### 5.1 Online conductance of rubber clay nanocomposites

The incorporation of nanoclay in the rubber matrix affects online measured electrical conductance (OMEC) of the nanocomposites. Generally, online conductance of the nanocomposites is the sum of conductance of the rubber and filler. It is given by following expression

$$\sigma_{comp} = \sigma_{rubber} + \sigma_{clay} \quad (5.1)$$

where

$\sigma_{comp}$  = Online conductance of the nanocomposites

$\sigma_{rubber}$  = Online conductance of rubber matrix

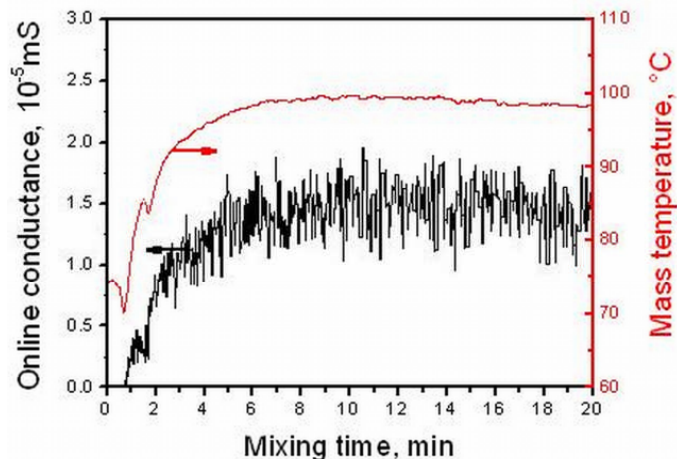
$\sigma_{clay}$  = Online conductance of the filler

The OMEC of the rubber clay nanocomposites is ionic in nature, which will be thoroughly discussed in the next chapter. It depends on the nature of the rubber matrix, types and loading of nanoclay as well as its intercalation/exfoliation in the polymer matrix.

### 5.2 Hydrogenated carboxylated acrylonitrile butadiene rubber XHNBR-clay nanocomposites

#### 5.2.1 Online conductance of XHNBR-clay nanocomposites

The online measured electrical conductance curve of the plain XHNBR versus mixing time is shown in figure 5.1. When the rubber was filled into the chamber, online conductance increased to a certain value and then remained constant. The increasing conductance is in line with the increasing mass temperature which on the one hand causes a better contact between the rubber and the sensor, and intensifies, on the other hand, the transport process of the charge carriers contained in the rubber. The material is masticated and the online conductance reaches its optimum value after 7 minutes; meanwhile the temperature also becomes constant.



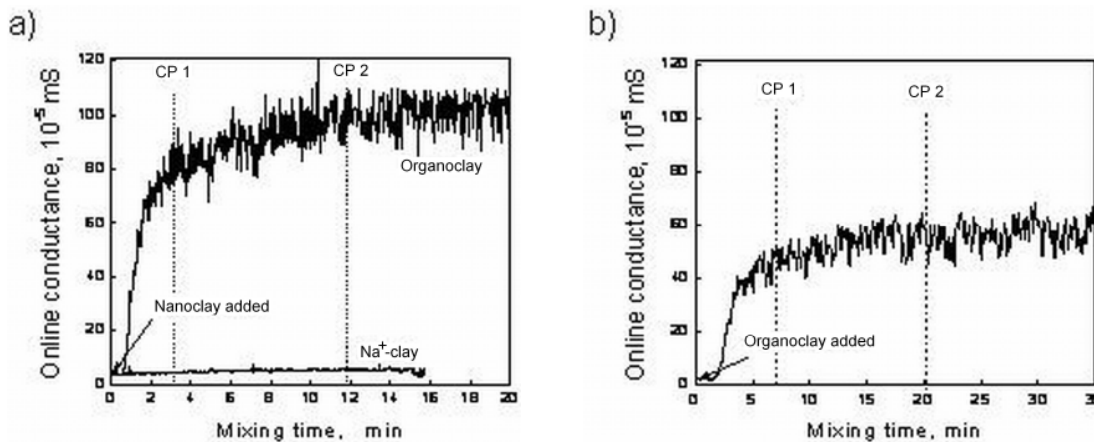
**Figure 5.1:** Online conductance of plain XHNBR

The conductance observed is ionic in nature which is due to the presence of ionic charged entities. They can be residual catalyst, impurity, hydrogen or hydronium ions, acids bases, salt impurities. Ionic conductivity is always possible when readily ionizable species are present in the polymer like possible degradation products or when purity is uncertain [141]. The ionic conductance is function of temperature. It increases for higher temperature and vice versa. It can be observed in figure 5.1 that increase of OMEC is inline with increase of temperature, when temperature is constant the OMEC value is also constant.

Figure 5.2 depicts the development of the online conductance after addition organoclay (Nanofil 9) into the XHNBR rubber matrix at the rotor speed of 70 rpm. The mixing time indicated is the time after organoclay addition. The conductance of organoclay increases significantly and passes through two distinct points which are assigned as the characteristic point 1 (CP 1) at 3 minutes and characteristic point 2 (CP 2) at 12 minutes before it reaches a plateau.

In the stage up to CP 1, a sharp increase of the conductance is observed. The development of the online conductance declines in the stage between CP 1 and CP 2. After CP 2 a plateau is reached and no change of the conductance is observed. When XHNBR was mixed with organoclay at rotor speed of 25 rpm the conductance curve is reduced to a lower level and prolonged to longer mixing time as shown in figure 5.2b. The CP 1 and CP 2 were delayed to longer time i.e. at 7 minutes and 20 minutes respectively. Considering the relevant literature [12,13,121,124 ] the rapid increase of the OMEC just after adding organoclay could be attributed to the ionic conduction.





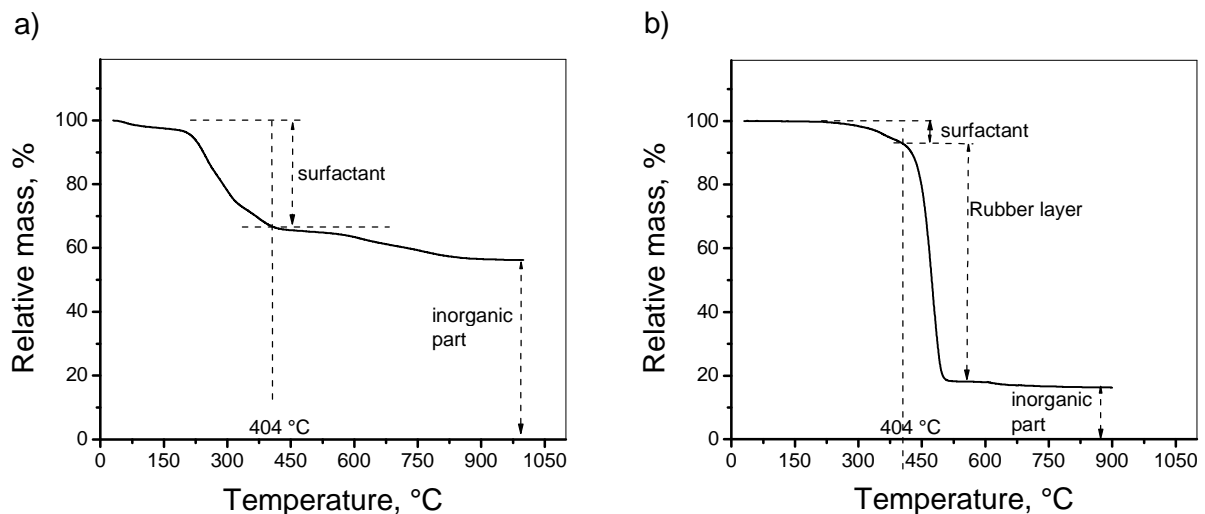
**Figure 5.2:** Online conductance of XHNBR-clay nanocomposites mixed by the rotor speed of (a) 70 rpm and (b) 25 rpm

Kortaberria et al. [12] have observed that epoxy resin of diglycidyl ether of bisphenol A shows higher conductivity on addition of organoclay. They mentioned that evolution of higher conductivity is due to the presence of ion of the surfactant present between the interlayer galleries. Motori et al. [142] have found that loading modified clay in the isotactic polypropylene increases the electrical conductivity of nanocomposites. They have attributed this increase of conductivity to the movement of ions in the amorphous part of i-PP, and increases the conductivity of the nanocomposites. Using online dielectric measurements, Bur et al. [8,119,130 ] detected electrical signals of polyamide (PA)-clay nanocomposites during the extrusion process. He supposed that the appearance of conduction may be related to the change of the microstructure of the composites, i.e. intercalation and exfoliation of the organoclay in the PA based nanocomposites. Some other authors have also reported the appearance of conductivity signals on the addition of organoclay in the polymer matrix [12,13,121,122 ].

*Determination of amount of surfactant remained in clay galleries after mixing process by thermogravimetric analysis of the rubber-clay gel*

The structural background of the online conductance chart of the polymer-clay nanocomposites has been characterized using different techniques, such as rubber layer experiment, (a method has been developed by Le et al. [139] and modified in this investigation) thermogravimetric analysis and small angle x-ray scattering.

The results of the thermogravimetric analysis of the organoclay and the rubber-filler gel are presented in figure 5.3a and b respectively. The mass loss of the surfactant,  $W_S$  is 34 % in the temperature range up to 404 °C is attributed to the degradation of the surfactant (figure 5.3a). The inorganic part of the organoclay  $W_I$  of 66 % was identified as the material remained beyond 600 °C. Figure 5.3b shows the relative mass curve of the rubber-filler gel. Analyzing the relative mass curve of rubber-filler gel reveals two distinct degradation processes. In the temperature range up to 404 °C, the surfactant degrades first. Its corresponding mass loss  $W_S$  is 7 %. In the subsequent temperature range between 404 °C and 507 °C XHNBR degrades. The mass loss of about 74 % in this range corresponds to the rubber layer  $L$  presented in figure 5.4.  $W_I$  of the inorganic part of the organoclay in the rubber-filler gel amounts 19 %. The ratio can be used as a measure to determine the loss of the surfactant, if it releases the organoclay galleries. The ratio  $W_S/W_I$  of 0.52 and 0.37 was calculated for organoclay and rubber-filler gel, respectively. It means that the surfactant remains inside the clay galleries after mixing only three fourth of that of the initial organoclay amount. It shows that one fourth of the surfactant amount has been released and moved into the rubber matrix causing an ionic conductance. When extraction experiment was performed to obtain rubber-filler gel, the released surfactants were extracted together with the unbound rubber.



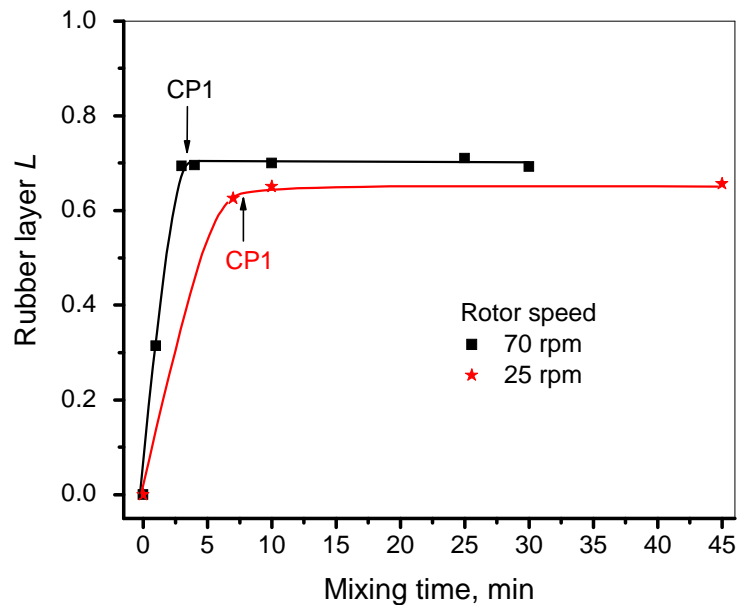
**Figure 5.3:** Thermogravimetric analysis of (a) organoclay (b) rubber-filler gel extracted from the sample taken out at 10 min mixing time

The organoclay is organophilic with a lower surface energy, and therefore it is more compatible with organic polymers. That results in the intercalation of polymer chains within the galleries. The nitrile group of XHNBR is a strong electron donor; therefore a hydrogen-bond formation exists between the ammonium ion of the intercalated amine and the nitrile group [42]. Such electrostatic interactions contribute to weaken the attractive forces between the cationic end group of the alkyl ammonium molecule and the negatively charged clay surface. The steady motion of rubber chains during the processing at high temperature facilitates the displacement of quaternary ammonium ions from one nitrile group to the other. Thus, even a large cation like alkyl ammonium could move easily in the rubber matrix causing an increase of conductance by two orders of magnitude compared to that of the virgin XHNBR.

## 5.2.2 Correlation between online conductance and structure of HNBR-clay nanocomposites

### 5.2.2.1 Rubber layer investigation

The rubber layer  $L$ , which is characteristic for the rubber amount that intercalates the clay galleries was determined for different nanocomposites using equation 4.4.

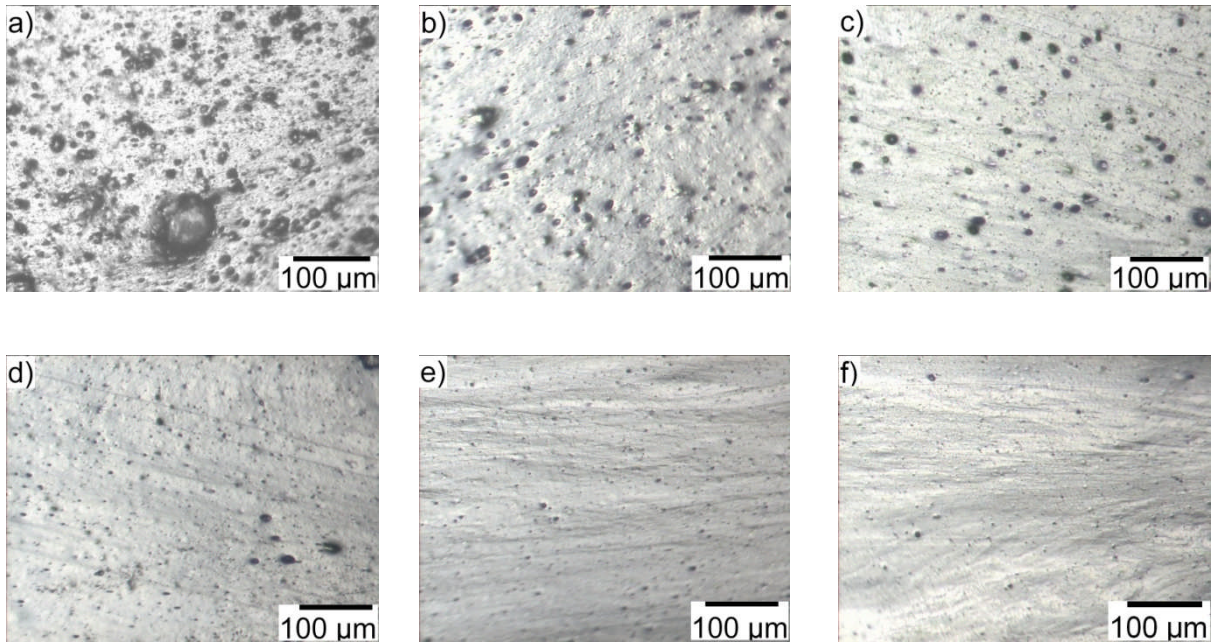


**Figure 5.4:** Rubber layer  $L$  bound on the clay surface of the mixtures versus mixing time for different rotor Speed

It can be seen clearly that for mixtures mixed at rotor speed of 70 rpm, the rubber layer  $L$  amount increases strongly in the stage up to CP 1, i.e. three minutes. The strong increase of rubber layer in the beginning of the process before CP 1 is due to diffusion of the rubber chains into the clay galleries. A plateau has been reached after CP 1 indicating that galleries of organoclay are already intercalated and the exfoliation process is yet in progress. It can be assumed that the most of intercalation process has been completed at CP 1. A similar behavior of surface saturation of wetted filler has also been observed for CB filled SBR composites [139]. There the authors have reported that the rubber layer increases along with mixing time as new surface is generated through the dispersion process. In the second mixing period, after reaching CP 1 the curve gets a plateau, which indicates the end of the intercalation process. At further mixing only exfoliation process of organoclay takes place. Figure 5.4 also shows the development of the rubber layer at lower mixing speed, i.e. 25 rpm. It clearly indicates that the CP 1 is shifted to longer mixing time. Low rotor speed imparts less mechanical force of mixing on the mixture, which ultimately slows down the dispersion process of clay. The value  $L$  of the mixture mixed at rotor speed, 25 rpm is lower than that of mixed at 70 rpm. This is related to the affectivity of the intercalation/exfoliation process when mixed with higher rate of energy input [143].

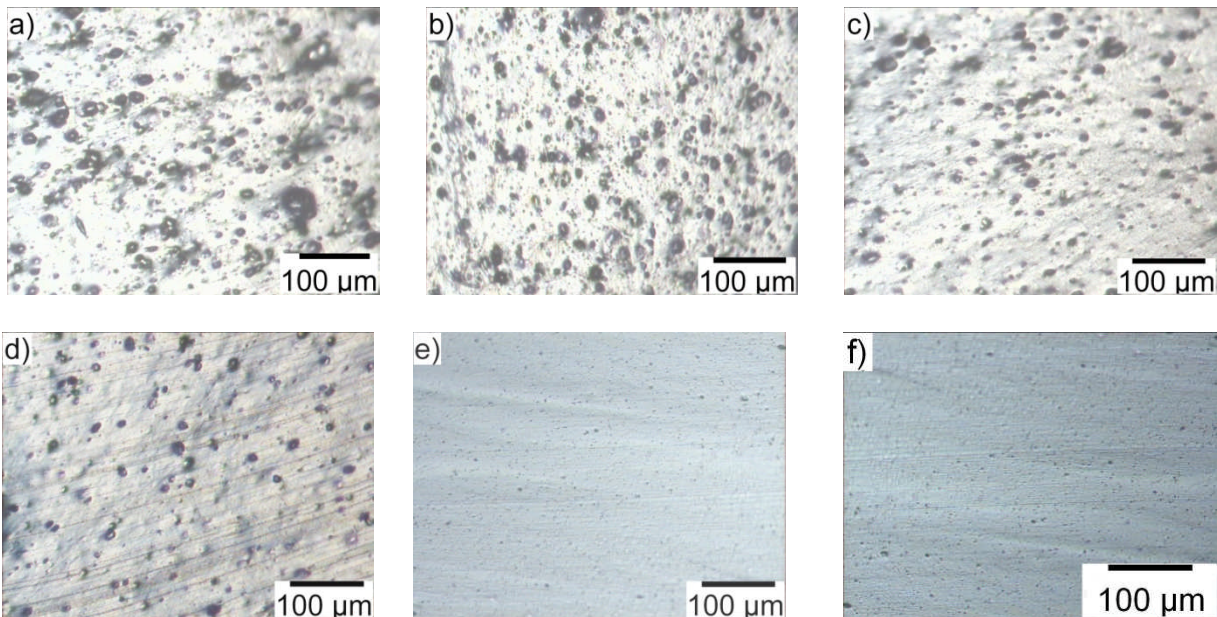
#### **5.2.2.2 Macrodispersion**

In order to characterize the macrodispersion of the organoclay the samples have been taken at different mixing times for the XHNBR-clay nanocomposites and were analyzed using the optical microscopy. Figure 5.5 shows the development of the morphology of the mixture mixed at 70 rpm. It is obvious that the number and size of the organoclay agglomerates decrease with the mixing time. This shows that the larger clay agglomerates are broken down into smaller aggregates (tactoids). When the size of tactoids is below 3  $\mu\text{m}$ , they become invisible in the optical micrographs, thus, they are considered as dispersed macroscopically (figure 5.5e-f). It can be observed from the micrographs that there were big agglomerates in start of mixing, as the time passes the tactoids size become smaller and smaller. The clay tactoids size approximately approaches to its optimum value at CP 2, a point which corresponds to plateau of the OMEC as shown in the figure 5.2a.



**Figure 5.5:** Development of morphology investigated by optical microscopy for XHNBR-organoclay compounds mixed at rotor speed of 70 rpm after (a) 1 min, (b) 3 min (CP 1), (c) 4 min, (d) 10 min (near CP 2), (e) 25 min, (f) 30 min

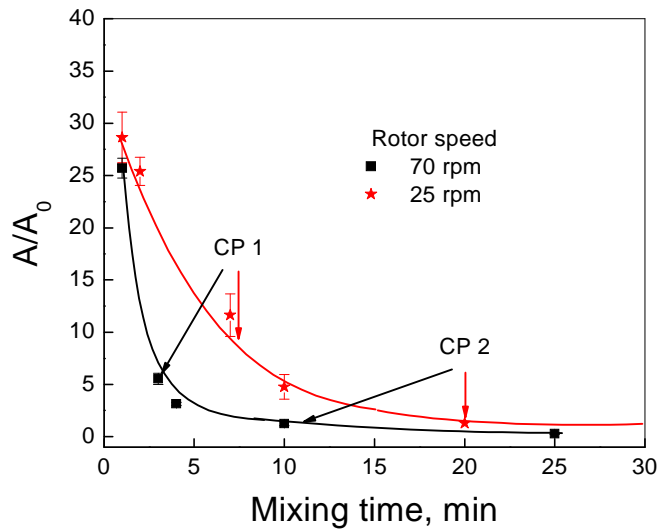
Figure 5.6 shows the change of morphology of the compound mixed at rotor speed of 25 rpm. It can be seen that the morphology change seems to be slowed down as compared to that of the mixed at rotor speed of 70 rpm.



**Figure 5.6:** Optical microscopic images of XHNBR-clay nanocomposites mixed at rotor speed of 25 rpm

after (a) 1 min, (b) 3 min, (c) 7 min (CP 1), (d) 10 min, (e) 20 min (CP 2), (f) 30 min

In order to quantify the morphology development of the mixture the macrodispersion, i.e. the ratio between filler area to the whole area  $A/A_0$ , has been calculated and presented in figure 5.7. With the mixing time the macrodispersion  $A/A_0$  decreases sharply in the first period up to CP 1 and reaches nearly a value of zero at the mixing time corresponding to the CP 2 for both rotor speeds.



**Figure 5.7:** Macrodispersion of XHNBR-clay nanocomposites prepared at different rotor speeds

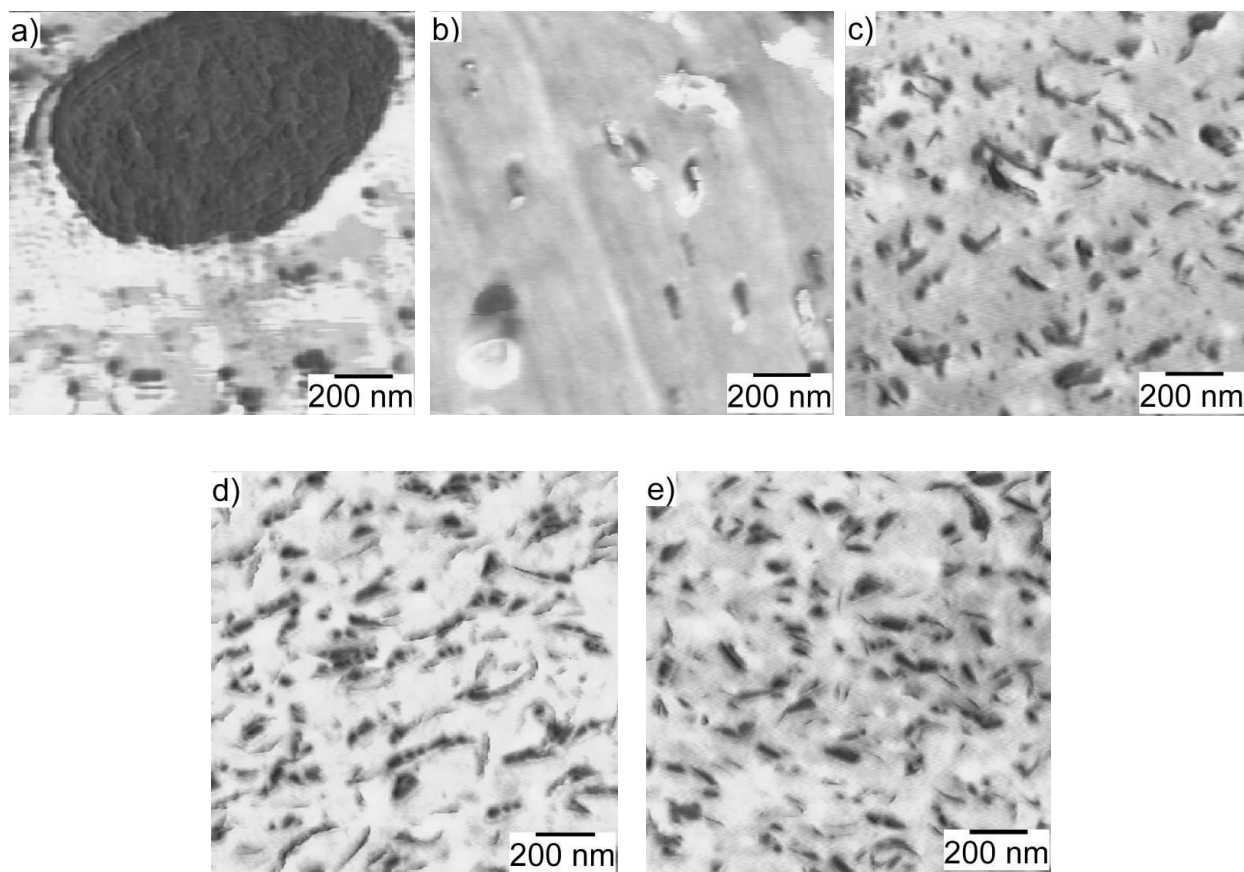
A value of zero means, that no more tactoids with a diameter larger than  $3 \mu\text{m}$  are available. It is clearly seen that the curve of the macrodispersion of the mixture mixed at 25 rpm shifts to a longer mixing time as discussed above.

### 5.2.2.3 Microdispersion

#### 5.2.2.3.1 Atomic force microscopy

The microdispersion of organoclay in rubber has been characterized by AFM and is presented in figure 5.8 for different mixing times. It can be seen that up to CP 1 the agglomerates are broken into small tactoids (figure 5.8a and b). The break-up process of larger agglomerates quickly establishes new clay surface that facilitates the diffusion process of rubber chains into the clay gallery. As a result, in this period the intercalation and the wetting of clay surface by rubber molecules mainly take place that has already been discussed in figure 5.4.

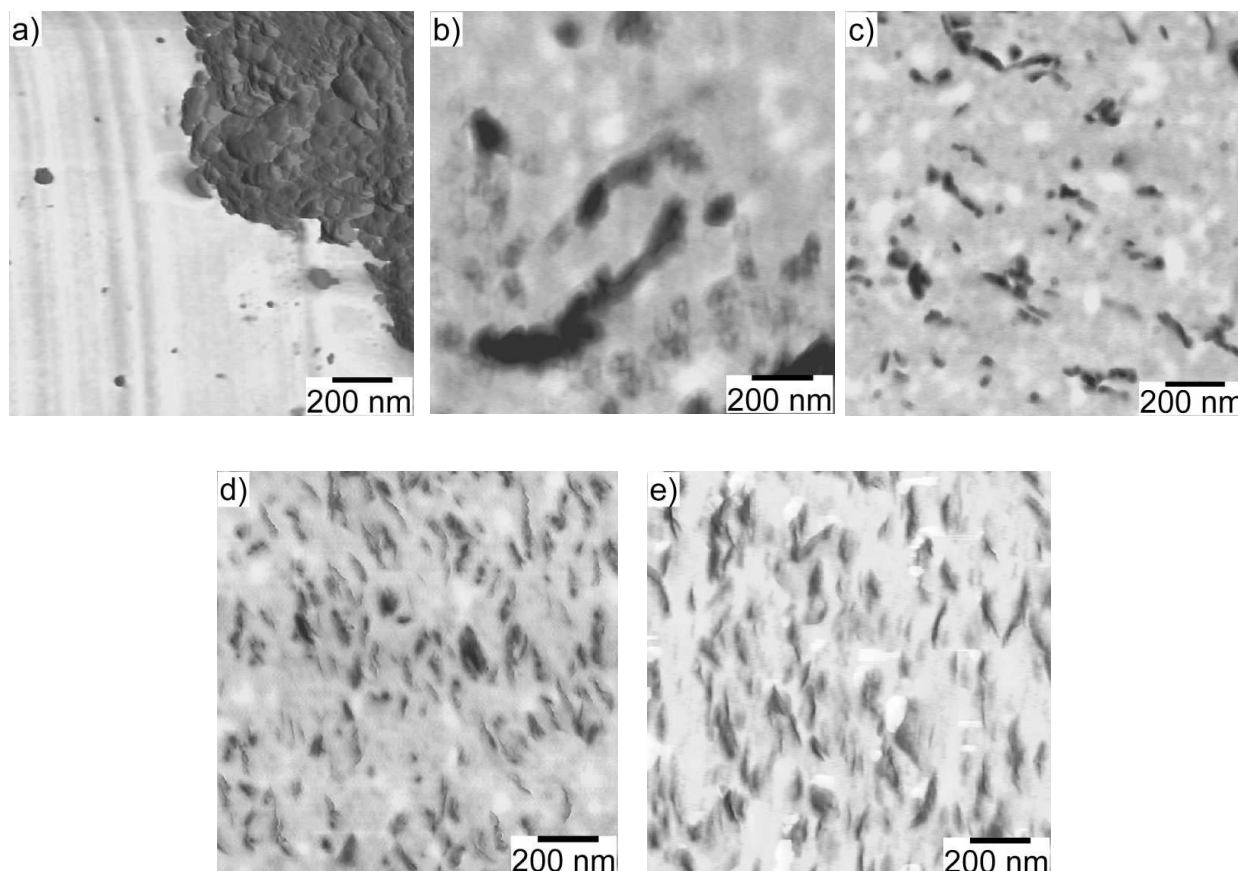




**Figure 5.8:** AFM images of XHNBR-clay nanocomposites mixed with a rotor speed of 70 rpm after (a) 1 min, (b) 3 min (CP 1), (c) 4 min, (d) 10 min (near CP 2), (e) 25 min

In the period between CP 1 and CP 2 the number of separated nanolayers increases due to the exfoliation process (figure 5.8c and d). Dennis et al. [65] proposed the delamination mechanism of organoclay in polyamide 6 which proceeds by sliding platelets apart followed by the insertion of polymer chains inside the clay galleries. As more polymer chains enter and further penetrate between the clay platelets, especially near the edge of the clay galleries and the platelets appear to peel apart. Park et al. [70] proposed in their study on epoxy nanocomposites that clay exfoliation starts at the surface layers of the tactoids and continues towards the center until all layers are exfoliated. Their proposed process is analog to the erosion process as described in the *onion model* used for the explanation of the dispersion process of carbon black in a polymer matrix [125]. As visible in figure 5.8d and e the morphology after CP 2 seems to remain unchanged that could explain the plateau of the online conductance in this period (figure 5.2a).

The constant conductance indicates that the clay dispersion has reached its final state. Further mixing only distributes the clay layers more homogeneously in the polymer matrix.



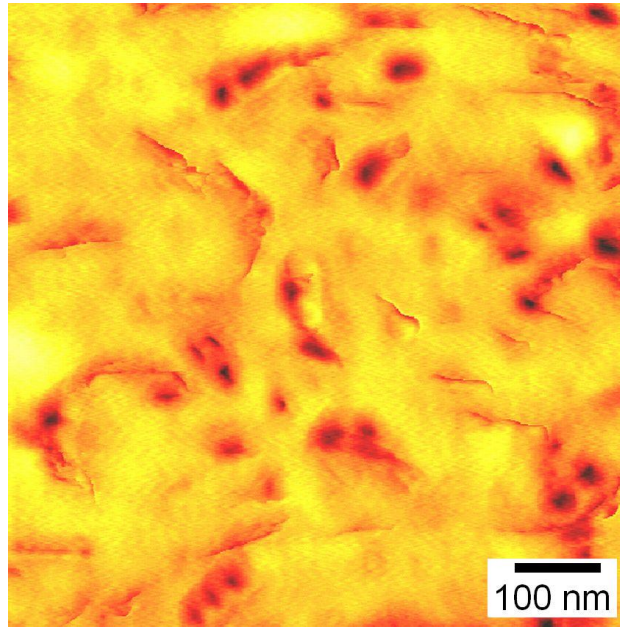
**Figure 5.9:** AFM images of XHNBR-clay nanocomposites mixed with a rotor speed of 25 rpm after (a)1 min, (b) 3 min, (c) 7 min (CP1), (d) 20 min (CP2), (e) 45 min

The microdispersion of the mixture prepared by the rotor speed of 25 rpm (figure 5.9) shows the similar tendency of the morphology change compared to the higher rotor speed (figure 5.8). However, at lower mixing speed the dispersion needs longer mixing time due to the lower energy input.

A magnified AFM micrograph of mixture mixed at 70 rpm for 25 minutes of mixing time is shown in the figure 5.10. Separated clay layers can be seen clearly which represents complete exfoliation. However, the separated nanolayers have a thickness of about 30 nm. The reason for the large thickness measured in comparison to the theoretically expected one could be the existence of a rubber layer bound on the surface of the nanolayer. Due to its restricted mobility



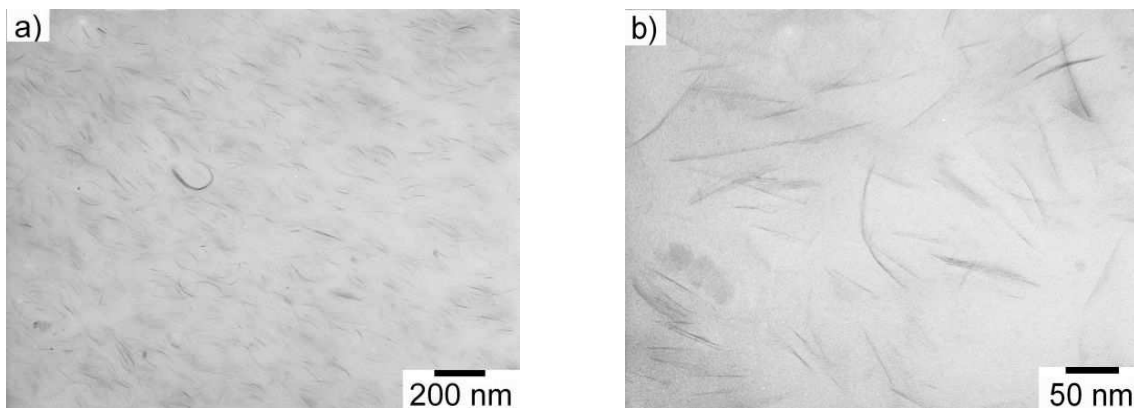
compared to unbound rubber the rubber layer appears in AFM images as a shell surrounding the platelets.



**Figure 5.10:** AFM image of XHNBR-organoclay nanocomposites mixed for 25 min with a rotor speed of 70 rpm

### 5.2.2.3.2 Transmission electron microscopy

One of the specimens, with mixing time of 25 minutes at rotor speed of 70 rpm was characterized by means of TEM. The results are presented in figure 5.11 on two magnifications, higher and lower one. It is obvious that individual layers with a thickness of about 5 nm exist in the matrix.



**Figure 5.11:** TEM images of XHNBR-organoclay nanocomposites mixed for 25 min with a rotor speed of 70 rpm

The layer thickness in the AFM seems to appear larger than in TEM. Major reasons may be the geometry of the tip in AFM, which is used for mechanical interaction with the specimen. There are several studies on polymeric and non-polymeric systems which yielded different results when analyzed by AFM and by TEM [144-147]. The bound rubber, however, is not visible in the TEM images, because there is no contrast between the rubber matrix and the phase boundary layer formed by the bound rubber. Clearly the well exfoliated clay layers can be observed in the figure 5.11b.

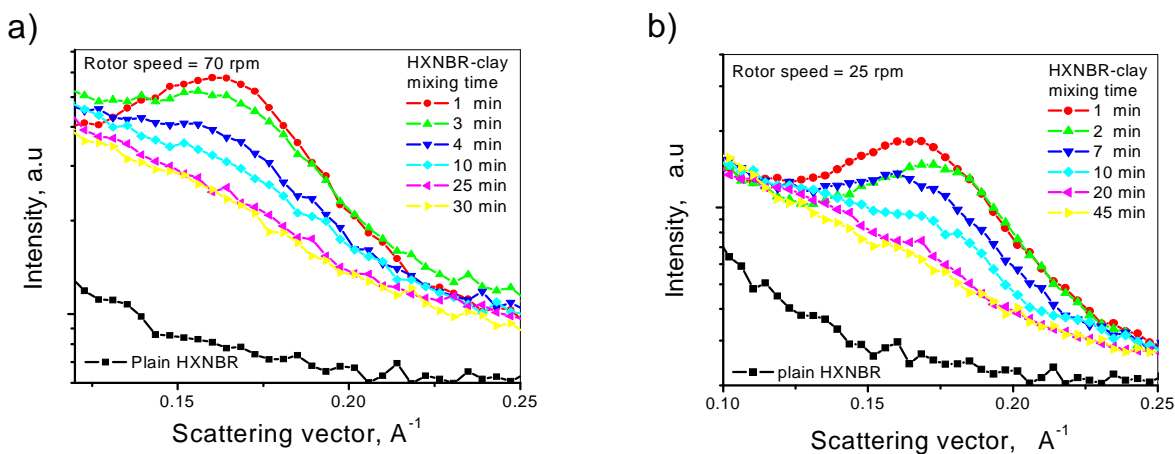
#### 5.2.2.3.3 Small angle X-ray scattering analysis

SAXS in combination with transmission electron microscopy is most frequently used for the characterization of morphology of the polymer-clay nanocomposites. TEM alone is not enough to determine the morphology of a nanocomposite. An intrinsic problem with TEM is that it can only observe a small portion of the sample, which may not be representative, whereas the use of SAXS alone can be very misleading [1], sometime both exfoliated and disordered structures will be SAXS silent (show no peak). The usual complement to TEM is SAXS.

Figure 5.12a and b show the SAXS analysis of the nanocomposites mixed at rotor speed of 70 and 25 rpm respectively. The large broad peaks representing the interlayer spacing of the organoclay changes their intensity with increasing mixing time. The height of the peak also quantitatively reflects the intercalated structure of the clay. The number of individual clay platelets per stack can also be calculated from the breadth of the XRD peak using the Scherrer equation [148]. Figure 5.12a shows that the position of the peaks does not change but the intensity of the peak decreases with mixing time. The data of the clay provider as well as our own investigations show that the organoclay has a basal spacing of 2.0 nm before compounding. The characteristic peak at the scattering vector  $q = 0.15 \text{ \AA}^{-1}$  corresponds to a basal spacing of about 4.2 nm of the organoclay in the nanocomposites. The peak reaches the highest level after a mixing time of about one minute due to the intercalation process. The following decrease of the peak height indicates that the regular structure in the nanocomposite is collapsed, i.e. delaminated, or the clay layers are already homogeneously dispersed.

As discussed above (figure 5.4) the intercalation process runs mainly up to CP 1. Thus, it can be concluded that up to CP 1 both intercalation and exfoliation take place simultaneously but

intercalation is dominant. They also affect the height of the peak in the opposite direction. Due to such an intensive intercalation and exfoliation process a larger amount of ionic species trapped inside the galleries could move now into the rubber matrix. This is the main reason why the online conductance increases so fast in the first stage of the mixing process.

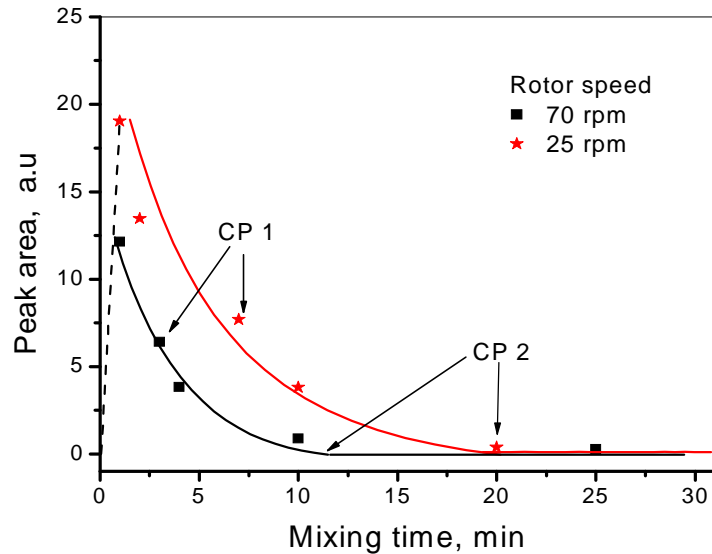


**Figure 5.12:** SAXS analysis of XHNBR-organoclay nanocomposites after different mixing times at rotor speeds (a) 70 rpm (b) 25 rpm

The decrease of peak intensity continues for samples taken till ten minutes of the mixing time, the time corresponds to CP 2 as discussed in figure 5.2a. In the stage between CP 1 and CP 2 only the exfoliation process causes a moderated increase of the online conductance since the release of the ionic species is more convenient. The disappearance of the peak in the SAXS curve after CP 2 means a constant morphology. Here in this case totally exfoliated state has been reached, which causes a constant conductance in this period as shown in figure 5.2.

The SAXS analysis in figure 5.12b show curves of the second series of nanocomposites mixed at rotor speed of 25 rpm. It can be seen clearly that the trend is similar to the former mixed at rotor speed of 70 rpm except the peak disappears after the mixing time of 20 minutes, which corresponds to the CP 2 (figure 5.2b).

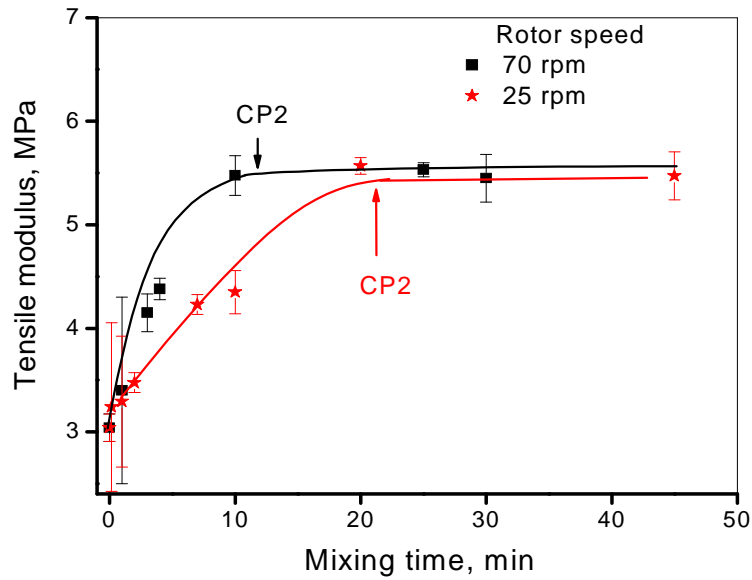
The calculated area under the peak for both rotor speeds is presented in figure 5.13. As the mixing time increases, the peak height and the area under the peak for both rotor speeds decrease. For both higher and lower mixing rate the area under the peak becomes approximately zero at the mixing time of 12 minutes or 20 minutes, respectively. This corresponds to the position of the characteristic point CP 2 of the mixture mixed at 70 rpm or 25 rpm, respectively.



**Figure 5.13:** Peak area under the SAXS curves of figure 5.12 for both rotor speeds

### 5.2.3 Mechanical properties


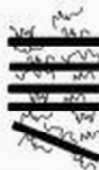
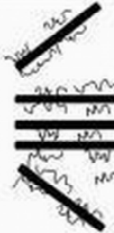

The tensile modulus of polymer clay composites is expected to depend on modulus of the polymer, modulus of the clay platelets, dispersion of the clay, clay loading, degree of crystallinity in the semi-crystalline polymer matrix, orientation of the clay tactoids or platelets, respectively, orientation of polymer crystallites and interfacial stress transfer mechanisms. In the present work, the investigated systems show a continuous change of morphology from larger agglomerates through intercalated tactoids towards separated nano platelets along the mixing time. It is interesting to observe that the development of the tensile modulus changes in connection to the monitored online conductance curve, as well as the morphology of the compounds. In figure 5.14 the tensile moduli of both series are presented in dependence on mixing time. For both rotor speeds (70 and 25 rpm) the modulus increases with mixing time when the organoclay undergoes different dispersion processes. The increase in the modulus is caused by the progressing intercalation and exfoliation, which is consistent with the development of the OMEC values. The modulus reaches a plateau approximately at the CP 2 when the online conductance becomes constant and the morphology is fixed as well. Tensile modulus improved by 80 % when organoclay is exfoliated in the polymer matrix.



**Figure 5.14:** Tensile modulus versus mixing time with different rotor speeds for XHNBR-organoclay nanocomposites

The lower rotor speed slows down the increase of modulus corresponding to the slower development of morphology. Other mechanical properties like stress at break, strain at break, modulus at 100 % or 200 % elongation also show a similar tendency that it changes until CP 2 then becomes constant like the online conductance.

For a better understanding, the correlation between the dispersion processes of organoclay and the online conductance, the rubber layer L, the macro- and microdispersion, as well as the tensile modulus is schematically presented in figure 5.15.

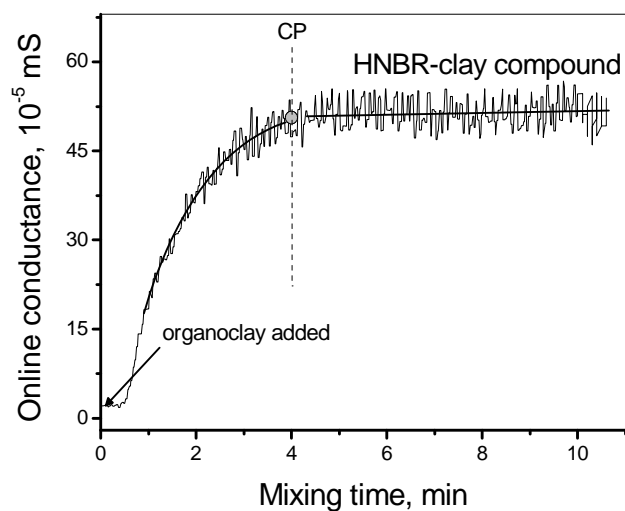
Mixing time	t=0	t = CP1	t = CP2	
Morphology				
Dispersion processes	Intercalation rupture erosion exfoliation	end of intercalation	exfoliation  end of exfoliation	
OMEC	rapid increase		slow increase plateau	
Rubber layer $L$	rapid increase	plateau		
Macrodispersion		increase	plateau	
Microdispersion	agglomerates	aggregates platelets	platelets	
Tensile modulus		increase	plateau	

**Figure 5.15:** Correlation between the dispersion processes of organoclay and the online conductance, rubber layer  $L$ , macro- and microdispersion, as well as the tensile modulus (schematic)

## 5.3 Hydrogenated nitrile butadiene rubber (HNBR)-clay nanocomposites

### 5.3.1 Online conductance chart of HNBR-clay nanocomposites

Figure 5.16 shows the development of OMEC of HNBR-clay nanocomposites in dependence on mixing time at rotor speed of 70 rpm. The OMEC chart indicates that the conductance increases significantly in the start of the clay addition. The development of the conductance passes through a characteristic point CP and then it remains constant. OMEC chart of HNBR-clay nanocomposites is similar to that of XHNBR-clay nanocomposites (figure 5.2, section 5.2) except that in former there is only one characteristic point and conductance level is lower than that of the later, where it passes through two characteristic points and the conductance level is also higher.



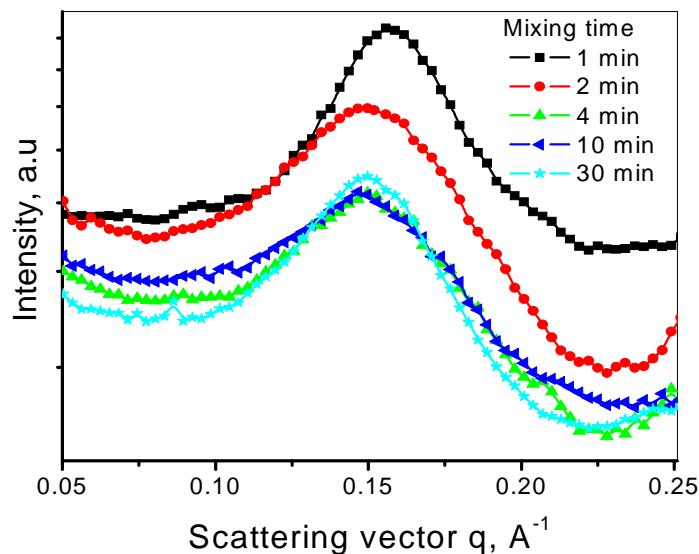
**Figure 5.16:** Online conductance HNBR-clay nanocomposites, in dependence on mixing time

Taking into account the polarity of the matrices an important difference can be observed. The presence of the carboxyl group in XHNBR strongly enhances the rubber-filler interaction and causes the appearance of the CP1 and CP2 at about 4 and 12 minutes (figure 5.2, section 5.2), respectively. There is no such strong electronegative group, carboxylic group, in HNBR which leads to comparatively less interaction of filler with the elastomer that result in the lower level of OMEC curve. Furthermore, only one characteristic point, at 4 minutes of mixing time is observed could be due to poor dispersion of organoclay in HNBR matrix.

### 5.3.2 Characterization of clay dispersion in HNBR

#### 5.3.2.1 SAXS analysis

The XRD spectra of SAXS analysis is shown in figure 5.17. The broad peak corresponding to the interlayer spacing of the organoclay in HNBR-clay nanocomposites evidences the pronounced intercalation with HNBR matrix. The peak position along the horizontal axis does not change, whereas the intensity of the peak changes with mixing times.



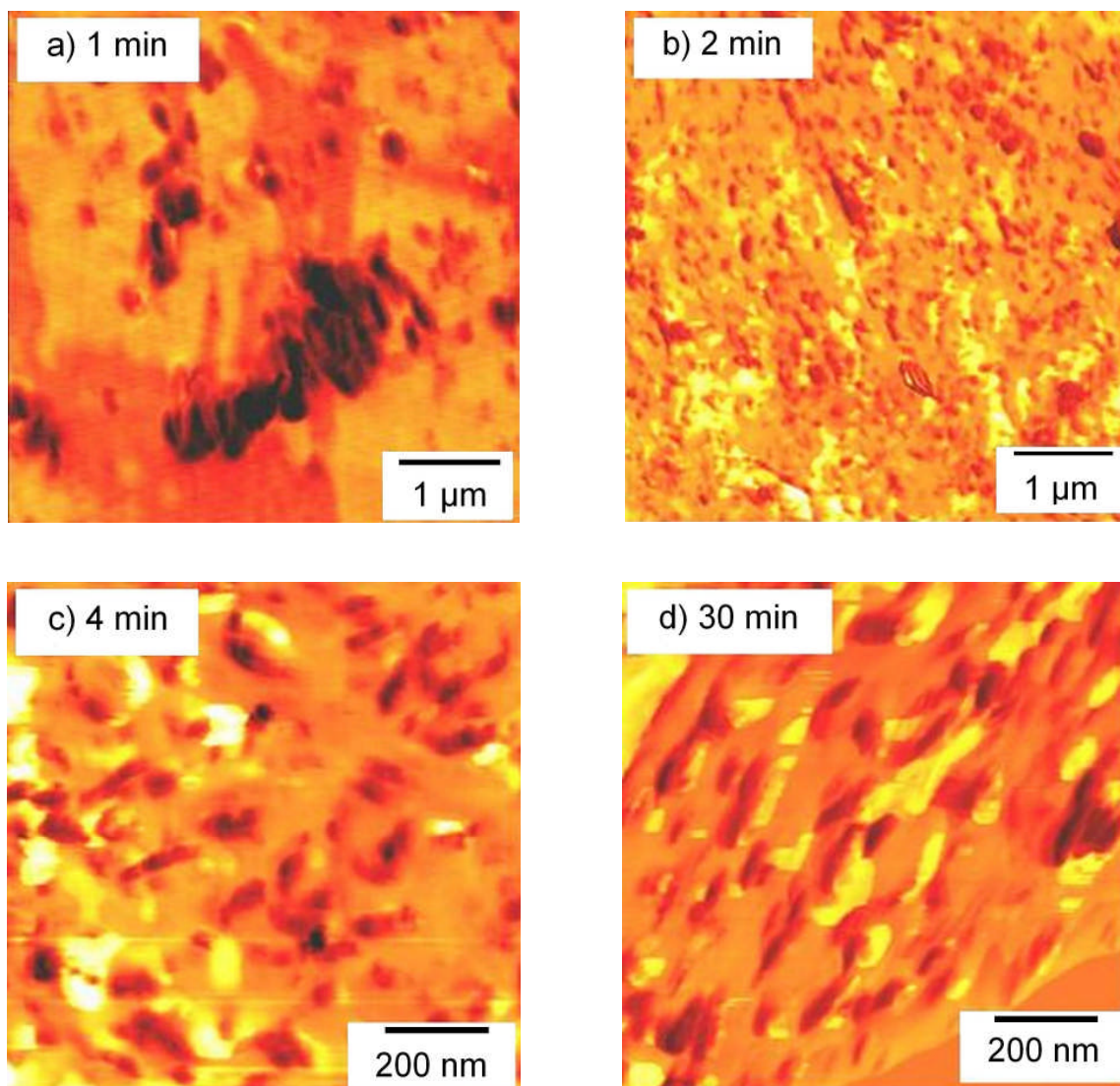
**Figure 4.17:** SAXS analysis of HNBR-clay nanocomposites in dependence on mixing time

The peak of the mixture taken out after 1 minute of mixing time at  $q = 0.155 \text{ \AA}^{-1}$  represents the interlayer spacing of 4.05 nm. The extent of the interlayer spacing is attributed to the intercalation process of HNBR into clay galleries. When the mixing time increases, more and more HNBR chains diffuse into clay galleries that shifts the position of peak to  $q = 0.15 \text{ \AA}^{-1}$  which indicates an interlayer spacing of 4.2 nm. However, no change in position of the peak after 2 minutes is observed, but the intensity decreases with the mixing time up to 4 minutes. Consequently, it may be reasonable to mention that the organoclay is partially exfoliated in the polymer matrix. However, in the period from 4 minutes to 30 minutes the height and position of the peak remains unchanged. That means the end state of morphology that consists of both the intercalated and exfoliated structure of clay, which is received already at 4 minutes. That explains the plateau of the online conductance after 4 minutes.

### 5.3.2.2 Atomic force microscopy

The morphological investigations have been carried out by atomic force microscopy. AFM micrographs of HNBR-clay nanocomposites as a function of mixing time are shown in figure 5.18.





**Figure 5.18:** AFM-images of HNBR-clay nanocomposites in dependent on the mixing time

It can be seen that up to CP (4 minutes) the agglomerates are broken into small tactoids (figure 5.18a and b). In figure 5.18c and d (after CP) clay aggregates with size of about 200-300 nm are visible and the morphology seems to remain unchanged; which is nicely correlated with the plateau of the OMEC (figure 5.16). Figure 5.18d demonstrates that further mixing distributes the clay layers more homogeneously in the polymer matrix, and does not exfoliate the clay any more. Note that the SAXS analysis does not deliver any experimental evidence for the exfoliation which is also corroborated by AFM micrographs.

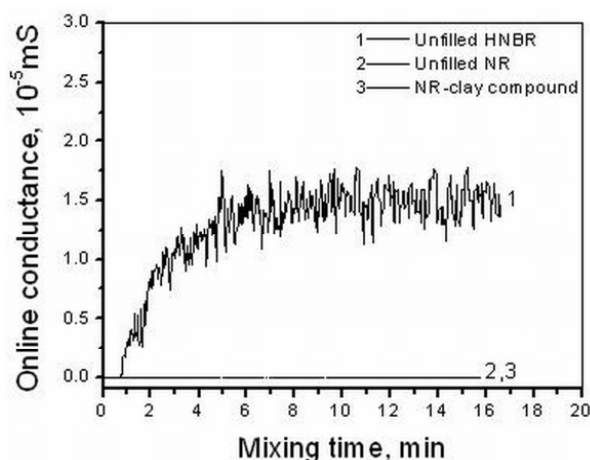
Comparing the AFM micrographs of HNBR-clay nanocomposites with XHNBR-clay nanocomposites (figure 5.8); it is interesting to note that former shows predominantly

intercalated morphology whereas later predominantly show well exfoliated clay structures. The reason of morphology difference can be attributed to different reactivity of the organoclay with HNBR and XHNBR matrices. This is also well corroborated by SAXS analysis (figure 5.17), which represents that the peak height remains constant, and OMEC chart (figure 5.16) shows that the conductance also remains constant after CP. Gatos et al. [44] have thoroughly investigated nanocomposites formation of hydrogenated nitrile butadiene rubber as a function of surfactant types in various organoclays and found on the basis of SAXS and TEM that both intercalated/exfoliated structures are obtained. There is no complete exfoliation, however better interaction has been observed for more polar organoclay. It has also been shown in a number of investigations that melt mixing of NBR with organoclay usually results in predominantly intercalated structures with tactoids sizes in the range of 20 nm whereas some part of the clay has been exfoliated [32,38,103,149-152 ]. However complete exfoliation has not been observed.

## 5.4 Natural rubber NR-clay nanocomposites

### 5.4.1 Conductance of NR-clay nanocomposites

The OMEC curve of the pure NR and HNBR versus the mixing time is shown in Figure 5.19. No conductance signal was recorded for NR (figure 5.19, curve 2), because it is non-polar. The measured conductance of HNBR is originated only in connection to the presence of additives and residues of catalysts used in the polymerization processes. In such a polar medium like HNBR matrix catalyst residues are dissociated into ions which act as charge carrier. The dissociation process of the catalyst residues does not take place in a non-polar medium like NR. Therefore, no electrical signal was received by compounding NR. The development of online conductance on addition of organoclay into NR and HNBR is depicted by figure 5.19, curve 3 and figure 5.16 respectively. While HNBR-clay increases significantly and reaches at a critical point a plateau after 4 minutes as has been discussed in details in section 5.3, the NR-clay does not show any electrical signal.



**Figure 5.19:** OMEC chart of pure NR, HNBR and NR-clay nanocomposites in dependence on mixing time

The absence of the online conductance in the case of NR-clay nanocomposites can be explained by the fact that the conductance term of NR,  $\sigma_{NR}$  is nearly zero (extremely small), thus, the  $\sigma_{comp}$  is too small and does not fall in the measuring range of the equipment, so it is considered as zero. The offline resistivity of the plain NR and NR-clay nanocomposites are shown in table 5.1. The decrease of the offline resistivity after addition of organoclay observed for NR-clay compounds is due to the contribution of the ionic conduction of surfactant released from clay galleries.

**Table 5.1:** Online conductance and offline resistivity of plain rubber and the nanocomposites

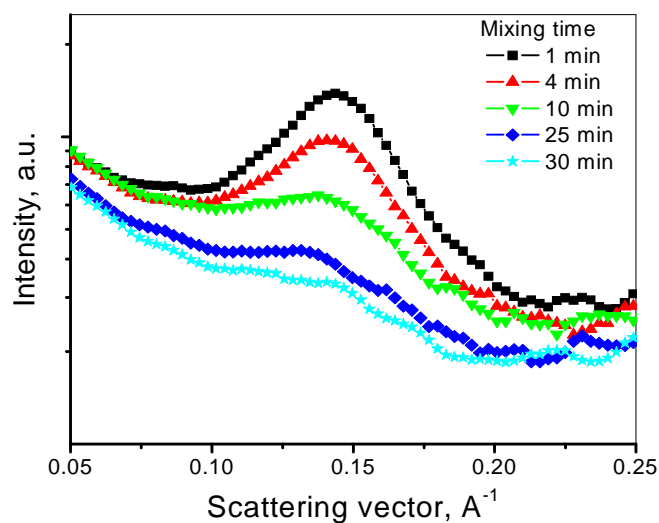
Sample	Online conductance, mS	Offline resistivity, $\Omega\text{cm}$
plain NR	Out of measuring range	$5.5 \times 10^{15}$
NR-clay nanocomposites (4 min mixing time)	Out of measuring range	$6.5 \times 10^{11}$
plain NBR	$1.5 \times 10^{-5}$	$2.3 \times 10^{11}$
HNBR-clay nanocomposites (4 min mixing time)	$51 \times 10^{-5}$	$6.5 \times 10^9$

The offline resistivity of the plain HNBR and of the HNBR-clay nanocomposites after 4 minutes of mixing time is also shown for comparison with NR in table 5.1. The decrease of the offline resistivity after addition of organoclay is as mentioned above observed for HNBR-clay due to the contribution of the ionic conduction of surfactant released from clay galleries.

## 5.4.2 Characterization of clay dispersion in NR

### 5.4.2.1 SAXS analysis

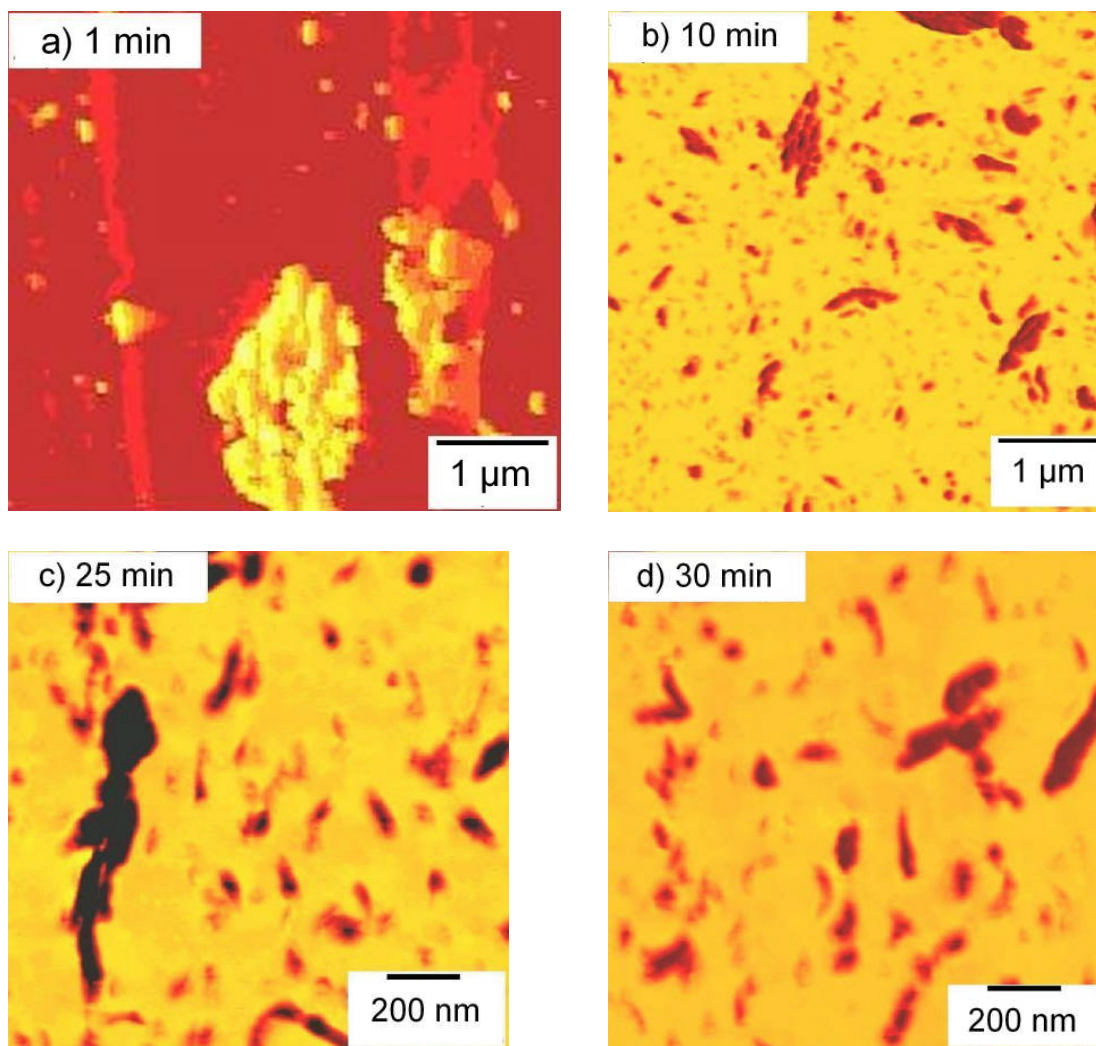
In figure 5.20 the SAXS curves of NR-clay compounds are presented in dependence on the mixing time. The characteristic peak at the scattering vector  $q = 0.14 \text{ \AA}^{-1}$  corresponds to an interlayer spacing of about 4.5 nm of clay in the nanocomposites, which is larger than that of the HNBR-nanocomposites. As the mixing time increases, the peak position remains unchanged, while the peak height decreases, because both intercalation and exfoliation processes take place simultaneously and they affect the height of the peak in the opposite direction, prolonging mixing decreases peak intensity. As the mixing time increase, more and more mechanical energy input during mixing cause the diffusion of polymer chains in clay galleries that ultimately leads to the exfoliation of the clay [65]. After 30 minutes of mixing time, there is only a small peak that corresponds to a predominantly exfoliated structure of clay in the NR matrix.



**Figure 5.20:** SAXS profiles for NR-clay nanocomposites in dependence on mixing time

#### 5.4.2.2 Atomic force microscopy

The kinetics of microdispersion of organoclay in NR in dependence of mixing time is characterized by AFM and is presented in figure 5.21. A continuous change from larger agglomerate through tactoids to separated clay layers can be observed with increasing mixing time. Organoclay has been dispersed better in the non-polar NR matrix as compared to the HNBR. The reason could be the better diffusion process of the linear chains of NR.

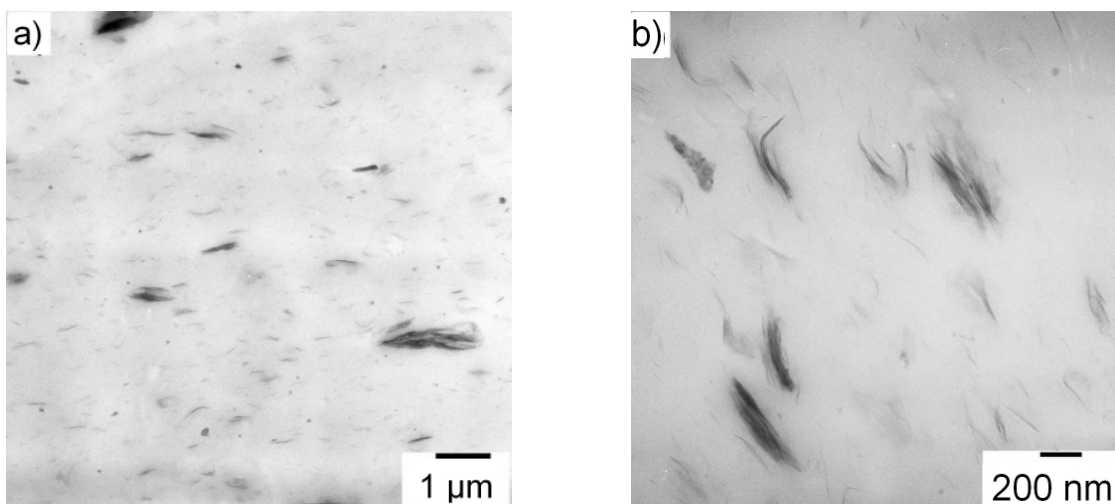


**Figure 5.21:** AFM-images of NR-clay nanocomposites at different mixing time

The SAXS analysis and the morphological investigations carried out by AFM show that the each of the interlayer distance and the tactoids sizes reduces with the increase of mixing time. The extent of intercalation/exfoliation depends on several factors such as polymer transport process through the agglomerate micro-pores, agglomerate size, diffusion of elastomer chains in clay layers and nature of the polymer itself [52].

#### **5.4.2.3 Transmission electron microscopy**

Figure 5.22 shows the TEM micrographs, both at high and low magnification, of NR-clay nanocomposites after 30 minutes of mixing time. It can be clearly analyzed that exfoliated clay layers also exist besides some small tactoids. Dark lines in this figure correspond to the clay layer evenly dispersed in the rubber matrix.



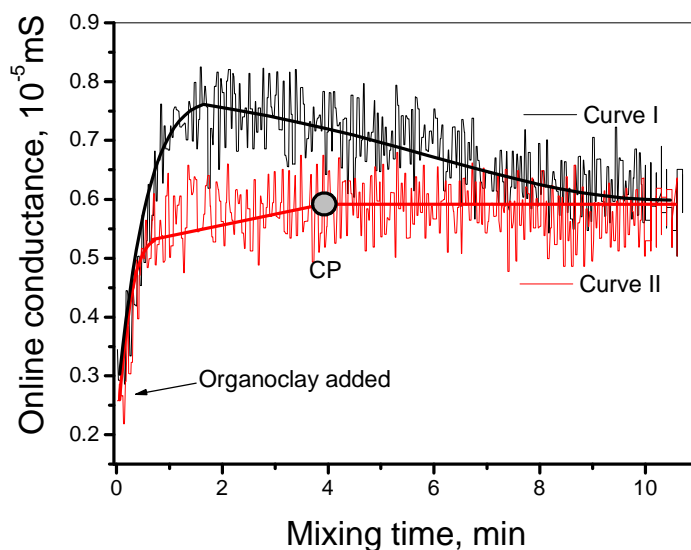
**Figure 5.22:** TEM images of NR-clay nanocomposites with 5 phr organoclay mixed for 30 min at (a) low magnification and (b) high magnification

It can be seen that the organoclay is intercalated (agglomerates, tactoids) and exfoliated (individual layers) in NR matrix. Similar morphological structures were also observed in investigations carried out by Varghese et al. [51] and Teh et al. [53]. The TEM images provide a direct evidence for the poor dispersion of organoclay in the NR matrix. Sharif et al. have melt mixed NR and clay and investigated the effect of clay on different properties [153]. They have shown that NR predominantly yields the intercalated structure of NR-clay nanocomposites.

## 5.5 Epoxidized natural rubber ENR-clay nanocomposites

### 5.5.1 Online conductance of ENR-clay nanocomposites

The development of online conductance of ENR-clay nanocomposites as a function of mixing time is shown in the figure 5.23. It shows that OMEC increases rapidly in the start of mixing, reaches a local maximum, and then decreases slightly. However, the important difference of the online conductance of XHNBR-clay nanocomposites and unmilled ENR-clay nanocomposites (curve I) is that the former passes through two characteristic points (assigned as CP1 and CP2 corresponding to intercalation and exfoliation respectively) and then remains constant whereas the later shows the similar behavior in comparison to XHNBR-clay nanocomposite in the start of mixing, i.e. increases significantly except that it reaches a maximum and then starts decreasing and finally a plateau is reached.



**Figure 5.23:** Online conductance ENR-clay nanocomposites (clay contents 5 phr) versus mixing times of unmilled (curve I) and milled at 120 g/25 min (curve II)

The quick increase of OMEC in the start of mixing is due to release of surfactants from the clay galleries. In case of ENR at the same time the surfactants are consumed due to the tendency to form H-bonding between epoxy group of ENR and surfactants [154]. It is expected that the consumption of surfactants continues at the uniform rate. In simpler words, there is competition between the release and consumption of the surfactants. In the start of mixing process the



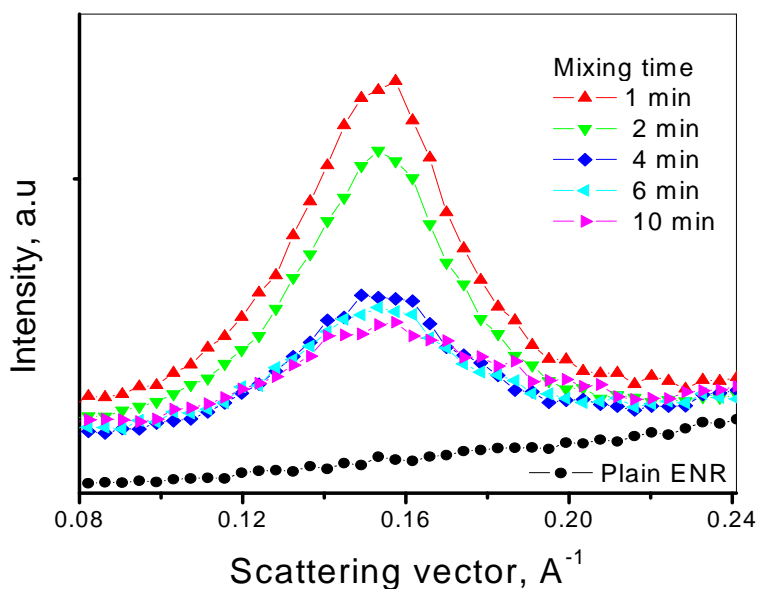
surfactant release process is faster as compared to the consumption process that results in an increase of conductance. After reaching a local maximum, the release of surfactant slows down but the consumption continues so in this mixing period the more surfactants are consumed than released. As a result, the OMEC decreases.

Similarly curve II shows the OMEC of ENR (which was milled at 120 g/ 25 minutes before mixing)-clay nanocomposites independence of mixing time. The OMEC value of curve II is lower than curve I. The viscosity of ENR decreases, when it was milled before mixing could be due to chain scission as discussed by Le et al. [14]. It is expected that the entities formed during the milling of ENR consumes surfactant more vigorously, so lower level of OMEC has been observed.

## **5.5.2 Characterization of clay dispersion in ENR**

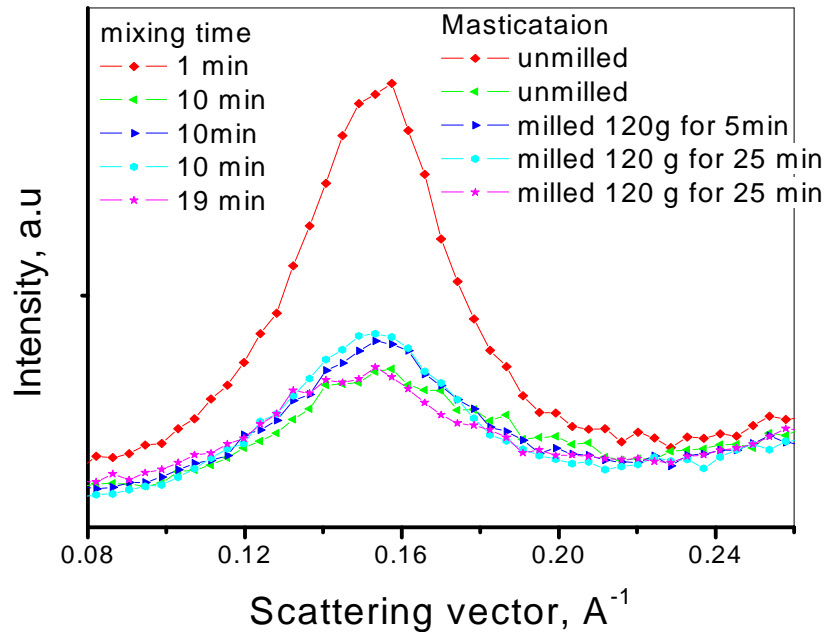
### **5.5.2.1 SAXS analysis**

SAXS analysis of unmilled ENR-clay nanocomposites in dependence on mixing time is shown in the figure 5.24. The peak represented in the figure at scattering vector  $0.15 \text{ \AA}^{-1}$  corresponds to the layer spacing (4.2 nm). The peak height is decreasing but the peak position remains unchanged. The decrease of peak height along the mixing time means that the regular structure is decreasing with mixing time, which implies that the clay layers are exfoliated in the polymer matrix. However, it can be analyzed that peak position in the SAXS investigation remains unchanged after 4 minutes of mixing time (CP), even after mixing for a longer time, the peak position and shape does not change (figure 5.24). This implies that a constant morphology has been reached after 4 minutes of mixing time. The final morphology could consist of intercalated and exfoliated structures. The characteristic point CP of ENR-nanocomposites corresponds to the CP 1 of the XHNBR-nanocomposites. Figure 5.25 shows the effect of mastication on SAXS analysis of ENR-clay nanocomposites. It reveals that the peak position remains constant for different mastication and mixing times.



**Figure 5.24:** SAXS analysis of plain and unmilled ENR-clay (5 phr) nanocomposites for different mixing times

It leads to the fact that for ENR-clay nanocomposites although during the mastication process undergoes chain scission, which ultimately leads to decreasing viscosity. The interaction of lone pair on oxygen and the surfactant could inspire the quick insertion of ENR chains into the clay galleries [154] during compounding with organoclay, which leads to a plateau of online conductance in short mixing time. At the same time due to bulky group formed by the interaction of surfactants and epoxy the mobility of ENR chains could decrease. The lower chain mobility causes the lower infiltration rate and therefore hampers the exfoliation process of the intercalated structures. The SAXS data is quite correlated with the online conductance of ENR-clay mixture, which shows that online conductance increases significantly in short time then a slow decrease up to 4 minutes of mixing time and finally become constant due to constant intercalated/exfoliated structures. These results also corroborate the conjecture that constant online conductance is due the uniform morphology. Varghese et al. [51] prepared ENR-clay nanocomposites using different types of clays with sulfur cure system. Both partly intercalated and partly exfoliated structures were obtained. It was also observed that for modified clay interlayer distance was also reduced than its original value before mixing. The reduction of the interlayer distance was argued due to a zinc sulfur-amine complex formation. Complete exfoliation structure were not obtained [51].

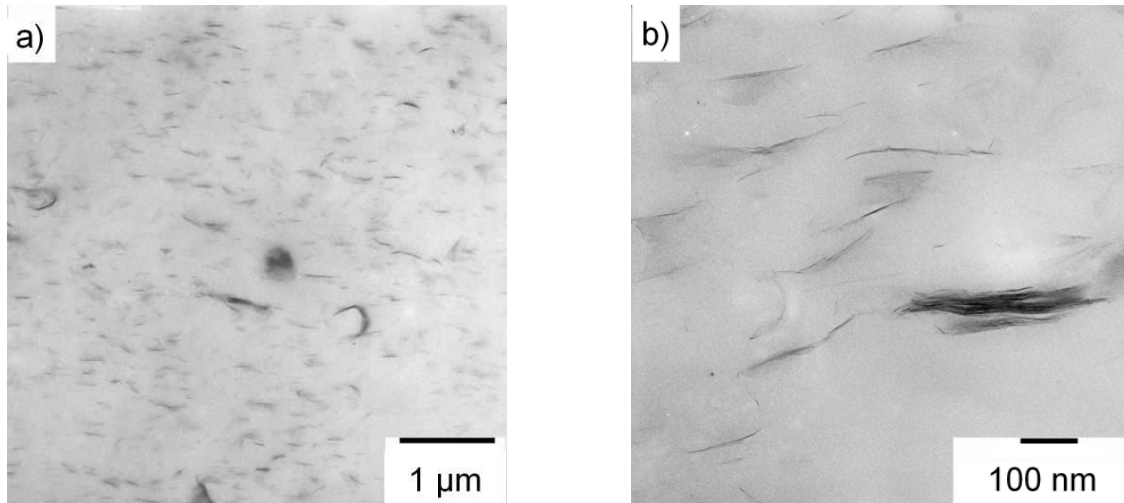


**Figure 5.25:** Mastication effect on the SAXS analysis of ENR-clay nanocomposites

Vu et al. [52] investigated the dispersion of clay in non-polar rubber matrix, i.e. cis-1,4-polyisoprene (IR) and the polar, i.e. ENR, by melt mixing and by dissolving the elastomer in solutions. They have shown only on the basis of WAXS results that intercalation was followed by exfoliation, but they have not given any morphological evidence for exfoliation of clay.

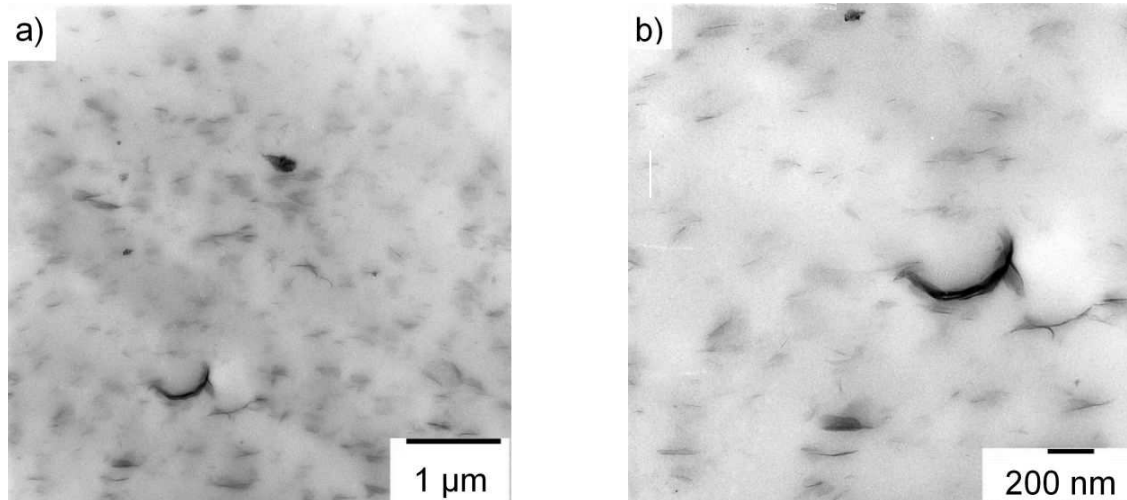
### 5.5.2.2 Transmission electron microscopy

Figure 5.26 shows the TEM analysis of the ENR-clay nanocomposites collected after 4 minutes of mixing time, both on high and low magnifications. Figure 5.26a shows the global view of the ENR-clay nanocomposites. It can be seen that clay is uniformly dispersed everywhere along some aggregates. Figure 5.26b shows the nanostructure of the nanocomposites. It can be clearly seen that intercalated/exfoliated structure are obtained. However, complete exfoliation is not obtained as seen by SAXS investigation. Similar results of intercalation/exfoliation of organoclay in ENR rubber matrix have also been observed by Varghese et al. [51]. Comparing the TEM micrographs of ENR-clay nanocomposites with that of NR-clay nanocomposites after 30 minutes (figure 5.22) it can be seen that ENR-clay nanocomposites show more exfoliated clay platelets with less tactoids than NR-clay nanocomposites.



**Figure 5.26:** TEM pictures of ENR clay (5 phr) nanocomposites after 4 minutes of mixing time (CP) taken at lower magnification (a) and at higher magnification (b).

This is due to the better interaction of organoclay with ENR than NR, which has arisen due to interaction of the epoxy groups of ENR with the amine group of the surfactant [154].



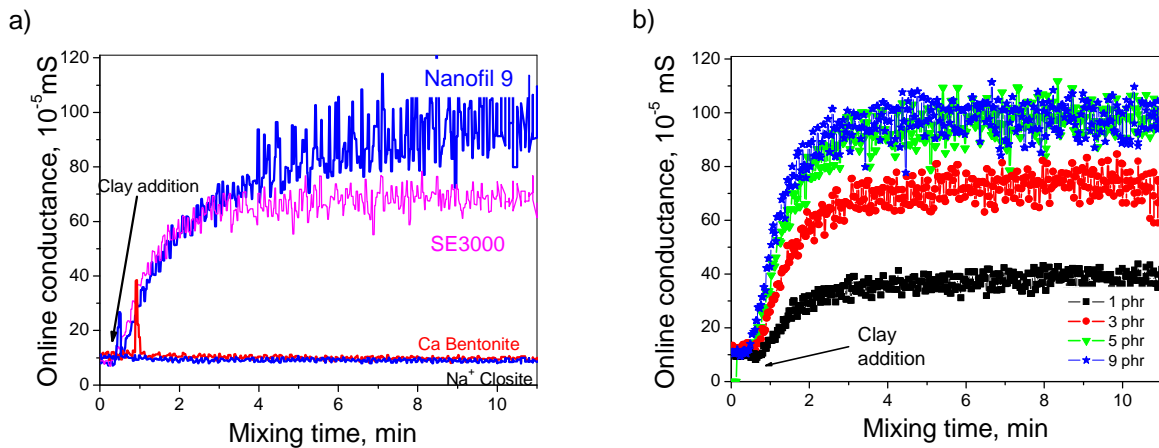
**Figure 5.27:** TEM pictures of ENR clay (5 phr) nanocomposites after 10 minutes of mixing time taken at lower magnification (a) and at higher magnification (b).

Figure 5.27 shows the morphology of the ENR-clay nanocomposites at mixing time of 10 minutes. This morphology is similar to that of nanocomposites mixed at 4 minutes as represented in figure 5.26. This implies that after 4 minutes morphology seems to remain unchanged.

However, the OMEC decrease after 4 minutes is due to the interaction of amine groups of surfactant with epoxy groups in the ENR chains [154].

### 5.5.3 Variation of clay types and concentrations of organoclay

Figure 5.28a shows the effect of different types of modified and unmodified clays on OMEC. Note that unmodified clay types ( $\text{Na}^+$  Cloisite and Ca Bentonite) do not show OMEC chart, whereas modified clay types (SE 3000 and Nanofil 9) shows increasing conductance with mixing time.



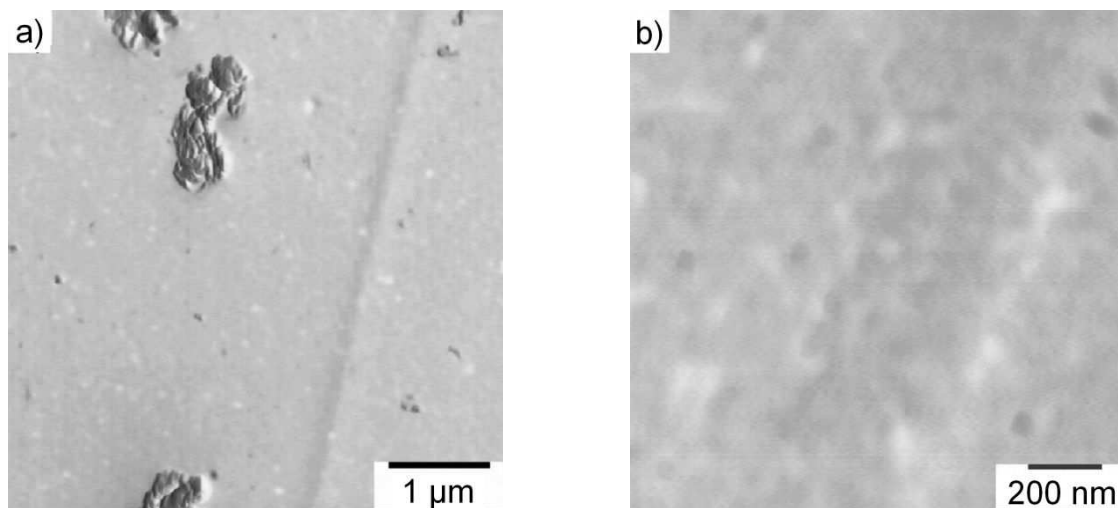
**Figure 5.28:** OMEC of XHNBR-clay nanocomposites with different (a) clay types (b) clay concentrations

It is obvious that Nanofil 9 and SE 3000 show OMEC spectra with different characteristic points. They have different surfactants which show different compatibility to the same rubber matrix. So the surfactants have different tendency to be released under same processing conditions. Therefore different dispersion behavior and the OMEC chart can be observed.

Unmodified clays ( $\text{Na}^+$  Cloisite and Ca Bentonite) do not show any OMEC as depicted in figure 5.28a. The absence of conductance can be explained by the fact, that clays are naturally hydrophilic, with  $\text{Na}^+$  cations bonded between the sheets of oxygen and silicon. Such unmodified layered clays have an interlayer spacing of approximately 1 nm. Therefore, as expected, due to the hydrophilic nature of  $\text{Na}^+$ -clay, it is hard to intercalate by the bulky chains of XHNBR.

In order to explore the background behind the absence of OMEC chart for unmodified clay, the morphology of rubber-Na Cloisite composites system has been analyzed. AFM micrographs shown in figure 5.29 clearly show some large clay tactoids that means unmodified clay is not

intercalated even for a longer mixing time. The unmodified  $\text{Na}^+$ -Cloisite agglomerates are simply incorporated into the rubber matrix. Also the AFM image with higher magnification does not show any separated nanolayers (figure 5.29b).



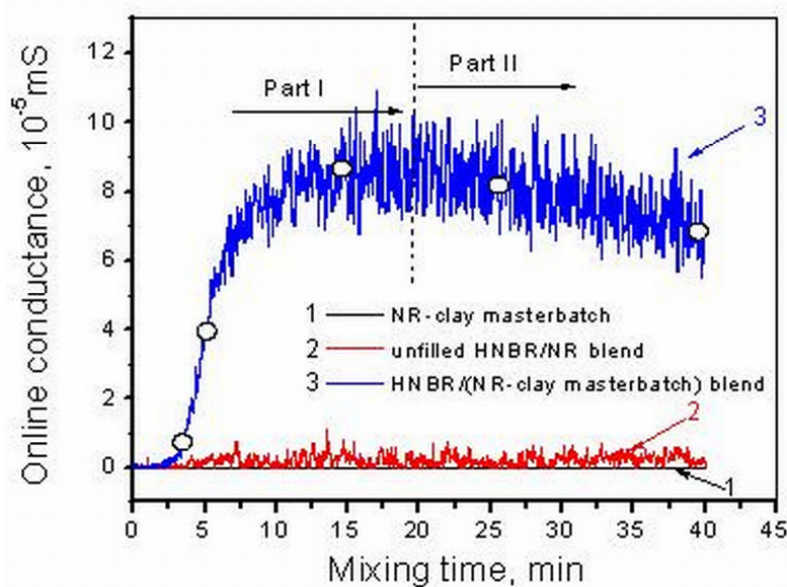
**Figure 5.29:** AFM images of HNBR- $\text{Na}^+$  Bentonite composite at different magnification

Sharif et al. [104] found an interlayer spacing of about 1.3 nm after compounding NBR and NR/EVA with  $\text{Na}^+$ -clay that means that no intercalation process took place. In this case,  $\text{Na}^+$  cations are trapped inside the clay galleries explaining why no electrical signal was observed in the XHNBR mixtures. Otherwise, the electrical signal obtained in  $\text{Na}^+$ -clay/PEO composites as mentioned in [122] is a result of a solution process that allows PEO to intercalate  $\text{Na}^+$ -clay. Such intercalated state imparts the nanocomposite ionic conduction due to the mobility of  $\text{Na}^+$  ions.

## 5.6 Blends of HNBR and NR (polar/non-polar blend system)

### 5.6.1 Correlation of online conductance and development of the structure of the blend

The NR-clay masterbatch was mixed with the pure HNBR to produce a HNBR/(NR-clay masterbatch) blend. The mixing time to produce the NR-clay masterbatch was kept as 10 minutes. The clay loading used in the masterbatch was 10 phr so that the HNBR/(NR-clay masterbatch) maintained 5 phr of clay. Thus, before blended with HNBR, it can be assumed that the NR-clay masterbatch shows a SAXS curve similar to the figure 5.20, the middle curve corresponding to 10 minutes of mixing time and a morphology corresponding to figure 5.21b (section 5.3). The OMEC charts of the NR-clay masterbatch, unfilled HNBR/NR blend and HNBR/(NR-clay masterbatch) blend are presented in figure 5.30.



**Figure 5.30:** Online conductance of NR-organoclay masterbatch (curve 1), unfilled HNBR/NR blend (curve 2), and HNBR/(NR-organoclay masterbatch) blend (curve 3) versus mixing time

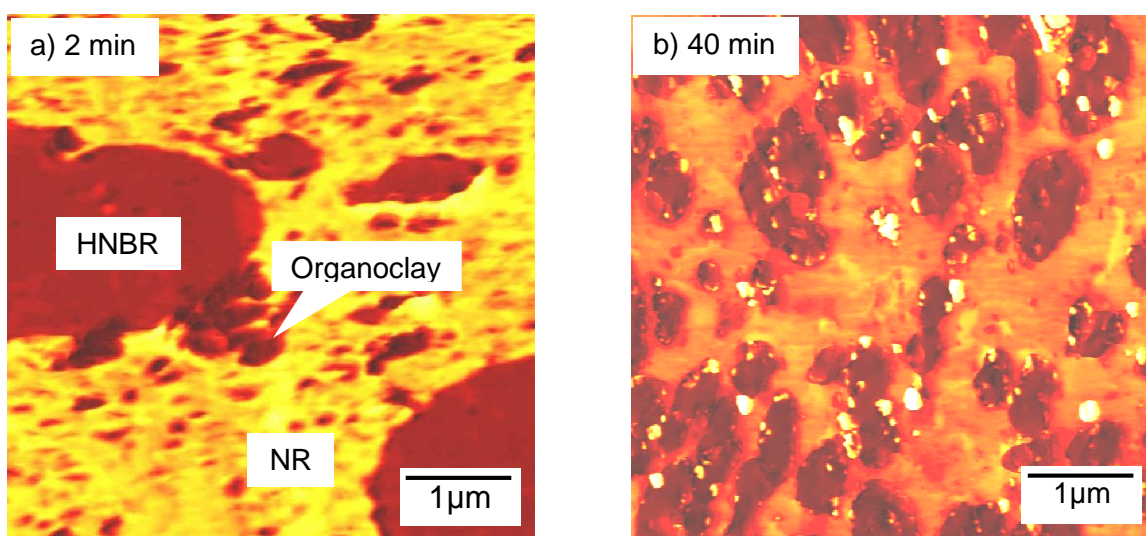
The conductance values of NR-clay masterbatch are below the range of the measuring equipment. They are considered as zero (figure 5.30, curve 1). The conductance curve of the unfilled 50/50 HNBR/NR blend (figure 5.30, curve 2) is also very low since in this blend the OMEC is originated only by the unfilled HNBR phase. Initially, when HNBR was mixed with NR-clay masterbatch it was expected that the conductance curve of the HNBR/(NR-clay masterbatch) blend will lie in the same level as that of the unfilled HNBR/NR blend. However, the OMEC

curve of HNBR/(NR-clay masterbatch) blend (curve 3) shows an unexpected chart with a higher conductance level compared to the unfilled HNBR/NR blend.

In order to explain the structural background of the online chart, the OMEC curve of HNBR/(NR-clay masterbatch) blends can be divided into two main parts. First part begins at the start of compounding the blend phases until the conductance reaches its maximum value. The second part begins from point where online conductance starts declining to the end of compounding process. The conductance curve and structure of the blend have been investigated by means of the extraction experiment, AFM, TEM and SAXS techniques.

### 5.6.1.1 Clay localization

The qualitative analysis of clay localization has been carried out by investigating the morphology of the blend-clay nanocomposite using AFM, TEM and SAXS. The clay migration becomes obvious by taking a look at the AFM images at the high magnification as presented in figure 5.31.



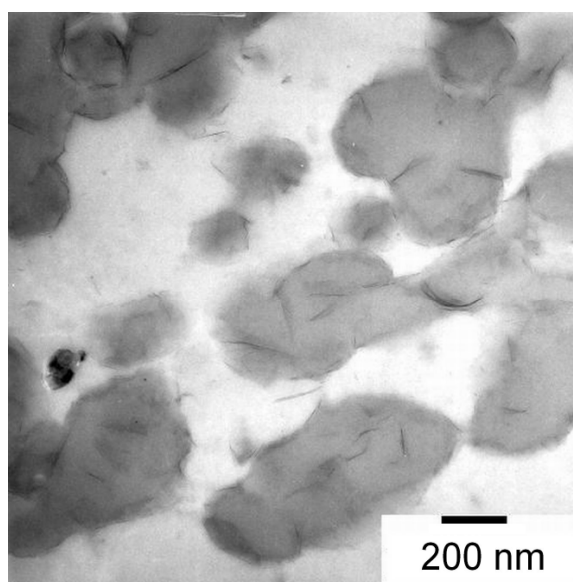
**Figure 5.31:** Clay immigration in HNBR/(NR-clay masterbatch) blend as a function of mixing time

After 2 minutes of mixing time, a number of clay agglomerates (black points) with a size of 500 nm is visible in the NR-phase (light area) and no clay in the HNBR phase (dark area). The clay tactoids migrates from NR to HNBR phase, with increasing of mixing time (figure 5.31). The AFM image of samples taken out at 40 minutes (figure 5.31b) reveals clearly a dominant localization of the clay tactoids in the HNBR phase. After 40 minutes of mixing time approximately all the organoclay has been immigrated to the more polar phase, i.e. HNBR.



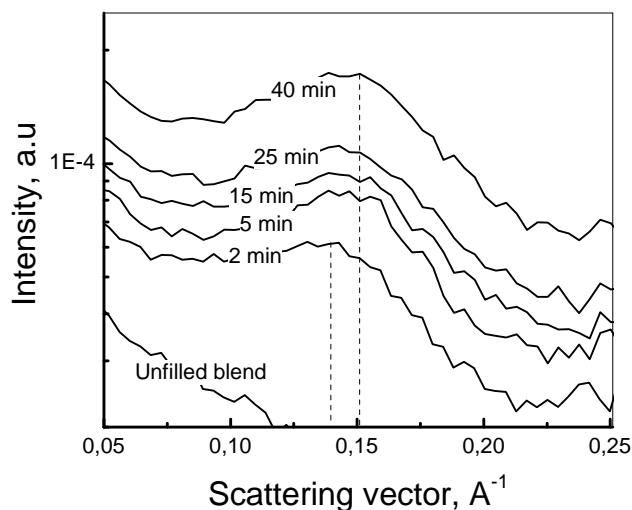
Comparing figure 5.30 and figure 5.31 it can be visualized that at the beginning of mixing process, when all the organoclay was in the NR phase, no online conductance has been observed, whereas for longer mixing time due to migration of clay from non-polar NR to polar HNBR phase higher OMEC value has been observed as depicted in the figure 5.30.

The hypothesis based on OMEC and AFM about a preferential location of the clay within more polar HNBR of the binary blend needs to be critically analyzed by means of further morphological analyses. TEM was employed to follow the nanostructure of the HNBR/(NR-clay masterbatch) blends. TEM image of randomly microtomed samples of HNBR/(NR-clay masterbatch) blend after 40 minutes of mixing time and a representative image is shown in the Figure 5.32.



**Figure 5.32:** TEM images HNBR/(NR-clay masterbatch) blends after 40 min of mixing time

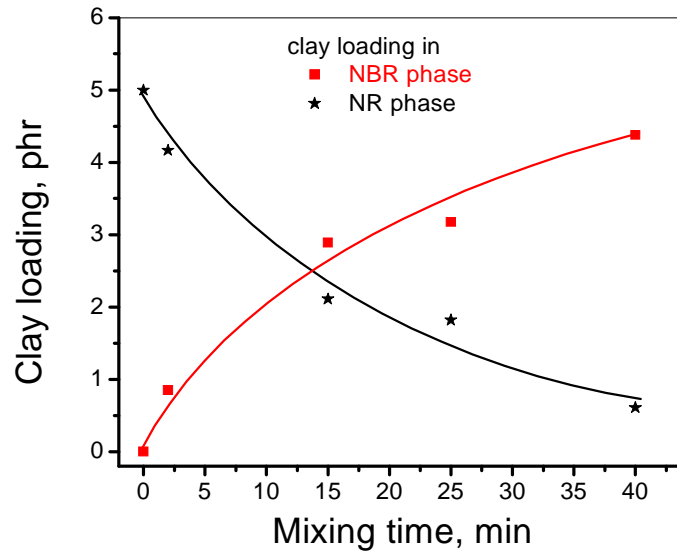
The clay appears as deep dark features in the dark gray dispersed phase, inline with the images taken by AFM, where preferential localization of organoclay stacks with thickness of few tens of nanometers has been observed.



**Figure 5.33:** SAXS analysis of HNBR/(NR-clay masterbatch) blends in dependence on mixing time

Figure 5.33 represents the SAXS analysis of unfilled HNBR/NR blend and HNBR/(NR-clay masterbatch) blends in dependence on mixing time. The SAXS curves show a large broad peak corresponding to the interlayer spacing of organoclay. It is obvious that the shape of intercalation peaks is not changed. That indicates a constant amount of the intercalated structure of clay in blends even after 40 minutes mixing time. With increasing mixing time the position of the peak maximum shifts from  $q = 1.4 \text{ \AA}^{-1}$  to  $q = 1.5 \text{ \AA}^{-1}$  corresponding to a reduction of the interlayer spacing from 4.5 nm to 4.2 nm. As seen in figure 5.17 (section 5.3) and 5.20 (section 5.4) the interlayer spacing of the clay in HNBR compound and NR compound is 4.2 and 4.5 nm, respectively. Thus, the reduction of the interlayer spacing of organoclay in the HNBR/(NR-clay masterbatch) blends in dependence on the mixing time is related to the fact that the NR chains available in the clay galleries were gradually replaced by the HNBR chains.

If HNBR partially replaces NR, both rubber chains co-exist in the clay galleries that cause the clay to reside at the interphase of the blend. When the NR chains are fully replaced by the HNBR chains, the interlayer spacing reduces from 4.5 nm to 4.2 nm, and the clay is considered as it has immigrated into the HNBR domains. When the clay tactoids leave the NR phase and enter the HNBR phase, they can maintain their intercalated structure, because it is poorly dispersed in the HNBR phase as discussed in connection to figure 5.18 (section 5.3).



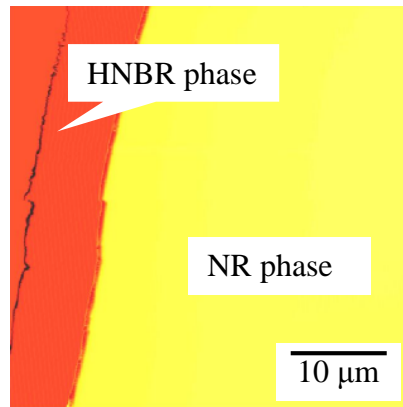
**Figure 5.34:** Clay distribution determined by extraction followed by TGA as a function of the mixing time

The quantitative analysis of clay migration has been carried out by investigation of the bound rubber analysis followed by the thermogravimetric analysis.

Figure 5.34 shows the quantitative analysis of the clay distribution in the blend phases. It can be seen clearly that the clay content in the NR phase, which was originally 5 phr, starts decreasing as the mixing process prolongs. The clay content has decreased in the NR phase from 5 phr to 1 phr after 40 minutes of mixing time. Meanwhile, the clay loading in the HNBR phase increases from zero to 4 phr. The better interaction of the clay with HNBR phase leads to migration of the organoclay from the NR to HNBR phase, which subsequently results in strong increase of the online conductance (figure 5.30, curve 3) in the first part of the curve (up to 15 minutes of mixing time). Le et al. [139] have also quantitatively investigated the phase specific localization of CB in one of the rubber phases. Other fillers like CB and silica also show the tendency to localize in a specific phase [108,155].

### 5.6.1.2 Morphology development in organoclay filled HNBR/NR blend

Figure 5.35 shows the AFM image of unfilled 50/50 HNBR/NR blend. The larger domains of both phases can be seen due to poor compatibility, weak interaction, difference in polarities, solubility parameters and large surface energy gap between both of the phases. Similar trend in results has also been reported by Tinker et al. [156].

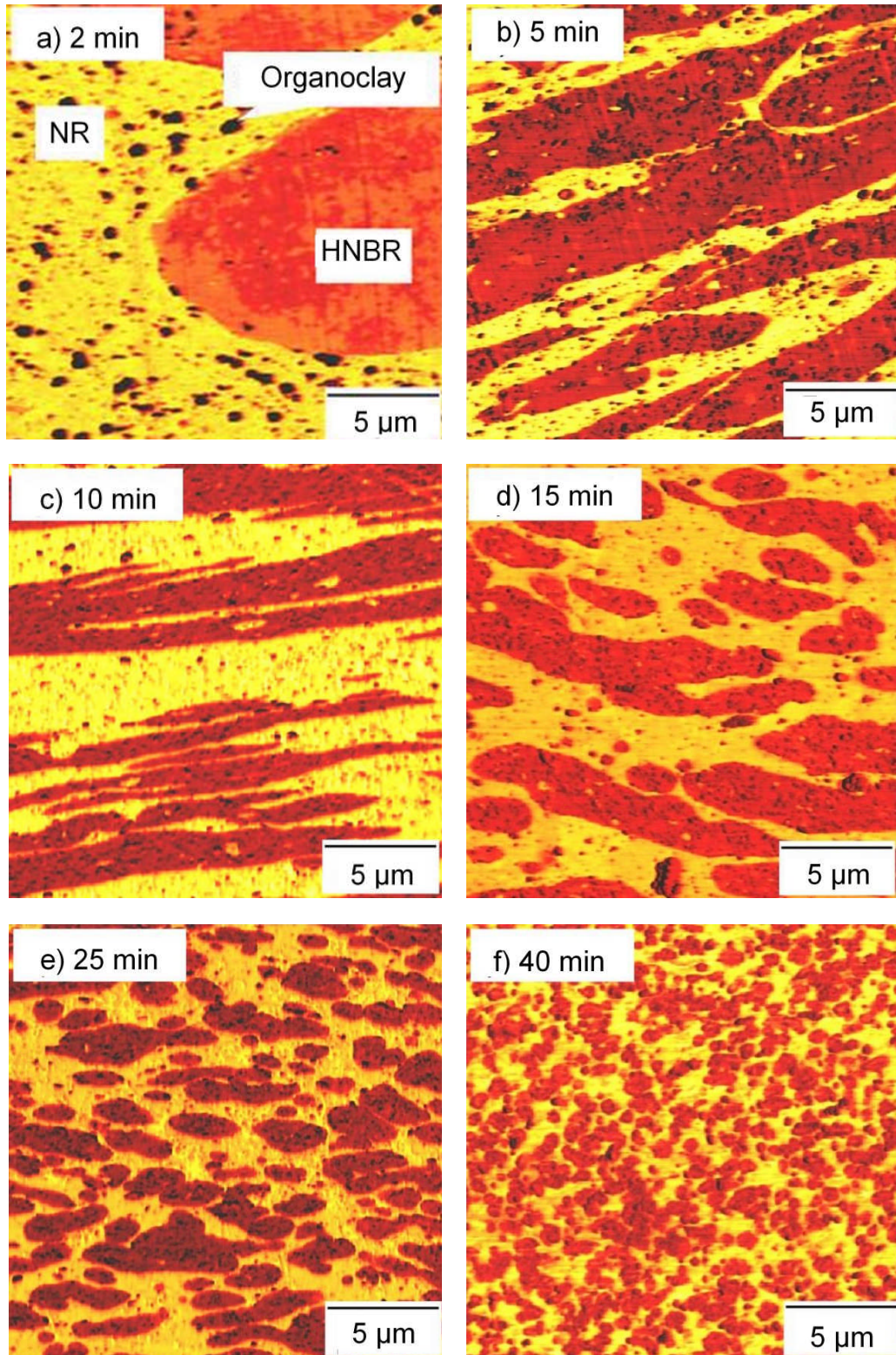


**Figure 5.35:** AFM image of unfilled HNBR/NR blend (50/50), mixing time 40 min

The micrograph in figure 5.35 also suggests that the phase morphology is nearly co-continuous, the HNBR (darker phase) appears to have a more discrete character with very big domain size. The high viscous HNBR phase will be the dispersed phase in the low viscous NR matrix.

In order to analyze the effect of organoclay on the development of the blend morphology, AFM micrographs at low magnification have been visualized. Figure 5.36 shows the AFM micrographs of development of the blend morphology as a function of mixing time. It is interesting to note that the morphology of the blend changes continuously with longer mixing time. In the start of mixing large domains of both phases are visible as can be seen in figure 5.36a. The morphology of the blends changes with increasing mixing time from very big domain to co-continuous and then to island-matrix type.

It can be noted that up to 15 minutes the HNBR phase still appears as a continuous phase which facilitates the ionic conduction in the blends. Indeed, after 15 minutes the co-continuous HNBR phase starts to break into domains that partly interrupt the motion of ionic species in the matrix. As a result the online conductance subsequently decays in the period between 20 minutes and 40 minutes. The extent of the conductance decay correlates with the reduction of the domain size of HNBR. In this period the diameter of HNBR domains reduces from about 2 μm to 0.5 μm and the corresponding online conductance from  $8.26 \times 10^{-5}$  mS to  $6.86 \times 10^{-5}$  mS.



**Figure 5.36:** Morphology development in HNBR/(NR-clay masterbatch) blend versus the mixing time (HNBR/NR ratio 50/50, 5 phr organoclay)

The better affinity of the organoclay to one of the components within the multi-component system leads to organoclay migration to the phase with more compatibility, which alters the viscosity ratio of the phases and improves the rheological properties of the component. It results in modification of the deformability of the droplets of the dispersed phase that in turn influence the breakup of the droplets. After 40 minutes of mixing time the HNBR domain size has become very fine in the range of 400 nm. This indicates that organoclay plays an important role in reducing the dispersed domain sizes of the HNBR phase. In short, this continuous change in morphology of HNBR/(NR-clay masterbatch) blend with mixing time originates from change in viscosity ratio, interfacial modification as well as rheological properties.

The rheological behavior of the used rubbers was characterized in an internal mixer PolyLab System Rheocord (Thermo Electron/Haake) at a temperature of 90 °C, rotor speed 50 rpm and fill factor 0.5. The torque has been used as a measure for the viscosity of rubbers. After reaching a plateau (about 10 min), the torque measured has been used for comparison of the viscosity between investigated rubbers as represented in the table 5.2.

**Table 5.2:** Development of torque in internal mixer during processing at  $T = 90\text{ }^{\circ}\text{C}$  and  $v_r = 50\text{ rpm}$

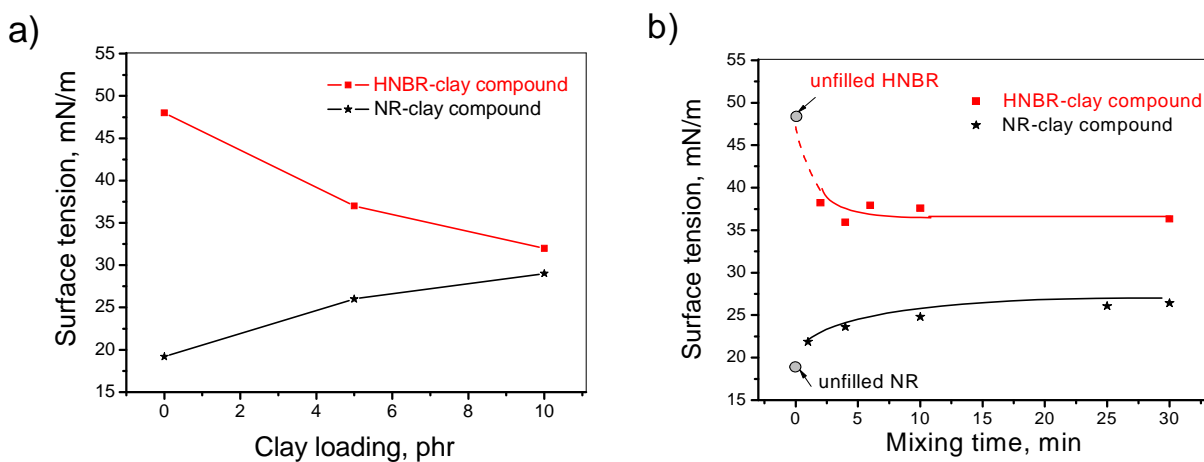
Rubber type	Torque, Nm
HNBR	20
NR	11
HNBR clay nanocomposites	21
NR clay nanocomposites	12

However, if organoclay loading is 5 phr, it has a significant influence on the viscosity of the polymer phase, and drives to a fine morphology of the dispersed phase, as depicted in figure 5.36f. Furthermore, there could be compatibilization effects of organoclay, which could lead to such a fine morphology. The interfacial tension of both phases before and after loading organoclay has been investigated in order to investigate the ability of organoclay to improve the compatibility of HNBR and NR phase.

Figure 5.37 shows the variation of surface tension with mixing time and organoclay loading. It reveals that addition of organoclay into HNBR and NR alters their surface tension strongly because of the existence of the surfactant ions which are released from the clay galleries during compounding. The surface tension of HNBR decreases from 48 mN/m to 33 mN/m, while that of



NR increases from 19 mN/m to 28 mN/m with 10 phr clay loading (figure. 5.37a). Figure 5.37b depicts that the surface tension of HNBR-clay compound decreases with the mixing time while that of NR clay compounds increases. Such behaviour can be explained by the release of surfactants from the clay galleries to the matrix. Furthermore, this also reveals that the surface tension of HNBR clay nanocomposites decreases rapidly and reaches a plateau in only 4 minutes of mixing time. In section 5.3, it has already been discussed that dispersion of organoclay in HNBR reaches its optimum value after 4 minutes of mixing time, which has been confirmed by online conductance, SAXS and AFM investigations. Similarly, in case of NR clay nanocomposites, the surface tension changes continuously throughout the mixing process until 30 minutes. It also conforms to the results of intercalation/exfoliation of organoclay in NR matrix as has been discussed in section 5.4. Based on the SAXS and microscopical investigations, it has been shown that prolonging the mixing time exfoliates more and more clay in the polymer matrix. More clay is intercalated/exfoliated, more surfactants are released.



**Figure 5.37:** Surface tension of HNBR clay and NR clay nanocomposites in dependence on (a) the clay loading and (b) mixing time

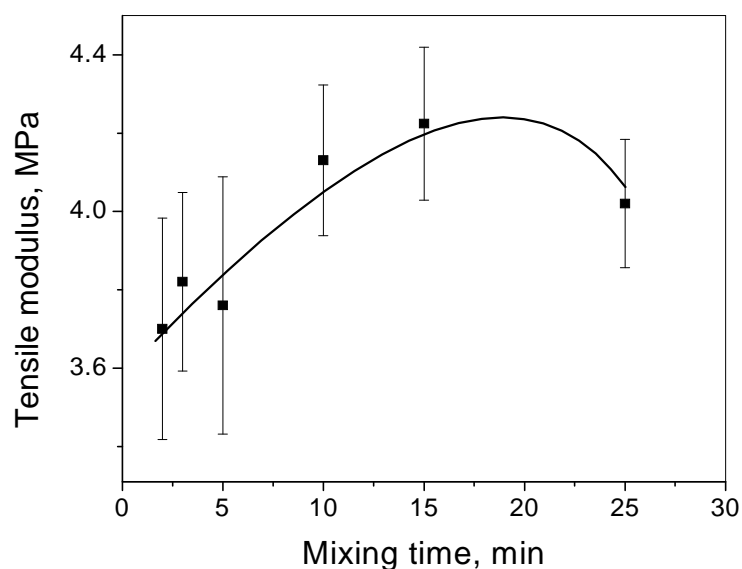
In HNBR/(NR-clay masterbatch) blend the interfacial tension reduces drastically when clay migrates from the NR phase to the HNBR phase. Therefore, organoclay influences the interfacial properties and viscosity ratio that are important factors in the determination of the droplet size of the dispersed phase during mixing. It is expected that the organoclay tactoids are very rigid, and have lower mobility as compared to block polymers in term of their ability to act as

compatibilizer. Therefore organoclay is located in the more compatible phase and heterogeneously distributed in the polar phase and along the interphase due to strong hydrodynamic forces. This may act in two directions, firstly, it refines the morphology of the blend and secondly it suppresses the coalescence of dispersed droplets. Former is caused by compatibilizing efficiency of clay, whereas later is introduced by the Marangoni force [157] and steric interaction [101].

## 5.6.2 Mechanical properties

### 5.6.2.1 Stress strain relationship

The development of tensile modulus of HNBR/(NR-clay masterbatch) in dependence on mixing time is shown in the figure 5.38. The development of the blend morphology and the phase specific distribution of clay strongly influence the mechanical properties of the nanocomposites. The tensile modulus increases within the mixing period up to about 20 minutes.

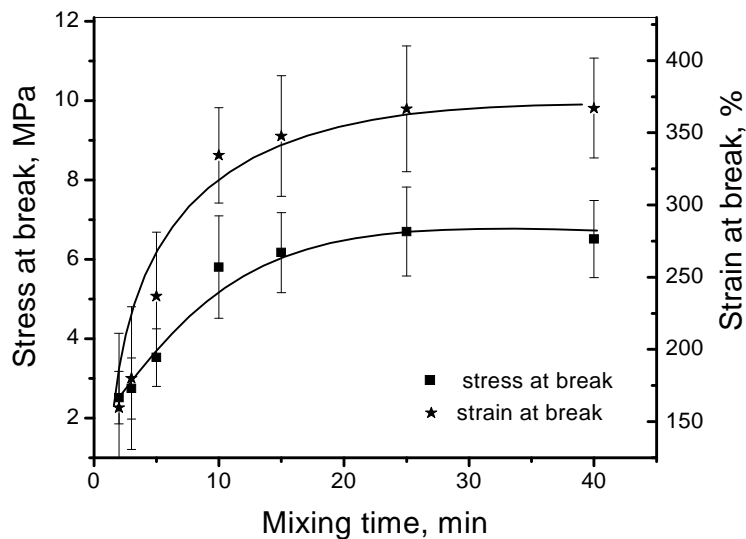


**Figure 5.38:** Tensile modulus of HNBR/(NR-clay masterbatch) blends in dependence on mixing time (HNBR/NR ratio 50/50, clay loading 5 phr)

According to figure 5.30 the OMEC curve also increases in this period and reaches a maximum at about 15 minutes. The modulus is a direct measure for the reinforcement effect of the nanofiller and it is strongly dependent on the phase specific distribution of the filler and development of morphology [139,158].



Thus, the increase of the tensile modulus is a result of the clay distribution within the blend phases. The modulus reaches the highest value, when a homogenous phase specific distribution of clay is reached, i.e. at about 15 minutes and a co-continuous morphology is developed [158]. Passing 20 minutes, clay continues to transfer into the HNBR phase, which causes an inhomogeneous distribution of clay and also results in the development of island-matrix morphology of the blend that result in lowering of tensile modulus. The NR matrix, with less contents of clay now determines the tensile modulus of the blend. The increase of tensile modulus of the blends with mixing time could also be attributed to the optimization of interfacial tension that ultimately leads to the increased interfacial area with refinement of the blend morphology [159].

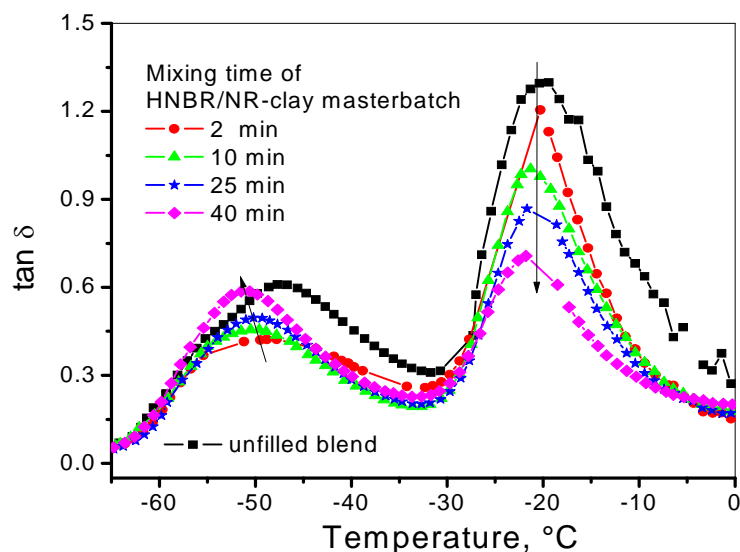


**Figure 5.39:** Stress and strain at break as a function of the mixing time of HNBR/(NR-clay masterbatch) blends (HNBR/NR ratio 50/50, clay loading 5 phr)

In figure 5.39 stress and strain at break of the HNBR/ (NR-clay masterbatch) blends are presented in dependence on the mixing time. Both the stress and strain at break increase with the mixing time up to 20 minutes and then nearly remain unchanged. The main reason for the improvement of stress and strain at break in this period is the better compatibility between the two blend phases.

### 5.6.2.2 Dynamic mechanical thermal analysis

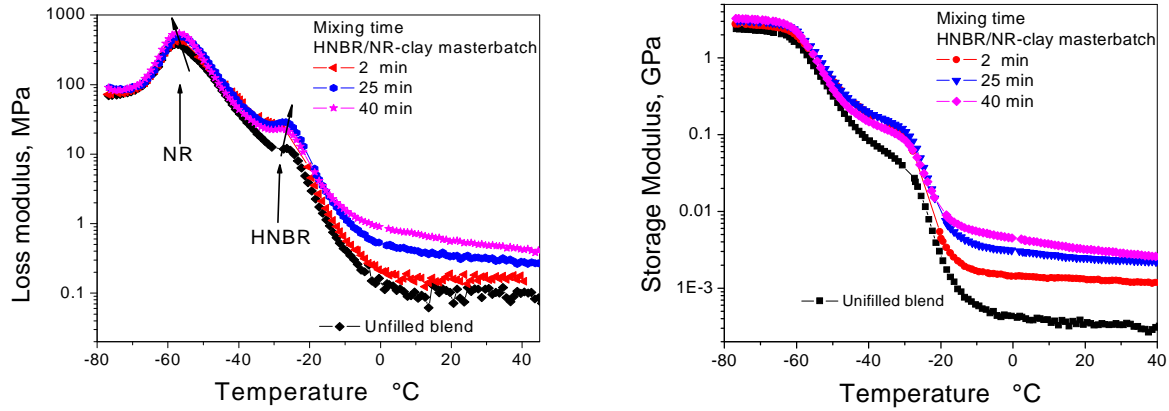
DMTA response of unfilled and filled HNBR/NR blends has been investigated over a wide range of temperature. The variation of loss factor,  $\tan \delta$ , of both HNBR and NR phases of the HNBR/(NR-clay masterbatch) blends is presented in dependence on the mixing time in figure 5.40. The position of the peak maximum of HNBR changes insignificantly, but the height of the peak changes depending on the localization of clay in the corresponding phase. The height of the peak is originated by the unbound rubber [140]. If the filler loading in one phase increases, the amount of the unbound rubber decreases and as a result the height of the peak also decreases.



**Figure 5.40:** Loss factor  $\tan \delta$  of the HNBR and NR phase of HNBR/NR unfilled blend and HNBR/(NR-clay masterbatch) blend in dependence on mixing time (HNBR/NR ratio 50/50, clay loading 5 phr)

The chart of loss moduli and storage moduli against temperatures are shown in Figures 5.41a and b, respectively. The  $T_g$  values are calculated from the peak position of loss moduli and found that, as the mixing time prolongs, the  $T_g$  of NR phase slightly shifted to a lower value whereas that of HNBR to higher temperature due to migration of organoclay from NR phase to HNBR phase. The trend can be attributed to better interaction of the organoclay with the polar phase, i.e. HNBR. The variation of  $T_g$  values, when the clay is either in NR or HNBR phase, may be due to

the existence of the interaction between nanolayers of organoclay and either NR or HNBR matrix that results in confinement of the motion of the macromolecular chains segment [160].



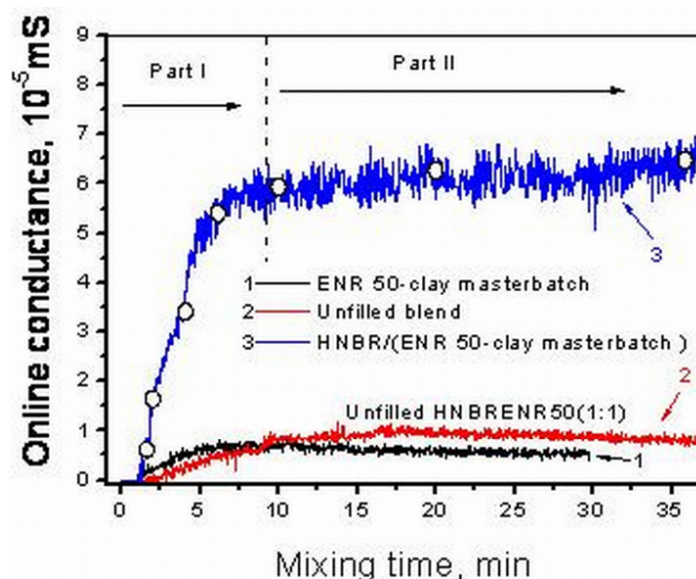
**Figure 5.41:** Loss moduli and storage moduli of unfilled and filled blends at different mixing time as a function of temperature (HNBR/NR ratio 50/50, clay loading 5 phr)

In short, it is the transfer of the filler from one phase to the other that tailors the viscoelastic properties of the blends. The interaction between the filler and the rubber is strong enough;  $T_g$  will shift to a lower (NR phase) or higher (HNBR phase) temperature.

## 5.7 Blends of HNBR and ENR (polar/polar blend system)

### 5.7.1 Online conductance of unfilled and filled HNBR/ENR-clay blends

Online measured electrical conductance of unfilled HNBR/ENR and HNBR/(ENR-clay masterbatch) blends as a function of mixing time is shown in figure 5.42. Curve 1 represents the OMEC of unfilled blend of HNBR/ENR (50/50). The online conductance of plain ENR is too low to be measured with the instrument being used to measure the online conductance. Therefore, it is considered as zero. The low conductivity of the ENR matrix may be due to less polarity of ENR phase. The OMEC chart in the curve 2 is quite low, originated by the HNBR phase in HNBR/ENR blends. Curve 3 in figure 5.42 depicts the development of OMEC of HNBR/(ENR-clay masterbatch) with mixing time of 40 minutes. It shows a quite higher online conductance than that of unfilled blend.



**Figure 5.42:** Online conductance of the ENR-clay masterbatch, unfilled HNBR/NR blend, and HNBR/(NR-clay masterbatch) blends in dependence on mixing time

Figure 5.42, curve 3, shows that when ENR-clay masterbatch was mixed with plain HNBR, the online conductance increases and reaches its maximum value in a very short time and a plateau of OMEC has been observed. In order to understand the background of the unusual behavior of the online conductance of the HNBR/(ENR-clay masterbatch), the curve 3 has been divided into two parts, i.e. part I and part II respectively. It is supposed that the former part of the curve could be due to two reasons, firstly, migration of organoclay from ENR, less polar phase to the more

polar HNBR phase, secondly, also at the same time there could be development of co-continuous morphology that facilitates the movement of charge carriers. The later part of the OMEC chart could be due to either co-continuous morphology of the clay bearing phase or island morphology with clay lies in the matrix phase.

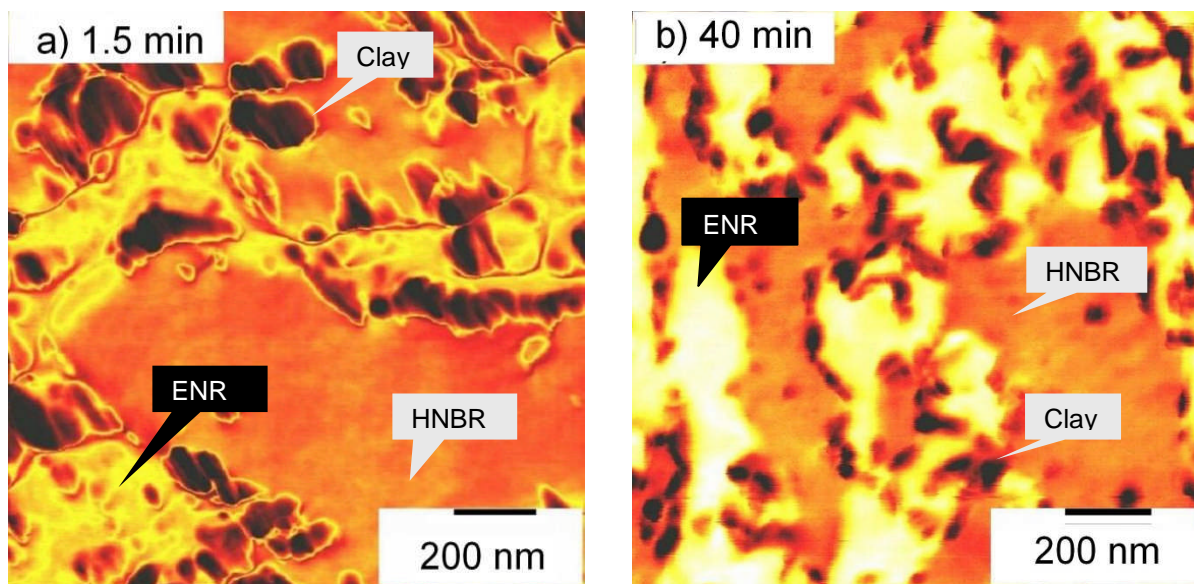
Note that, if figure 5.42 is compared with 5.30, it can be analyzed that the OMEC chart of the HNBR/(ENR-clay masterbatch) with that of the HNBR/(NR-clay masterbatch), an important difference can be noted that former shows plateau for longer mixing time, whereas for later it starts decreasing after 15 minutes of mixing time. In order to explore the background for the online conductance curves for organoclay filled and unfilled HNBR/ENR blends, the dispersion and distribution of organoclay as well as the kinetics of development of blend morphology has been extensively studied using different characterization techniques like AFM, TEM, SAXS. The performance of the blend nanocomposites has also been analyzed by investigating the stress-strain behavior and correlated with the development of online conductance.

## **5.7.2 Relationship between online conductance and morphology of blends**

### **5.7.2.1 Investigation of clay transfer and distribution**

The distribution of fillers and various processing aids in heterogeneous elastomer blends can be nonuniform due to the greater solvation between the filler and one of the polymers in the melt-mixed blends [109]. In order to observe the location of the clay, higher magnification AFM micrographs of HNBR/(ENR-clay masterbatch) in the start of mixing process (after 90 seconds) and at end of mixing process (40 minutes) were obtained and are shown in the figure 5.43a and b, respectively. The dark brown phase corresponds to the HNBR phases. The light yellow phase corresponds to the ENR phase and the black area corresponds to the clay platelets/tactoids. Since ENR-clay masterbatch was mixed with the HNBR phase to get the blend, so in the start of mixing process all the clay was in the ENR phase. If these two images are compared, two factors are obvious. First, after 90 seconds of mixing time, there is not or very small discernible clay in the brown phase (HNBR), as show in figure 5.43a, but after 40 minutes of mixing time the case is reversed, i.e. most of the clay has migrated to dark phase (HNBR) where as only a little quantity of clay stayed in light yellow phase (ENR) as shown in the figure 5.43b. Secondly, the clay tactoids are of big size, well distributed in ENR phase (figure 5.43a), whereas their migration to HNBR phase after 40 minutes of mixing time then not only reduces the size of the clay tactoids but also it predominantly localized at phase interfaces. Extensive organoclay

transfer from the ENR phase to the HNBR phase have occurred, regardless of masterbatch mixing procedure, is due to better interaction of organoclay in the HNBR phase. The localization of the clay at phase interface is due to similar polarity of both of the blend phases [87,110].

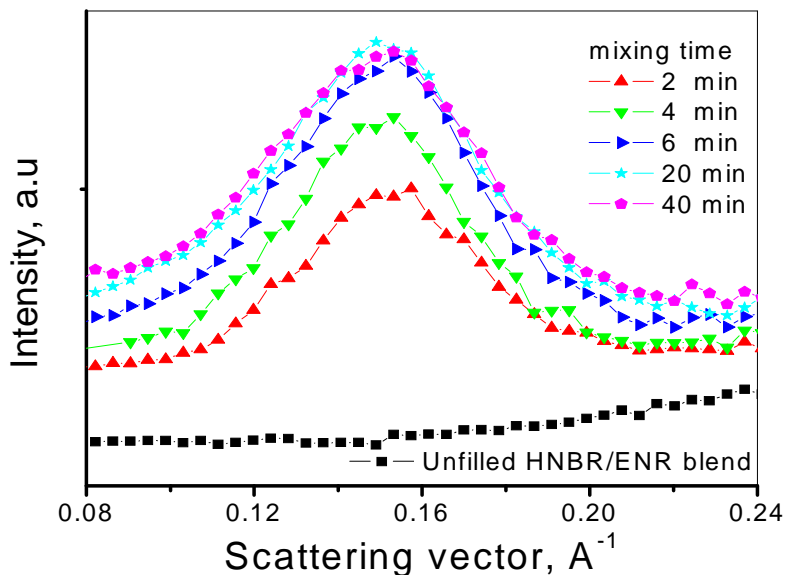


**Figure 5.43:** AFM micrographs of HNBR/(ENR-clay masterbatch) blends after (a) 90 seconds (b) 40 minutes

The clay migration and localization of the organoclay nicely supports the conjuncture based on the online conductance (figure 5.42) that increase of the conductance is due to transfer of organoclay from ENR phase to HNBR phase. Predominantly, localization of organoclay at the interphase has also been observed by other authors [87,110,161 ], while analyzing the role of organoclay in the immiscible blends. Ray et al. [161] explained, that when organoclay have similar interactions with both of the blend phases then clay predominantly localizes at phase interface.

Figure 5.44 shows the SAXS analysis of HNBR/(ENR-clay masterbatch) blends at different mixing times and unfilled HNBR/ENR blends mixed for 40 minutes. The peak position at scattering vector  $0.15 \text{ \AA}^{-1}$  represents the interlayer spacing of organoclay 4.2 nm. The SAXS pattern shows that the peak position along abscissa does not change that means that the intercalated structures remains constant. However, the peak position changes along the ordinate with different mixing time but after 4 minutes the peak position remains constant even after longer mixing time. A possible explanation for change of peak position along the ordinate is due to the transfer of organoclay from ENR phase to HNBR phase and development of the blend

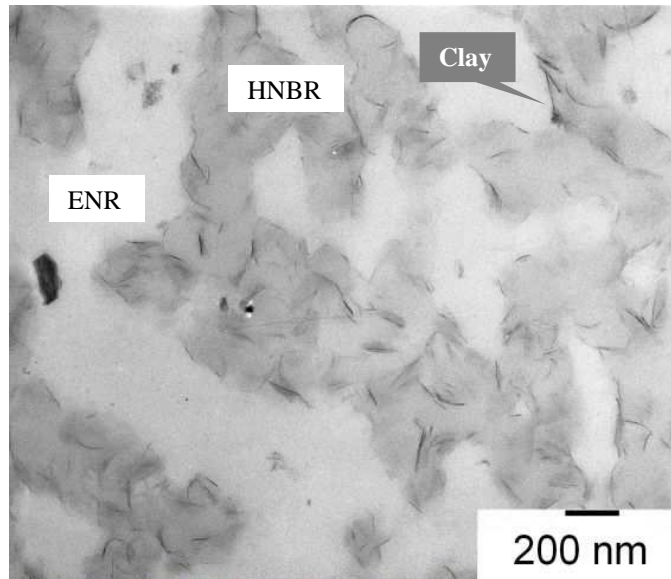
morphology. However, note that the peak position, which does not change after 4 minutes, could be due to the constant morphology.



**Figure 5.44:** SAXS analysis of unfilled HNBR/ENR and filled blends of [HNBR/(ENR-clay masterbatch)] at different mixing times.

However, comparing the SAXS analysis of HNBR/(ENR-clay masterbatch) for different mixing time with that of the previous investigation of HBR/(NR-clay masterbatch), it can be analyzed that there was a continuous vertical upward shift (along y-axis) of the SAXS peak. That has been explained with the continuous change of the morphology along with the migration of clay. But in this case the peak positions along the y-axis remain constant after 4 minutes of mixing time, which is due to constant morphology.

TEM images of randomly microtomed sample of the blends after 40 minutes of mixing time is shown in the figure 5.45. A complex morphology both on micro- and nanoscale can be noticed. The clay appears as deep dark features in the dark gray continuous phase, so that it is detectable on the micron size.

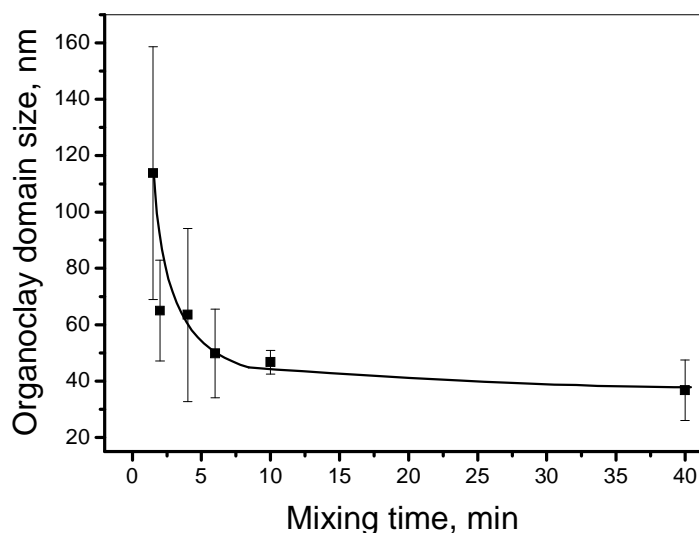


**Figure 5.45:** TEM images HNBR/(ENR-clay masterbatch) blends, (dark gray area represents HNBR phase, light gray area represents ENR phase and the black lines in dark phase corresponds to clay)

It can also be observed that most of the clay lies at the phase interface. The visual appearance of TEM micrograph confirms such statement of preferential localization of organoclay in the phase interface. The stacks with thickness of few tens of nanometers are also observable. It can also be analyzed the size of organoclay tactoids became smaller after 40 minutes of mixing time.

The variation of organoclay domains size in HNBR/(ENR-clay masterbatch) blends in dependence on mixing time is shown in the figure 5.46. The figure depicts that at the start of mixing process big domains exist. As the mixing time prolongs the organoclay domains reduces in size and become constant after about 10 minutes. This is well correlated with the online conductance (figure 5.42), which increases in start of compounding and become constant after about 10 minutes of mixing. The big domains of organoclay in start could be explained by taking into account on the basis of poor dispersion of organoclay in ENR phase as already discussed in section 5.5.



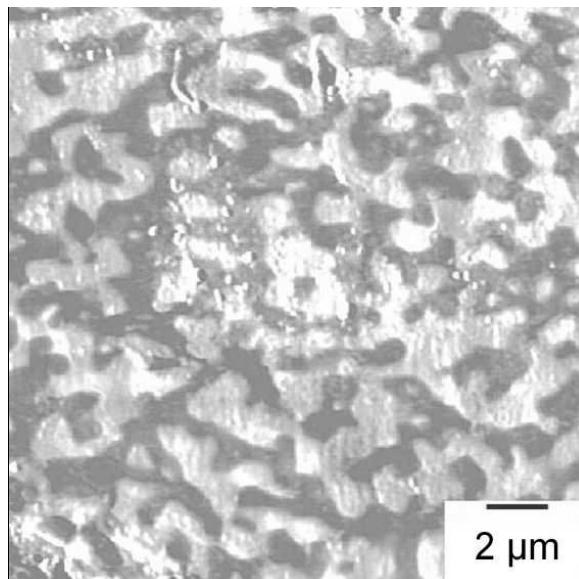


**Figure 5.46:** Clay domain size in HNBR/(ENR-clay masterbatch) blend in dependence on mixing time

As the mixing time prolongs more and more, organoclay transfers from ENR phase to HNBR, where it becomes better dispersed and distributed than in the ENR phase. This clearly can be seen by analyzing the AFM images (figure 5.43) and TEM images (figure 5.44). Comparing figure 5.43a and b, it is obvious that there exist big clay tactoids in the former case, whereas the later shows finely dispersed and distributed clay structures. TEM analysis of HNBR/(ENR-clay masterbatch) also shows that clay exists well intercalated/exfoliated in the HNBR phase that could be explained due to better filler-elastomer interaction (figure 5. 44).

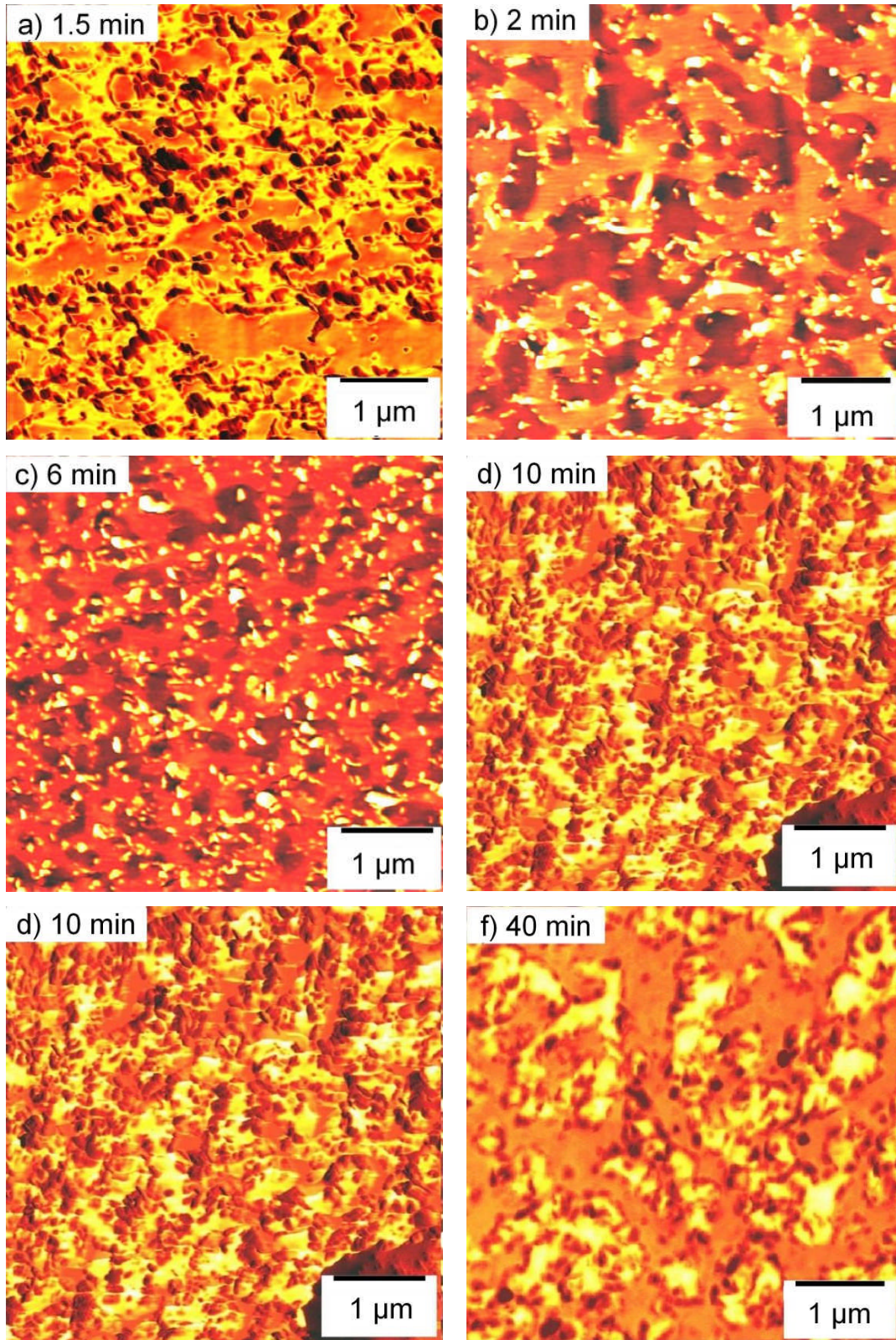
### 5.7.2.2 Morphology development in organoclay filled HNBR/ENR blends

Figure 5.47 shows the AFM image of unfilled blend of HNBR/ENR (50/50). The morphology of the blends is usually determined by the melt viscosity ratio, interfacial tension and the composition. When HNBR and ENR phases are blended in 50/50 ratio, a co-continuous morphology is obtained due to similarity in polarity of both phases. A similar co-continuous morphology for HNBR/ENR (50/50) blend has also been observed by Mathai et al. [162].



**Figure 5.47:** AFM micrograph of HNBR/ENR blend (50:50) with mixing time of 40 min, rotor speed 70 rpm

The development of morphology of the HNBR/(ENR-clay masterbatch) blend as a function of mixing time is shown in figure 5.48. Analyzing the kinetics of morphological changes of the blends not only leads to understand the second part of OMEC curve (figure 5.42) but guides to realize the mechanism of clay transfer from ENR to HNBR phase as well as the phase inversion of blend morphology. After 90 seconds of mixing time clay tactoids are in the ENR phase and a very small amount of discernible clay is found in the HNBR phase. As the mixing time increases under the influence of strong shear forces, organoclay starts to move to the HNBR phase. At the same time co-continuous morphology starts changing to island-matrix morphology as is shown in figure 5.48b and c. It can be analyzed that after 2 minutes of mixing time most of the organoclay has moved towards the ENR interface. The movement of organoclay to the phase interface and circumscription of HNBR phase causes the change from co-continuous to island-matrix morphology. Simultaneously, clay tactoids are broken to smaller sizes to surround more HNBR domains. This process continues as the mixing time prolongs. After 6 minutes of mixing time a fine morphology with HNBR dispersed in the ENR matrix has been obtained (figure 5.48c). At the same time dispersed HNBR phase starts to unite again at the points of organoclay. The organoclay act as bridge to unite the dispersed HNBR phase. Again a phase inversion from island-matrix to co-continuous morphology can be observed.



**Figure 5.48:** AFM micrographs taken at different time intervals during mixing process of HNBR/NR-clay masterbatch) blends

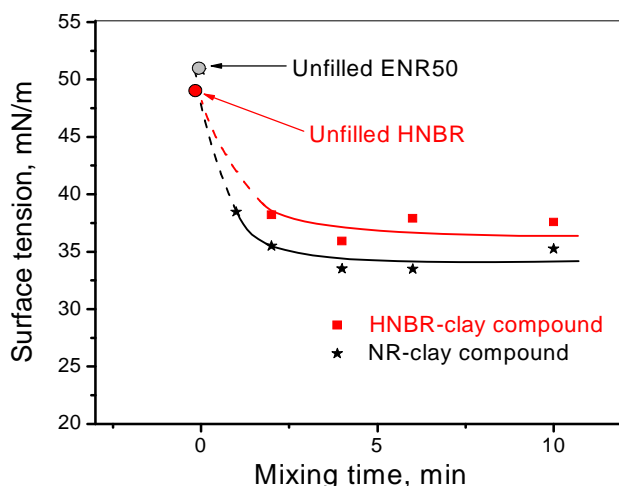
The kinetics of development of blend morphology is controlled by several factors, e.g. the presence of fillers, viscoelastic flow of elastomers, shear force and interfacial tension between the phases [90]. Li et al. [100] have studied the morphology development in PPO/PA6 clay nanocomposites and noted that addition of organoclay to the blend inverts the PPO dispersed phase to co-continuous phase due to high aspect ratio of clay platelets, which may exert significant effects on the phase coalescence during melt mixing. When the dispersed HNBR phase coalesces, the organoclay shifts inside the HNBR phase. It can be noted in figure 5.48d that after 10 minutes of mixing time most of clay has transferred to either in the HNBR phase or at the interface. This also explains the maximum value of online conductance after 10 minutes of mixing time, which also corresponds to the second part of the OMEC curve (figure 5.42). The morphology after 10 minutes remains unchanged.

The morphology development during melt processing is mainly determined by a flow-induced process. In this process, the dispersed phase particles deform, break up, coalesce, and finally reach a dynamic equilibrium state. Two most common approaches have been used to explain this effect. Firstly, the selective localization of clay may increase the viscosity of the specific phase, which controls the morphology of the blends. Secondly, the thermodynamic approach focuses on the changes of the free energy of the components due to the inclusion of organoclay [163]. The selective localization of the organoclay along the interface of the two polymeric components can alter the interfacial tension between the two phases, essentially affecting their mutual adhesion and wetting between the two immiscible polymers of the matrix. In fact, both of the two mechanisms may act in parallel and synergistically. It is apparent, that the morphological characteristics and spatial organization of the polymer domains are sensitive to the nature of organoclay and the blend phases.

In order to have a deeper insight into changes of the surface energy of the components due to inclusion of organoclay in the blends, the interfacial tension has been investigated. The effect of organoclay on the surface tension of HNBR and ENR with mixing time is shown in figure 5.49. It is obvious that the surface tension decreases strongly with mixing time and reaches a plateau after only 4 minutes for both of the elastomers. The surface tension of HNBR and ENR decreases from 48 mN/m to 36 mN/m and 51 mN/m to 34 mN/m respectively, after addition of 5 phr of organoclay.

The localization of organoclay in the phases strongly changes the surface energy of the blend phase [163]. Figure 5.48b shows that after 2 minutes of mixing time organoclay is evenly

distributed in both of the phases; so that the surface tension for both the phases is approximately equally decreased. This will compatibilize both of the blend phases, which leads to the inversion of the morphology from co-continuous to island-matrix morphology. Figure 5.48c shows that HNBR is finally dispersed in the ENR matrix. As the mixing continues, more and more clay is transferred to the HNBR phase that will also increase the surface tension gap between both of the phases, i.e. the surface tension of HNBR decrease where as that of ENR increase. The dispersed domain will start coalesce, and again change of morphology from island-matrix to co-continuous morphology has been observed as can be seen in figure 5.48d.

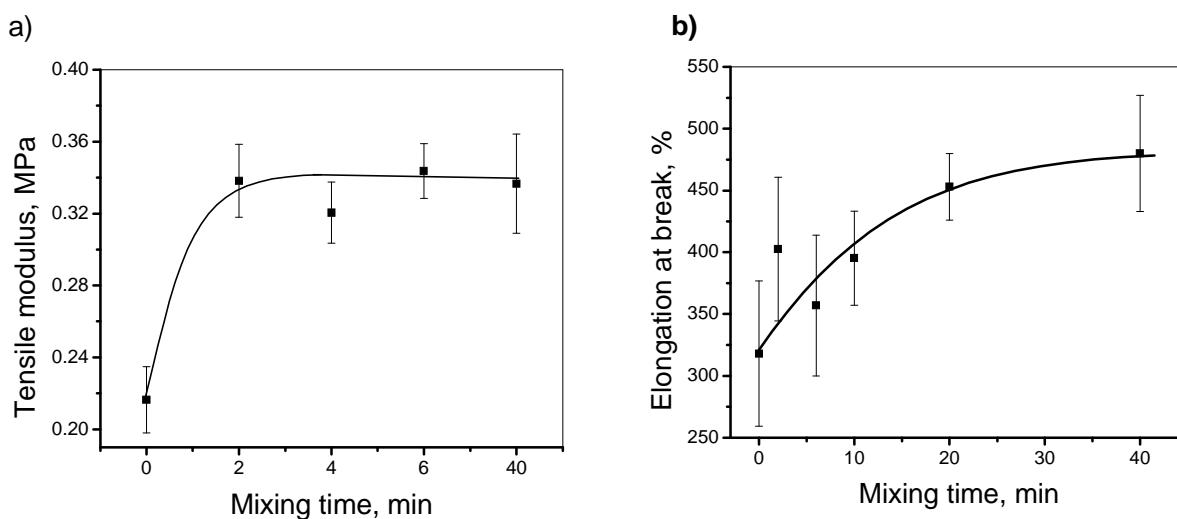


**Figure 5.49:** Surface tension of the HNBR clay and ENR clay nanocomposites in dependence on the mixing time

There are two important factors that could influence significantly on the phase coalescence during the melt mixing of HNBR/(ENR-clay masterbatch). Firstly, the migration of organoclay from the ENR phase to HNBR drastically changes the surface tension of both of the phases and increases the surface energy gap between them. Secondly, high aspect ratio of clay may exert significant effects to yield the co-continuous morphology [100]. The change of surface energy of the blend phases not only influences the blend morphology, but also the performance of the blends.

### 5.7.3 Investigation of mechanical behavior of the blend nanocomposites

In order to explore the effect of organoclay on the performance of blend nanocomposites, the mechanical properties of the virgin and organoclay modified blends were investigated. The results are reported in the figure 5.50a and b for E-modulus and elongation at break, respectively. Figure 5.50a shows the increase in modulus in dependence on mixing time. It can be analyzed that the modulus of HNBR/(ENR-clay masterbatch) increases slightly by loading of 5 phr of organoclay than that of virgin blends. The mechanical properties are mainly controlled by the morphology of blend, filler localization and polymer-polymer or polymer-filler interactions. The co-continuous structure is very important from the practical point of view. It is known that blends with co-continuous structures have improved properties as compared to the blends with island-matrix morphology [158].



**Figure 5.50:** Tensile test results of HNBR/(ENR-clay masterbatch) as function of mixing time and corresponding unfilled blend; (a) tensile modulus, (b) elongation at break

The increase in the modulus of the filled blends is due to the reinforcing effects of organoclay and good interaction of the filler with the phases as well as co-continuous morphology of the blends. It has been observed that both ENR and HNBR show intercalated/exfoliated structures with organoclay, so a favorable interaction exists between both phases in the blends. Ray et al. [106] have observed an increase in modulus of organoclay filled blends and described it due to

reinforcing efficiency and ability of the nanofiller to promote the interfacial adhesion between the immiscible phases. Figure 5.50b shows the elongation at break as function of mixing time. The localization of organoclay at the interface strengthens the phase adhesion and increases the resistance to failure. The tensile strength and elongation at break depend on the interfacial adhesion between phases [164]. If adhesion is not perfect, fissures can induce sample break originated at the interfacial region. The low adhesion makes this region weak. The increasing of strain at break along with the mixing time could be due to better dispersion and distribution of organoclay in the HNBR phase or along the interface.



## 6 Summary

The online measured electrical conductance (OMEC) method was applied to characterize dispersion and distribution of nanoclay during the mixing process of rubber compounds and blends. Accordingly, making use of OMEC spectra versus mixing time, time required for the development of optimum morphology of rubber clay nanocomposites was proposed. Afterward, the method was extended to detect and analyze aspects related to the filler phase specific localization and organoclay induced morphology in polar/non-polar and polar/polar rubber blends.

It was analyzed that different types of nanoclays showed different OMEC charts. Unmodified clay did not show online conductance. Morphological investigation has revealed that unmodified clay did not disperse in the rubber matrix and big agglomerates have been visualized. The background of the OMEC spectrum has been analyzed by characterizing the kinetics of clay dispersion using offline techniques, such as rubber layer  $L$  determination, optical microscopy, SAXS, TEM, AFM and was nicely correlated with the online conductance curves. It was proposed on the basis of the rubber layer  $L$  experiment that the intercalation process was completed up to a critical point 1, afterwards only exfoliation process takes place. The effect of rotor speed on the development of morphology of the nanocomposites has also been analyzed. It was found that lowering the rotor speed shifts exfoliation to longer mixing time. Additionally, a deeper insight into the mechanism of melt mixing process of organoclay filled rubber compounds has been found by analyzing the mechanical performance of the nanocomposites. The mechanical properties like tensile modulus, stress at break and strain at break increase with longer mixing time, until a plateau is reached.

XHNBR clay nanocomposites showed higher conductivity than either of virgin XHNBR or organoclay. Higher conductivities of the nanocomposites were due to better dispersion of clay that imparts more surfactant ions in the polymer matrix. The OMEC chart of XHNBR clay nanocomposites passed through two characteristic points indicating intercalation and exfoliation. Equipped with the knowledge obtained on XHNBR clay nanocomposites, rubber compounds with different polarities, ranging from moderately polar to non-polar (HNBR, ENR and NR) have been selected to perform further experiments. The OMEC chart of HNBR clay nanocomposites was similar to the XHNBR clay nanocomposites except that firstly, it passed through only one characteristic point, secondly, the conductance level was lower than the later.



The kinetics of development of the morphology was characterized using SAXS and AFM. It was found that the morphology of the HNBR clay nanocomposites remained constant after the characteristic point, even if it was mixed for a longer mixing time. Only one characteristic point in HNBR clay spectra was due to poor dispersion of organoclay in the HNBR matrix that was explained taking into account the higher polarity of XHNBR due to carboxylic group. The online conductance of pure ENR was too low to be measured with the instrument; therefore it is considered as zero. The OMEC spectra of ENR clay nanocomposites was recorded and found that it showed different behavior from both rubbers which has already been discussed above. The conductance level was very low and it decreased after the maximum. Former was due to less polarity of ENR and later was due to thermal degradation of ENR at the processing temperature. In order to discard the effect of thermal degradation, ENR was milled prior to mix with organoclay. It was found that OMEC spectra obtained was similar to that of HNBR. The kinetics of the clay dispersion was systematically characterized by SAXS and TEM. It has been shown that the morphology remains constant after the characteristic point. Similarly, the method was extended to non-polar rubber, i.e. NR. The OMEC spectrum of the nanocomposites on the basis of NR clay could not be detected; because the values of the OMEC laid out of the measuring range of the equipment due to non-polar nature of the rubber matrix. However, the AFM analysis of the NR-clay nanocomposites, which showed that the big clay tactoids were broken into smaller ones with longer mixing time. It was nicely correlated with the SAXS analysis that showed that peak position decreases with longer mixing time.

Moreover, the method has been successfully applied to investigate the effect of organoclay in HNBR/(NR-clay masterbatch) blend. The online conductance of HNBR/NR blend was very low, which was originated by HNBR component. It was observed that when NR-clay masterbatch was mixed with HNRB, the online conductance increased, reached a maximum and then decreased. The OMEC curve was divided into two parts; first part corresponds to increasing portion of the conductance curve, whereas the second portion corresponds to the decreasing portion of the OMEC curve. The structural background of the conductance curve was discussed by taking into consideration the results of different structural investigations like AFM, SAXS and extraction experiment as well as surface tension measurement. It was found that the main reason for the OMEC of the HNBR/(NR-clay masterbatch) blends is the migration of organoclay from NR phase to HNBR phase. The migration of organoclay from NR to HNBR phase has been qualitatively observed by analyzing the AFM and TEM images at higher magnification. The

quantitative analysis of the filler transfer was analyzed by extraction experiment followed by TGA. The clay migration from NR phase to HNBR phase is a result of favorable interaction of clay to the HNBR phase which has higher polarity than that of the NR phase. The decreasing portion of the conductance curve is due to change of blend morphology from co-continuous to island-matrix as a result of the compatibilization effect of clay. Surface tension investigations showed that the loading organoclay drastically influence the surface energies of both blend components. Mechanical properties of the blends have been investigated and nicely correlated with the OMEC spectrum.

The OMEC method was also applied to investigate the effect of organoclay in the polar-polar, i.e. HNBR/ENR blends. Like HNBR/NR blends, the online conductance of HNBR/ENR blend was also very low that was originated by HNBR component. It was analyzed that when ENR-clay masterbatch was mixed with plain HNBR, the conductance increased and reached a plateau after some time. The online conductance curve was divided into two portions; first increasing portion and second the plateau or constant conductance portion. The increasing portion of OMEC chart was due to migration of the filler from ENR to more polar HNBR phase. The morphological investigations have been carried out by AFM and TEM at higher magnification that clearly revealed the migration of organoclay from ENR to HNBR phase. The SAXS analysis showed that the peak position corresponds to interlayer spacing of organoclay; shifted upward with longer mixing time and it did not change once the plateau of OMEC has been achieved. The kinetics of development of morphology of HNBR/(ENR-clay masterbatch) was characterized by AFM. It was observed that there is an inversion of morphology taking place from co-continuous to island-matrix morphology and again to co-continuous morphology. The inversion of morphology was due to the migration of the filler in blend from less polar to more polar phase. It was also analyzed that when the plateau of online conductance is reached then there is no change of morphology. Moreover, the organoclay preferentially resided at the HNBR phase interface that was attributed to the polarities of both of the phases.

It can be concluded that OMEC method offers a suitable economically and industrial viable way to characterize online the intercalation/exfoliation of organoclay in the rubber compounds. However the method has certain limitations; it cannot be applied to thermally unstable, non-polar and high processing temperatures materials. It can also be concluded that when organoclay is mixed in the blends, the higher OMEC is due to migration of the organoclay from less polar to more polar rubber matrix, where it is thermodynamically more stable. After maximum value of

the online conductance curve, there are two possibilities; either it decreases or stays constant. Former is due to the development of island-matrix with organoclay lies in the dispersed phase. The later is either due co-continuous morphology or island-matrix morphology, with clay lies in the matrix phase so that a continuous path is provided for the electrical conductance.

The success of online conductance method on laboratory scale, to study the nanoclay dispersion process in rubber compounds and rubber blend, will initiate the application of the method to to study the nanoclay dispersion process and to monitor the quality of rubber-clay nanocomposites on industrial scale.

## 7 Zusammenfassung

Die Methode der Erfassung des Online-Leitwerts (OMEC) wurde zur Charakterisierung der Dispersions- und Distributionsvorgänge von Schichtsilikaten (Nanoclay) während des Mischprozesses in Kautschukkompositen und -blends angewandt. Mit Hilfe der Online-Leitwertkurve wurde die Entwicklung einer optimalen Morphologie von nanoclaygefüllten Kautschukmischungen beabsichtigt. Im Nachhinein konnte die Methode erweitert werden, um auch die phasenspezifische Füllstoffverteilung, sowie die durch Schichtsilikat induzierte Morphologiebildung in polaren-unpolaren sowie polaren-polaren Kautschukblends aufzudecken und zu analysieren.

Verschiedene Nanoclaytypen führten zu unterschiedlichen Leitwertkurven. Des Weiteren zeigten unmodifizierte Schichtsilikate keine online Leitfähigkeit. Morphologische Untersuchungen verdeutlichten, dass sich unmodifizierte Schichtsilikate nicht in Kautschuk dispergieren lassen, was zu großen Agglomeraten in der Matrix führte. Der Hintergrund der Online-Leitwertkurve lässt sich durch Charakterisierung der Füllstoffdispersion mittels verschiedener Offlinetechniken analysieren. Untersuchungsmethoden, wie die Bestimmung der Kautschukschicht L, optische Mikroskopie, Transelektronenmikroskopie (TEM), Atomic-Force-Microscopy (AFM), sowie die Röntgenkleinwinkelstreuung (SAXS) korrelieren sehr gut mit der online Leitwertkurve. Mit Hilfe der Lösungsversuche und der Bestimmung der Kautschukschicht L wurde gezeigt, dass der Interkalierungsprozess bis zu einem kritischen Punkt 1 abgeschlossen ist, anschließend findet nur der Exfolierungsprozess statt. Auch der Einfluss der Rotordrehzahl auf die Morphologieentwicklung der Nanokomposite ist analysiert wurden. Dabei konnte gezeigt werden, dass mit abnehmender Rotordrehzahl eine Verschiebung der Exfolierung zu längeren Mischzeiten stattfand. Durch die Analyse der mechanischen Eigenschaften der Nanokomposite konnte zusätzlich ein tieferer Einblick in die Mechanismen des Schmelzemischprozesses der nanoclaygefüllten Kautschukblends gegeben werden. Die mechanischen Kennwerte, wie Zugmodul, Bruchspannung und Bruchdehnung erhöhten sich mit längeren Mischzeiten, bis ein Plateau erreicht wurde. XHNBR-Nanoclay-Nanokomposite zeigten höhere Leitwerte als ungefülltes XHNBR oder Organoclay. Höhere Leitwerte der Nanokomposite bedeuten bessere Füllstoffdispersion, was auf mehr grenzflächenaktive Ionen in der Matrix schließen lässt. Die Online-Leitwertkurve der nanoclaygefüllten XHNBR Nanokomposite verläuft durch zwei charakteristische Punkte, die durch Interkalierung und Exfolierung gekennzeichnet sind. Mit dem

erlangten Wissen über nanoclaygefüllte XHNBR-Nanokomposite wurden Kautschuke mit unterschiedlicher Polarität von mäßig polar bis unpolar (HNBR, ENR and NR) für weitere Untersuchungen ausgewählt. Die Online-Leitwertkurven der nanoclaygefüllten HNBR-Komposite glichen denen der gefüllten XHNBR-Komposite, außer dass nur ein charakteristischer Punkt durchlaufen wurde und der Leitwert über die gesamte Mischzeit niedriger war. Die Kinetik der Morphologiebildung wurde mittels SAXS und AFM charakterisiert. Dabei zeigte sich, dass sich die Morphologie der claygefüllten HNBR-Nanokomposite nach dem charakteristischen Punkt der Leitwertkurve mit steigender Mischzeit nicht mehr änderte. Eine Verlängerung der Mischzeit erzielte gleiche Ergebnisse. Aufgrund der geringen Dispersion von Schichtsilikat in HNBR konnte nur ein charakteristischer Punkt in der Online-Leitwertkurve ermittelt werden; in Bezug dazu muss die höhere Polarität von XHNBR aufgrund der Carboxylgruppen gesehen werden. Die online Leitfähigkeit von reinen ENR war zu gering für den gerätebedingten Messbereich, so dass sie als null gesetzt wurde. Die Online-Leitwertkurve von nanoclaygefüllten ENR zeigte einen unterschiedlichen Verlauf zu den eben diskutierten Materialien. Die Leitfähigkeit war sehr gering und sie nahm nach dem Maximum weiter ab, was sowohl der geringen Polarität des ENR, als auch der thermischen Degradierung bei Verarbeitungstemperatur geschuldet ist. Um dem Effekt der thermischen Degradation vorzubeugen, wurde ENR vor dem Einmischen von Organoclay gewalzt. Die ermittelten Online-Leitwertkurven glichen denen des HNBR. Die Kinetik der Schichtsilikatverteilung wurde systematisch mittels SAXS und TEM charakterisiert. Dabei konnte gezeigt werden, dass sich die Morphologie nach dem charakteristischen Punkt der Online-Leitwertkurve nicht weiter ändert. Die Methode wurde auch in gleicher Weise auf unpolare Kautschuke wie NR angewandt. Dabei konnte keine Online-Leitwertkurve für das Nanokomposit auf Basis von NR und Schichtsilikat detektiert werden, da die Leitwerte außerhalb des Messbereiches des Messgerätes lagen, aufgrund des unpolaren Charakters der Kautschukmatrix. Die AFM Analyse der gefüllten NR Komposite zeigte indessen, dass die großen Füllstofftakteide mit steigender Mischzeit in kleinere zerteilt wurden, was sehr gut mit den SAXS-Messungen korreliert. Diese zeigt, dass die Position des Peaks mit steigender Mischzeit abnimmt. Des Weiteren konnten die Methoden auch erfolgreich zur Untersuchung des Einflusses von Schichtsilikat in HNBR/(NR-Schichtsilikat Masterbatch) Blends angewandt werden.

Die online gemessene Leitfähigkeit des HNBR/NR-Blend war sehr gering, was der HNBR Komponente geschuldet ist. Es konnte zuerst ein Anstieg, gefolgt von einem Plateau und einem

anschließenden Absinken des Online-Leitwert festgestellt werden, wenn das NR-Schichtsilikat-Masterbatch mit HNBR gemischt wurde. Die Online-Leitwertkurve lässt sich somit in zwei Abschnitte unterteilen, wobei der erste Abschnitt dem Anstieg und der zweite dem Absinken des Online-Leitwertes entspricht. Der strukturelle Hintergrund der Leitwertkurve wurde in Betracht zu den Ergebnissen der verschiedenen strukturellen Untersuchungen wie AFM, SAXS, Lösungsuntersuchungen und Oberflächenspannungsmessungen diskutiert. Dabei konnte als Hauptursache die Migration von Organoclay von der NR- zur HNBR-Phase gefunden werden. Diese Migration des Füllstoffes wurde qualitativ durch Vergrößerung der AFM- und TEM-Aufnahmen festgestellt. Die quantitative Bestimmung des Füllstofftransfers wurde mit Hilfe der Lösungsuntersuchung mit anschließender TGA durchgeführt. Der Füllstofftransfer von der NR- zur HNBR-Phase ist ein Ergebnis der bevorzugten Wechselwirkung zwischen dem Schichtsilikat mit der höher polaren HNBR-Phase, als mit der unpolaren NR-Phase. Das Absinken der Online-Leitwertkurve im zweiten Abschnitt ist mit einer Änderung der Morphologie von kokontinuierlich zur Insel-Matrix-Morphologie, als Ergebnis der Zusammenlagerung der Schichtsilikate verbunden. Die Oberflächenspannungsuntersuchungen ergaben einen starken Einfluss des Füllstoffanteils auf die Oberflächenenergien der beiden Blendkomponenten. Die Untersuchungen der mechanischen Eigenschaften ergaben sehr gute Korrelationen zur Online-Leitwertkurve.

Die Methode der Online-Leitfähigkeitsmessung wurde auch zur Untersuchung des Einflusses von Schichtsilikat in rein polaren Blends wie HNBR/ENR-Blends untersucht, dabei zeigte sich auch eine sehr geringe Leitfähigkeit, ähnlich dem HNBR/NR-Blend, die durch die HNBR-Komponente hervorgerufen wurde. Es konnte gezeigt werden, dass die Leitfähigkeit nach einem Anstieg mit steigender Mischzeit in ein Plateau übergeht, wenn das ENR-Schichtsilikat-Masterbatch mit reinem HNBR gemischt wurde.

Die Online-Leitwertkurve lässt sich auch hier in zwei Abschnitte unterteilen, wobei der erste Abschnitt durch einen Anstieg der Leitfähigkeit und der zweite durch ein Plateau gekennzeichnet ist. Somit ist der erste Abschnitt der Leitwertkurve mit der Migration des Füllstoffs von der ENR zur stärker polaren HNBR-Phase verbunden. Die morphologischen Untersuchungen mittels AFM und TEM verdeutlichen bei höherer Vergrößerung den Füllstofftransfer von der ENR- zur HNBR-Phase. Die Ergebnisse der SAXS-Untersuchungen zeigten eine sehr gute Übereinstimmung mit den Abständen in der Zwischenschicht. Mit steigender Mischzeit kam es zunächst zur Abnahme der Peaks. Mit Erreichen des Plateaubereiches der Online-Leitwertkurve,

wurden konstante Peaks mit Hilfe der Kleinwinkelröntgenstreuung erzielt. Die Kinetik der Morphologieentwicklung des HNBR/(ENR-Schichtsilikat-Masterbatch) wurde mittels AFM charakterisiert. Hier zeigte sich eine Umkehrung der Morphologie mit steigender Mischzeit von kokontinuierlich zu Insel-Matrix-Morphologie und wieder zu kokontinuierlich. Die Umkehrung der Morphologie ist dem Füllstofftransfer von der niedrig polaren zur polaren Blendphase geschuldet. Weiterhin konnte festgestellt werden, dass nach dem Erreichen des Plateaus in der Online-Leitwertkurve keine Änderung der Morphologie stattfand. Der Füllstoff, welcher sich an der Interphase des HNBR befindet, ist in der Polarität der beiden Phasen begründet.

Die Online-Leitfähigkeitsmessung stellt eine geeignete ökonomische und industriell realisierbare Methode zur Charakterisierung der Interkalierung und Exfolierung von Schichtsilikaten in Kautschukmischungen dar. Dennoch weist die Methode wenige Grenzen auf, da sie nicht auf thermisch instabile, unpolare und hochtemperaturbeständige Materialien angewendet werden kann. Weiterhin lässt sich schlussfolgern, dass wenn Schichtsilikate als Füllstoff in Blends eingemischt werden, der höhere Wert der Leitwertkurve in Verbindung mit einem Füllstofftransfer von der niedrig polaren zur stark polaren Phase des Blends steht. Nach dem Erreichen des Maximum des Online-Leitwertes ergeben sich zwei mögliche Kurvenverläufe; ein Absinken oder ein konstantes Verhalten. Ein Absinken der Leitwertkurve ist mit der Ausbildung einer Insel-Matrix-Morphologie verbunden, wobei der Füllstoff in der dispersen Phase dispergiert ist. Ein Plateau in der Online-Leitwertkurve kennzeichnet eine kokontinuierliche oder Insel-Matrix-Morphologie, wobei der Füllstoff in der Matrixphase dispergiert ist und ein durchgängiges Netzwerk für die elektrische Leitfähigkeit darstellt.

Die erfolgreiche Einführung der Online-Leitwertmessung zur Charakterisierung des Dispersionsprozesse von Schichtsilikaten in Kautschukmischungen und -blends im Labormaßstab ermöglicht eine Anwendung im Industriemaßstab zur Beurteilung der Füllstoffdispersion, sowie der Qualität von Kautschuk-Schichtsilikat-Nanokompositen.

## 8 Literature

1. A.B. Morgan, J.W. Gilman; *J. Appl. Polym. Sci.* 87 (2003) 1329.
2. S. Sadhu, A. K. Bhowmick; *J. Mater. Sci.* 40 (2005) 1633.
3. R.A. Vaia, W.D. Liu, H. Koerner; *J. Polym. Sci. B: Polym. Phys.* 41 (2003) 3214.
4. S. Bourbigot, D.L. Vanderhart, J.W. Gilman, W.H. Awad, R.D. Davis, A.B. Morgan, C.A. Wilkie; *J. Polym. Sci. B: Polym. Phys.* 41 (2003) 3188.
5. L.S. Loo, K.K. Gleason; *Macromolecules* 36 (2003) 2587.
6. H.J.M. Hanley, C. D. Muzny, D. L. Ho, C. J. Glinka; *Langmuir* 19 (2003) 5575.
7. J. Zhao; A.B. Morgan; J.D. Harris; *Polymer* 46 (2005) 8641.
8. A.J. Bur, Y. Lee, S.C. Roth, P.R. Start; *Polymer* 46 (2005) 10908.
9. I. Alig, D. Fischer, D. Lellingner, B. Steinhoff; *Macromol. Symp.* 230 (2005) 51.
10. A. Malinauskas, R. Holze; *J. Appl. Polym. Sci.* 73 (1999) 287.
11. Th. Rohe, W. Becker, A. Krey, H. Negele, S. Kölle, N. Eisenreich; *J. Near Infrared Spectr.* 6 (1998) 325.
12. G. Kortaberria, L. Solar, A. Jimeno, P. Arruti, C. Gomez, I. Mondragon; *J. Appl. Polym. Sci.* 102 (2004) 5927.
13. F. Hussain, J.H. Chen, M. Hojjati; *Mater. Sci. & Eng., A: Structural Mater.: Properties, Microstructure and Processing* 445 (2007) 467.
14. H.H. Le, S. Ilisch, B. Jakob, H.-J. Radosch; *Rubber Chem. Technol.* 77 (2004) 147.
15. H.H. Le, G.R. Kasaliwal, S. Ilisch, H.-J. Radosch; *Rubber Chem. Technol.* 81 (2008) 767.
16. F. Hussain, M. Hojjati, M. Okamoto, R.E. Gorga; *J. Comp. Mater.* 40 (2004) 1511.
17. *Encyclopaedia of Science and Technology* 4; McGraw-Hill, page 491.
18. H. va Olphen, J.J. Fripiat, "Data Handbook for Clay Minerals and other Non-Metallic Minerals" Pergamon Press, Elmsford NY 1979
19. C. Park, O. Park, J. Lim, H. Kim; *Polymer* 42 (2001) 7465.
20. L.A. Utracki, "Clay containing polymer nanocomposites" Rapra Technology Shawbury, Shrewsbury, Shropshire, SY4 4NR, United Kingdom 2004.
21. L. Pérez-Maqueda, F. Franco, M.A. Avilés, J. Poyato, J.L. Pérez-Rodríguez; *Clay and Clay Minerals* 51 (2003) 701.
22. M.A. Osman, M. Ploetze, P. Skrabal; *J. Phys. Chem. B* 108 (2004) 2580.
23. T.D. Fornes, P.J. Yoon, D.L. Hunter, H. Kesula, D.R. Paul; *Polymer* 43 (2002) 5915.
24. E. Hackett, E. Manias, E.P. Giannelis; *J. Chem. Phys.* 108 (1998) 7410.
25. G. Lagaly; *Solid State Ionics* 22 (1984) 43.
26. R.A. Vaia, R.K. Teukolsky, E.P. Giannelis; *Chem. Mater.* 6 (1994) 1017.
27. L.Q. Wang, J. Liu, G.J. Exarhos, K.Y. Flangan, R. Bordia; *J. phys. Chem. B* 104 (2000) 2810.
28. R.A. Vaia, H. Ishii, E.P. Giannelis; *Chem. Mater.* 5 (1993) 1694.
29. J. Karger-Kocsis, C.-M. Wu; *Polym. Eng. Sci.* 44 (2004) 1083.
30. R. Sengupta, S. Chakraborty, S. Bandyopadhyay, S. Dasgupta, R. Mukhopadhyay, K. Auddy, A.S. Deuri; *Polym. Eng. Sci.* 47 (2007) 1956.
31. Y. Wang, L. Zhang, C. Tang, D. Yu; *J. Appl. Polym. Sci.* 78 (2000) 1879.
32. Y.P. Wu, L.Q. Zhang, Y.Q. Wang, Y. Liang, D.S. Yu; *J. Appl. Polym. Sci.* 82 (2001) 2842
33. A. Usuki, M. Kawasumi, Y. Kojima, A. Okada, T. Kurauchi, O. Kamigaito; *J. Mater. Res.* 8 (1993) 1179.
34. S. Sadhu, A.K. Bhowmick; *J. Appl. Polym. Sc.* 92 (2004) 698.
35. Y. Kojima, K. Fukumori, A. Okada, T. Kurauchi; *J. Mater. Sci. Letters* 12 (1993) 889.
36. A. Akelah, N. Salahuddin, A. Hiltner, E. Baer, A. Moet; *Nanostructured Materials* 4 (1994) 965.
37. C. Nah, J.J. Ryu, S.H. Han, J.M. Rhee, M.H. Lee; *Polym. Int.* 50 (2001) 1265.
38. J. Fritzsche, A. Das, R. Jurk, K.W. Stöckelhuber, G. Heinrich, M. Klüppe; *eXPRESS Polymer Letters* 2 (2008) 373.
39. A. Das, K.W. Stöckelhuber, P. Sen Majumder, T. Engelhardt, J. Fritzsche, M. Klüppel, G. Heinrich; *J. Material Science-A: Pure Appl. Chem.* 46 (2009) 7.
40. R. Rajasekar, K. Pal, G. Heinrich, A. Das, C.K. Das; *Material and Design* 30 (2009) 3839.



41. J. T. Kim, T.S. Oh, D.H. Lee; *Polym. Int.* 52 (2003) 1058.
42. S. Sadhu, A.K. Bhowmick; *J. Polym. Sci. Part B: Polym. Phys.* 42 (2004) 1573.
43. Y.R. Liang, W.L. Cao, X.B. Zhang, Y.J. Tan, S.J. He, L.Q. Zhang; *J. Appl. Polym. Sci.* 112 (2009) 3087.
44. S. Kalaivani, V. Vijayabaskar, M. Thunga, M. Stephan, H.Dorschner, G. Heinrich, A. K. Bhowmick; U. Wagenknecht; *Plastics, Rubber and Composites* 38 (2009) 39
45. K. G. Gatos, N. S. Sawanis, A. A. Apostolov, R. Thomann, J. Karger-Kocsis; *Macromol. Mater. Eng.* 289 (2004) 1079.
46. K. G. Gatos, L. Százdi, B. Pukánszky, J. Karger-Kocsis; *Macromol. Rapid Commun.* 26 (2005) 915
47. P.L. Teh, Z.A. Mohd Ishak, A.S. Hashim, J. Karger-Kocsis, U.S. Ishiaku; *Eur. Polym. J.* 40 (2004) 2513.
48. M.A. López-Manchado, M. Arroyo, B. Herrero, Biagiotti; *J. Appl. Polym. Sci.* 89 (2003) 1.
49. A. Jacob, P. Kurian; A. S. Aprem; *Int. J. Polym. Mater.* 54 (2007) 593.
50. S. Varghese, J. Karger-Kocsis; *J. Appl. Polym. Sci.* 91 (2004) 813.
51. S. Varghese, J. Karger-Kocsis, K.G. Gatos; *Polymer* 44 (2003) 3977.
52. Y.T. Vu, J.E. Mark, L.H. Pham, M. Engelhardt; *J. Appl. Polym. Sci.* 82 (2001) 1391.
53. P. L. Teh, Z. A. Mohd Ishak, A. S. Hashim, J. Karger-Kocsis, U. S. Ishiaku; *J. Appl. Polym. Sci.* 100 (2004) 1083.
54. K.G. Gatos, J. Karger-Kocsis, *Polymer* 46 (2005) 3069.
55. C.D. Silva, B. Haidar, A. Vidal, J. Miehe-Brendle, R. Le Dred, L. Vidal; *J. Mater. Sci.* 40 (2005) 1813.
56. A. Usuki, A. Tukiase, M. Kato; *Polymer* 43 (2002) 2185.
57. W.C. Young, Y. Yungchul, R. Seunghoon, C. Nah; *Polym. Int* 51 (2002) 319.
58. Y.P. Wu, Y. Ma, Y.Q. Wang, L.Q. Zhang; *Macromol. Mater. and Eng.* 289 (2004) 890.
59. L. Zhang, Y. Wang, Y. Wang, Y. Sui, D. Yu; *J. Appl. Polym. Sci.* 78 (2000) 1873.
60. R. Rajasekar, G. Heinrich, A. Das, C.K. Das; *Research Letters in Nanotechnology* 2009 doi:10.1155/2009/405153.
61. T.D. Fornes, P.J. Yoon, H. Keskkula, D.R. Paul; *Polymer* 42 (2001) 9929.
62. M. Kawasumi, N. Hasegawa, M. Kato, A. Usuki, A. Okada; *Macromolecules* 30 (1997) 6333.
63. L. Zhu, M. Xanthos; *J. Appl. Polym. Sci.* 93 (2004) 1891.
64. J.W Cho, D.R. Paul; *Polymer* 42 (2001) 1083.
65. H.R. Dennis, D.L. Hunter, D. Chang, S. Kim, J.L. White, J.W. Cho, D.R. Paul; *Polymer* 42 (2001) 9513.
66. R.A. Vaia, E.P. Giannelis; *Macromolecules* 30 (1997) 7990.  
R.A. Vaia, E.P. Giannelis; *Macromolecules* 30 (1997) 8000.
67. M.E. Mackay, A. Tuteja, P.M. Duxbury, C.J. Hawker, B. Van Horn, Z. Guan, G. Chen, R.S. Krishnan; *Science* 311 (2004) 1740.
68. S.W. Kim, W.H. Jo, M.S. Lee, M.B. Ko, J.Y. Jho; *Polymer Journal*, 34 (2002) 103.
69. T. Koyama, S. Tanoue, Y. Iemoto, T. Maekawa, T. Unryu; *Polymer Composites* 30 (2008) 1065.
70. J. Park, S.C. Jana; *Macromolecules*, 36 (2003) 2758.
71. A. Hasook, H. Muramatsu, S. Tanoue, Y. Iemoto, T. Unryu; *Polymer Composites* 29 (2008) 1.
72. M.A. Scott, K.A. Carrado, P.K. Dutta; "Hand Book of Layered Materials" CRC press 2004.
73. L. Jiankun, K. Yucai, Q. Zongneng, Su Y. Xiao; *J. Polym. Sci. B: Polym. Phys.* 39 (2001) 115.
74. G. Strobl; *Physics of Polymers*. 2nd Edn., Springer Verlag, Berlin Heidelberg New York, 1997, P 285.
75. H. Ishida, S. Campbell, J. Blackwell; *Chem. Mater.* 12 (2000) 1260.
76. A. Usuki, M. Kawasumi, Y. Kojima, A. Okada, T. Kurauchi, O. Kamigaito, *J. Mater. Res.* 8 (1993) 1179.
77. K. Yano, A. Usuki, A. Okada, T. Kuraychi, O. Kamigaito, *J. Polym. Sci., Part A: Polym Chem.* 31 (1993) 2493.
78. M.A. López-Manchado, B. Herrero, M. Arroyo; *Polym Int* 53 (2004) 1744.
79. J.T. Kim, D.Y. Lee, T.S. Oh, and D.H. Lee, *J. Appl. Polym. Sci.* 89 (2003) 2633.
80. N. Hasegawa, M. Kawasumi, M. Kato, A. Usuki, A. Okada; *J. Appl. Polym. Sci.* 67 (1998) 87.
81. J.H. Lee, D. Jung, C.E. Hong, K.Y. Rhee, S.G. Advani, *Compos. Sci. Technol.* 65 (2005) 1996
82. E. Manias, A.Touny, L.Wu, K. Strawhecker, B. Lu, T.C. Chung; *Chem. Mater.* 13 (2001) 3516.
83. L. Liu, Z. Qi, X. Zhu; *J. Appl. Polym. Sci.* 71 (1999) 1133.
84. N. Tokita; *Rubber Chem. Technol.* 50 (1977) 292.
85. L.A. Utracki; *Polymer blend handbook*, Kulver academic Publishers, Dordrecht 2002.

86. C.B. Wang, S.L. Cooper; *J. Polym. Sci.; Polym. Phys.* 21 (1983) 11.
87. Z. Fang, C. Harrats, N. Moussaif, G. Groeninckx; *J. Appl. Polym. Sci.* 106 (2007) 3125.
88. D. Vulgaris, D. Petrides; *Polymer* 43 (2002) 2213.
89. W.S. Chow, Z.A. Mohd Ishak, J. Karger-Kocsis, A.A. Apostolov, U.S. Ishiaku; *Polymer* 44 (2002) 7427.
90. J.E. Mark, B. Erman, F.R. Eirich; *Science and Technology of Rubber*, Elsevier Academic Press, Burlington USA, 2005.
91. J. Noolandi, K.M. Hong; *Macromolecules* 15 (1982) 482.
92. V.J. Grossmann, P. Putsch; *Kunststoffe* 9(2005) 180.
93. L. Priya, P.J. Jog; *J. Polym. Sci., part B: Polym. Phys.* 40 (2002) 1682.
94. M.Y. Gelfer, H.H. Song, L. Liu, B.S. Hsiao, B. Chu, M. Rafailovich, M. Si, V. Zaitsev; *J. Polym. Sci., Polym. Phys.* 41 (2003) 44.
95. B.B. Khatua, D.J. Lee, H.Y. Kim, J.K. Kim; *Macromolecules* 37 (2004) 2454.
96. Y. Wang, Q. Zhang, Q. Fu; *Macromol. Rapid Commun.* 24 (2003) 231.
97. H. Essawy, D. El-Nashar; *Polymer Testing* 23 (2004) 803.
98. B.B. Khatua, D.J. Lee, H.Y. Kim, J.K. Kim; *Macromolecules* 37 (2004) 2454.
99. K. Yurekli, A. Karim, E.J. Amis, R. Krishnamoorti; *Macromolecules* 37 (2004) 507.
100. Y. Li, H. Shimizu; *Polymer* 45 (2004) 7381.
101. J.S. Hong, Y.K. Kim, K.H. Ahn, S.J. Lee, C.Y. Kim; *Rheol. Acta* 46 (2007) 469.
102. R. Fisher, M.W. Zhang, X. Hu, M. Lin, D. Gersoppe, J. Sokalov, M. Rafailovich, M. Rubenstein, A. Winesett, H. Ade; *Proceedings of the 7th International Conference on Atomically Controlled Surfaces*, 14–20 November, Nara, Japan, 2003.
103. K. Wang; S. Liang; R.N. Du; Q. Zhang; Q. Fu; *Polymer* 45 (2004) 7953.
104. J. Sharif, W.M.Z.W. Yunus, K.J. Dahlan, M.J. Ahmad; *J. Appl. Polym. Sci.* 100 (2004) 353.
105. S.S. Ray, M. Bousmina; *Macromol. Rapid Commun.* 26 (2005) 1639.
106. S.S. Ray, M. Bousmina; *Macromol. Rapid. Commun.* 26 (2005) 450.
107. L.T. Vo, E.P. Giannelis; *Macromolecules* 40 (2007) 8271.
108. J.E. Callan, W.M. Hess, C.E. Scott; *Rubber Chem. Technol.* 44 (1971) 814.
109. S. Datta, D.J. Lohse; *Polymeric Compatibilizers: Uses and Benefits in Polymer Blends*, Hanser Gardner Publications, Munich, 1996
110. M. Si, T. Araki, H. Ade, A.L.D. Kilcoyne, R. Fisher, J.C. Sokolov, M.H. Rafailovich; *Macromolecules* 39 (2004) 4793.
111. L. As'habi, S.H. Jafari, B. Baghaei, H.A. Khonakdar, P. Pötschke, F. Böhme; *Polymer* 49 (2008) 2119.
112. A.F. Santos, E.L. Lima, J.C. Pinto; *J. Appl. Polym. Sci.* 70 (1998) 1737.
113. K. Ito, T. Kato, T. Ona; *J. Raman Spectroscopy* 33 (2002) 466.
114. H. Keuter, D. Ackfeld, A. Limper; *Kautsch. Gummi Kunstst.* 53 (2000) 566.
115. J. Tatibouet, M.A. Huneault; *Polym. Processing* 17 (2002) 49.
116. G.D. Smith, E.C. Brown, D. Barnwell, K. Martin, P.D. Coates; *Plastics Rubber and Composites* 32 (2003) 248.
117. J.A. Covas, O.S. Carneiro, P. Costa, A.V. Machado, J.M. Maia; *Plastic Rubber and Composites* 33 (2004) 55.
118. N.H. Abu-Zahra; *Mechatronics* 14 (2004) 789.
119. N. Noda, Y.H. Lee, A.J. Bur, V.M. Prabhu, C.R. Snyder, S.C. Roth, M. McBrearty; *Polymer* 46 (2005) 7201.
120. R. A. Vaia, S. Vasudevan, W. Krawiec, L. G. Scanlon, and E. P. Giannelis; *Adv. Mater.* 7 (1995) 154.
121. W.Y. Jang, S.D. Hwang, J.D. Nam; 33rd ISTC, Seattle, WA, November 5-8, 2001.
122. P. Aranda, J.C. Galvan, B. Casal, E. Ruiz-Hitzky; *Electrochim. Acta* 37 (1992) 1573.
123. M. Okamoto, S. Morita, and T. Kotaka; *Polymer* 42 (2001) 2685.
124. F.F. Fang, H.J. Choi, J. Joo; *J. Nanosci. and Nanotech.* 8 (2008) 1559.
125. H.H. Le, I. Prodanova, S. Ilisch, H.-J. Radsch; *Rubber Chem. Technol.* 77 (2004) 815.
126. H.H. Le, M. Tiwari, S. Ilisch, H.-J. Radsch; *Kautsch. Gummi Kunstst.* 58 (2005) 575.
127. H.H. Le, Z. Qamer; S. Ilisch, B. Jakob, H.-J. Radsch; *Rubber Chem. Technol.* 79 (2006) 621.
128. H.H. Le, M. Tiwari, S. Ilisch, H.-J. Radsch; *Rubber Chem. Technol.* 79 (2006) 610.
129. S. Shiga, M. Furuta; *Rubber Chem. Technol.* 58 (1985) 1.
130. R. D. Davis, A. J. Bur, M. McBrearty, Y.-H. Lee, J. W. Gilman, P. R. Start; *Polymer* 45 (2004) 6487.
131. Therban product information, Lanxess Energizing Chemistry, <http://www.therban.com>.

132. Zeptol technical information, Zeon Chemicals, <http://www.zeonchemicals.com>.
133. Standard Malaysian Rubber comparison chart, Altlett Rubber Inc., <http://www.astletterubber.com>.
134. Epoxidized natural rubber, Weber & Schaer GmbH & Co., <http://www.weber-schaer.com>.
135. Cloisite Na+, Southern Clay products "www.scpod.com".
136. P.K. Freakley, S.R. Patel; *Rubb. Chem. Technol.* 52 (1979) 134.
137. J.L. Leblanc; *Prog. Trends Rheol. II* (1988) 32.
138. C. Leigh-Dugmore; *Rubber Chem. Technol.* 29 (1954) 1303.
139. H. H. Le, S. Ilisch, G. R. Kasaliwal, H.-J. Radsch; *Kautsch. Gummi Kunstst.* 60 (2007) 241.
140. S. Maiti, S.K. De, A.K. Bhowmick; *Rubber Chem. Technol.* 65 (1992) 293.
141. H.A. Pohl; *J. Polym. Sci. Sym.* 17 (1947) 13.
142. A. Motori, G.C. Montanari, A. Saccani, F. Patuelli; *J. Polym. Sci. B; Polymer Physics* 45 (2007) 705.
143. R. A. Vaia, K. D. Jant, E. J. Kramer, E. P. Giannelis; *Chem. Mater.* 8 (1994) 2628.
144. H. Zhou, G.L. Wilkes; *Polymer* 38 (1997) 5735.
145. A. Kathryn, A. Ramirez, L.R. Kathy; *Langmuir* 14 (1998) 2562.
146. W. Stocker, J. Beckmann, R. Stadler, J. Rabe; *Macromolecules* 29 (1994) 7502.
147. E.A. Radovanovic, E. Carone, M.C. Goncalves; *Polymer Testing* 23 (2004) 231.
148. J. Zhang, E. Manias, C.A. Wilkie; *J. Nanosci. and Nanotech.* 8 (2008) 1597.
149. Y.P. Wu, Q.X. Jia, D.S. Yu, L.Q. Zhang; *J. Appl. Polym. Sci.* 89 (2003) 3855.
150. F. Schön, R. Thmann, W. Gronski; *Macromol. Symp.* 189 (2002) 105.
151. J. Kim, T. Oh, D. Lee; *Polym. Int.* 53 (2004) 406.
152. Y. Kojima, K. Fukumori, A. Usuki, T. Kurauchi; *J. Mater. Sci. Lett.* 12 (1993) 889.
153. J. Sharif, W.M.Z.W. Yunus, K. Z.M. Dahlan, M.H. Ahmad; *Polym. Testing*, 24 (2005) 211.
154. Z.A.M. Ishak, P.Y. Wan, P.L. Wong, Z. Ahmad, U.S. Ishiaku, J. Karger-Kocsis; *J. Appl. Polym. Sci.* 84 (2002) 2265.
155. P. Sae-oui, C. Sirisinha, T. Wantana, K. Hatthapanit; *J. Appl. Polym. Sci.* 104 (2007) 3478.
156. A.J. Tinker, K.P. Jones; *Blends of Natural Rubber*, Chapman and Hall, London 1998.
157. S. Lyu, T.D. Jones, F.S. Bates, C.W. Mocosko; *Macromolecules* 35 (2002) 7845.
158. S.H. Jafari, P. Pötschke, M. Stephan, H. Warth, H. Alberts; *Polymer* 43 (2002) 6985.
159. R.G. Larson; *The structure and rheology of complex fluids*, Oxford University Press; ch 9, 1999.
160. L. Liu, D. Jia, Y. Luo, B. Guo; *J. Appl. Polym. Sci.* 100 (2004) 1905.
161. S. S. Ray, S. Pouliot, M. Bousmina, L.A. Utracki; *Polymer* 45 (2004) 8403.
162. A.E. Mathai, S. Thomas; *J. Appl. Polym. Sci.* 97 (2005) 1561.
163. A. Kalarakis, E.P. Giannelis, K. Yoon; *Polymer* 48 (2007) 7567.
164. M. Ganter, W. Gronski, H. Semke, T. Zilg, C. Thomann, R. Mühlhaupt; *Kautsch. Gummi Kunstst.* 54 (2001) 144.

## Resume

**Full Name:** Zulfiqar Ali  
**Date of Birth:** 20<sup>th</sup> April 1974  
**Place of Birth:** Kassoki, Hafizabad, Pakistan  
**Nationality:** Pakistani

### Academic Qualification

**1997-1999** Master of Science (Chemistry) Department of Chemistry, Quaid-i-Azam University Islamabad, Pakistan.  
**2002-2004** Master of Science (Applied Polymer Science) Department of Engineering, Martin-Luther University Halle-Wittenberg, Germany  
**Dec 2005-2009** PhD Student, Center for Engineering Sciences, Polymer Technology, Martin Luther University Halle-Wittenberg, Germany

## **Erklärungen**

### **Erklärung über die selbständige Anfertigung der Arbeit**

Hiermit erkläre ich, dass ich meine Arbeit selbständig und ohne fremde Hilfe verfasst, andere als die von mir angegebenen Quellen und Hilfsmittel nicht benutzt und die den benutzten Werken wörtlich oder inhaltlich entnommenen Stellen als solche kenntlich gemacht habe.

### **Erklärung über Vorstrafen und Ermittlungsverfahren**

Hiermit erkläre ich, dass gegen mich keinerlei Vorstrafen vorliegen und kein Ermittlungsverfahren eingeleitet ist.

### **Erklärung über etwaige frühere Promotionsverfahren**

Hiermit erkläre ich, dass ich mich zuvor an keiner anderen Institution um den Doktorgrad beworben und dass ich keinerlei vergebliche Promotionversuche unternommen habe.

Halle 05.08.2009

Zulfiqar Ali